Doctoral Dissertation

Studies on Controlling the Dissolution/disintegration Behavior of Polysaccharide-based Blend Films by Incorporating Intermolecular Crosslinks

（分子間架橋の導入による多糖ベース混合フィルムの水中崩壊挙動の制御に関する研究）

Yuxiang Jia

June 2023

Graduate School of Engineering,
Osaka University

Table of Contents

General Introduction

GI.1. Single-use plastic films (SUPs) and marine plastics issue

While SUPs greatly improved quality of life and facilitated economic growth, a large amount of discarded SUPs were being leaked to the marine environment. Among the non-fiber plastic produced from 1950 through 2015, short-term applications, mostly packaging, consumed more than 40% of total produced amount, most of which leave service in the first year.[1] Due to the improper waste management, these single- or short-term-use materials find their way into the marine environment after being discarded,[2] and it has been found that these discarded SUPs accounted for most of the marine plastics found globally.[3] These discarded plastics have caused significant adverse impacts on the marine ecosystem[4]. Additionally, the change in lifestyle consequent to the COVID-19 pandemic has also significantly boosted demand for SUPs,[5] which further complicates the plastic waste management.[6]

Plastics films have a diverse array of applications, including packaging and non-packaging applications such as agricultural and building applications; accordingly, plastic films also represents a major part of the plastic waste.[7] With the advancement of plastics recycle technology, various recycling strategies including mechanical and chemical recycling have seen different degree of success;[1] however, recycling process currently available is far from free of limitations, and recycle options can be even more limited when it comes to recycling plastic films. Due to the nature of plastic film applications, many plastic film wastes can be heavily contaminated, which requires complex sorting operations and reduced profitability in recycling, as a result plastic films are usually considered as non-recyclable in waste management.[7] Thus, it is highly likely that plastic films have a higher chance of leaking to the marine environment. In fact, it has already been reported that film-type plastics were the major type of plastic in nearshore areas.[3] Thus, lessening the burden put on marine ecosystem by plastic films is one important aspect to solving the marine ecosystem, and there is a necessity for designing alternatives to current plastic films that poses less risk to marine ecosystem even when failed to be recycled and being leaked to the marine environment.

GI.2. Issues of current biodegradable plastics as a solution to marine plastics

Biodegradable plastics refer to a group of plastics that is degradable at the action of naturally occurring micro-organisms, for example bacteria, fungi and algae.[8] In the past decades, a wide variety of biodegradable plastics, both artificially synthesized ones such as polylactic acid (PLA)[9] and polycaprolactone (PCL)[10], and microorganism-synthesized ones such as polyhydroxyalkanoates (PHA)[11], have been developed (**Figure 1**). These plastics show much faster biodegradation rates in certain environments when compared against conventional synthetic polymers,[8] and thus have been

widely considered to be an opponent solution to a series of environmental and ecological issues caused by leakage of discarded SUPs to the natural environment.

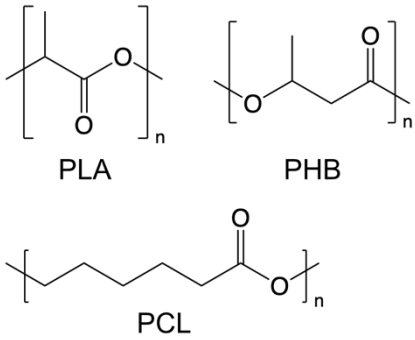

Figure 1 Molecular structures of some current biodegradable polymers: PLA, PHB (one type of PHA), and PCL.

Due to their ability to biodegrade under microorganism action and vanish in natural environments, it may seem apparent that these biodegradable polymers are the solution to marine plastics. However, whether they can be utilized as a true solution to the marine plastics issue remains to be open for debate. A significant limiting factor is their production. Out of 335 Mt of plastics produced globally in 2016, biodegradable plastics merely accounted for 0.5%; although biodegradable plastics production are expected to increase to about 2.26 Mt in 2023 and are still expected to increase beyond that, it is unlikely that the supply becomes sufficient enough that conventional plastics can be replaced entirely in the near future.[12] Also, the manufacturing cost of biodegradable plastics is still considerably higher than that of conventional plastics; while it is possible to decrease the manufacturing cost by economies of scale, the attempts of increasing manufacturing capability are usually constrained by the cost of scaling up facilities.[13]

While the supply and cost of current biodegradable plastics could be a major limiting factor in the utilization of these plastics as marine ecosystem-friendly alternatives, the real barrier comes from their inherent properties, i.e., the capability to degrade in marine environments. For these current biodegradable polymers, highly controlled environments (e.g. compost) are almost always required to achieve optimum biodegradability.[14] In environments that are not as nearly meticulously controlled, their biodegradability tends to decrease substantially. Specifically, the biodegradation rates of common biodegradable polymers such as PLA and PCL reduces drastically in aqueous environments including seawater, to an extent that they might no longer be considered to be biodegradable.[15,16] For example, even after 1 year of incubation in seawater, the weight loss of PLA is barely noticeable (**Figure 2**).[15] The reduced degradability of these biodegradable polymers owes primarily to the lower total amounts of microorganisms, fewer specific microbial species, and lower temperature than those in optimum environments.[17] The discarded plastics that are discharged into marine environment are encountered by ocean wildlife primarily by the entanglement, ingestion, and interaction (including collisions, obstructions, and

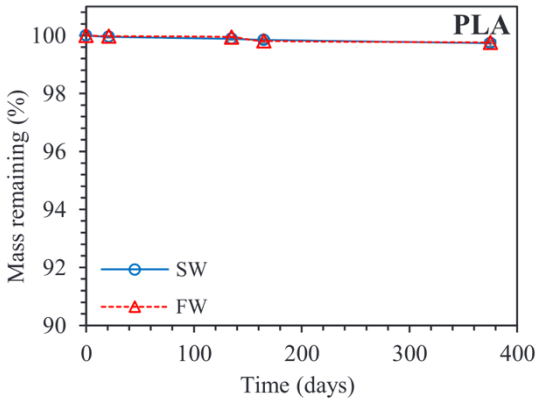

Figure 2 Mass reduction of PLA in aqueous environments over time. SW: seawater. FW: freshwater.[15]

abrasions)[4]. All these patterns of encountering require plastic debris to possess a certain shape and a certain degree of mechanical strength. Owing to the prolonged time required for completely breaking down or vanishing in marine environments, these biodegradable plastics might not quickly vanish in marine environment, thus there is a large time window during which the material retains a distinct shape and considerable strength for encountering ocean wildlife.

The ecological impact that current biodegradable plastics have on marine ecosystem still needs to be investigated in better detail. Nevertheless, even at the very early stage of such investigations, evidence of slowly degrading biodegradable plastics can possibly negatively affect the marine ecosystem at both macro-[18] and microplastic levels[19–23], as with conventional plastics[24], has already been reported. Therefore, while current biodegradable plastics generally represent a great step on alleviating the environmental and ecological issue caused by discarded SUPs leaked to the natural environment, they might be less advantageous over conventional synthetic polymers in terms of eco-safeness or "friendliness" to marine ecosystem. Current biodegradable plastics might not be the final answer to the marine plastics issue, and new biodegradable plastic materials that is capable of addressing this issue must be developed.

GI.3. Starch as a potential source material of marine ecosystem-friendly SUPs

Starch is a natural carbohydrate consisted almost entirely of two major polysaccharides, amylose and amylopectin; both consists of chains of α-(1,4)-linked D-glucose residues interconnected through α-(1,6)-glycosidic linkages, with the difference being that amylose are mostly linear long chains with hundreds or even thousands of glucose residues, whereas amylopectin is extensively branched and have comparatively shorter chains (**Figure 3**).[25] Starch is the end-product of photosynthesis and serves as the chemical energy storage of plants, and can be widely found in all kinds of plant tissue, including the leaves of all green plants and in the seeds, stems, roots of most plants.[26]

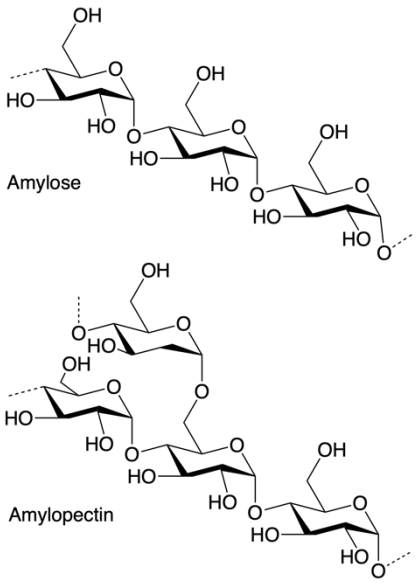

Figure 3 Molecular structures of two components of starch, amylose and amylopectin.

While starch is mostly being considered as a nutrition source of human, it can also be a potential material for the preparation of sustainable polymer materials. Benefiting from the biodegradability of starch, starch-based materials can have faster biodegradation rate and reduced landfill requirements as compared to conventional plastics.[27] Due to the -OH groups on C-2, C-3 and C-6, starch is chemically reactive and can be easily modified by a slew of chemical reactions, which can be mainly be categorized into oxidation, esterification and

etherification.[26] The chemical and physical properties of starch can be altered significantly by chemical modifications, which provided good flexibility for designing starch-based plastics with different properties based on the requirements of the application in question. With all these excellent properties, there is a growing emphasis on starch-based plastics, and previously a variety of starch-based plastics have been developed.[27] Additionally, as mentioned above, starch is extremely abundant in nature, and it can be mass produced by a wide variety of crops, each with adaptations to different climate conditions, including but not limited to potato, casava and wheat; the global production of starch has been estimated between 88.1 and 97.7 Mt in 2020.[28] The price of starch is on par with or even lower than conventional petrochemical polymers,[29] and significantly lower than current biodegradable plastics.[29,30] With this abundant supply and low cost, it is likely that the production and consumption of starch-based plastics would be economically viable, which further increases the attractiveness of using starch as a source material for the preparation of future plastic materials.

Aside from the properties already discussed, starch also have some additional properties that make starch not only an ideal starting material for developing sustainable polymer materials, but also particularly suitable for the development of polymer materials that pose low risk to marine ecosystem. While the biodegradability of starch in soil has already been widely known, starch has also been recognized as a polymer that readily biodegrades in seawater.[17,31] Furthermore, recent evidence showed that when blended with other biopolymers, starch can even potentially promote the biodegradation of the whole composite; for example, the biodegradation of a cellulose nanofiber film in marine environment was accelerated by starch, which has been identified to enhance the attachment of microorganisms on the surface of the film.[32] Therefore, starch is not only generally suitable for the substitution of petrochemical plastics, but also a promising starting material for the development of marine-ecosystem-friendly polymeric materials.

GI.4. Starch as a source material for plastic films, and issues of starch-based blend films

As previously mentioned, plastic film is an important category of plastic materials with high demands and a wide variety of applications, and plastic films used for many applications can have higher risks of being leaked to the environment. Therefore, there is always a strong interest in developing alternatives using sustainable and biodegradable starting materials. With many properties suitable for the development of plastic materials, starch is also a popular starting material for the development of said alternatives. Previously, a wide variety of starch films have already been prepared, and the relationship between different factors (biological source of starch, plasticizer, humidity etc.) and film physico-chemical properties has been investigated.[33–38] Starch-based blend films prepared by blending starch with a wide variety of different polymers was also developed; for example, including but not limited to natural polymers, agar[39], chitosan[40], guar gum[41], and synthetic polymer like LDPE[42] and P(3HB)[43]. Blending starch with other polymers can yield films with improved physical properties

over starch or the other components, due to the synergistic effects between starch and the other components. And these blend films generally show comparable physical properties comparable to some conventional polymer films, especially strength (around 10 to a few tens of MPa), which makes them suitable for SUPs films.

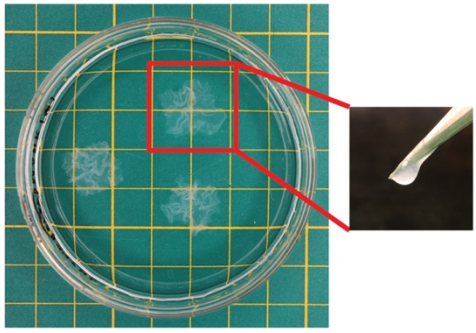

Figure 4 Tapioca starch films immersed in water for 10 min, showing its dissolution.

However, the application prospect of starch or starch-based blend films can be limited by a few issues. For these films to be used practically for single-use applications, these issues must be addressed. The most prominent issue would be the lack of water resistance, which is a much-desired property for SUPs. While conventional plastics have great stability in water and thus products based on conventional plastics have great water resistance, starch-based films tend to swell, dissolve, or disintegrate rapidly in water,[34,44,45] after which their mechanical strength is severely degraded. As shown in **Figure 4**, a tapioca starch film completely dissolved after being immersed in water. This low water resistance can be attributed to not only the high hydrophilicity of starch, whose molecular structure is rich in hydrophilic hydroxyl groups, but also the change in polymer chain conformation during the preparation process of films. When being synthesized in plants, starch is deposited in the form of granules, which is formed by crystalline and semi-crystalline lamellar of highly ordered starch molecular chains.[46] This highly ordered arrangement consequently promoted formation of inter- and intramolecular hydrogen bonds, which held the molecular chains together and rendered the granules cold water-insoluble.[26] Nevertheless, to process starch into any starch-based plastics including films, starch must go through a gelatinization process (**Figure 5**) under high temperature and

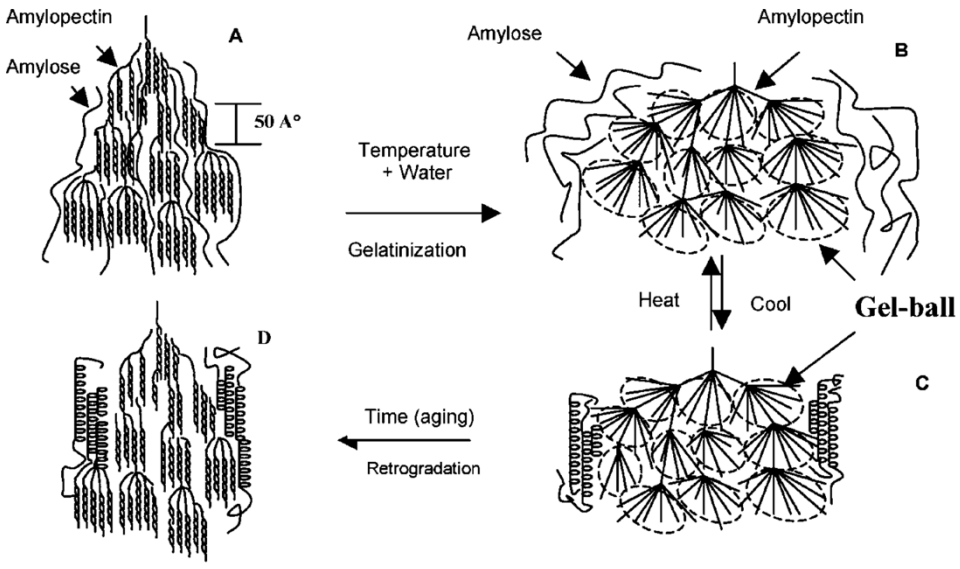

Figure 5 Schematic illustration of gelatinization and retrogradation.[48]

existence of plasticizer, during which ordered molecule arrangement and the granule structure are disrupted.[47] This process is irreversible, due to the incompatibility between amylose and amylopectin and their partial separation during the gelatinization process; although the hydrogen bonds can regenerate partially as time passes (retrogradation), the polymer chains cannot fully return to the previous ordered state, and the newly formed hydrogen bonds are insufficient for holding the molecular chains together in water.[48] The loss of aligned structure also prevented the formation of dense crystalline structure, which can retard water penetration. The loss of aligned structure, combined with the inherent hydrophilicity of starch, caused the low water resistance of starch.

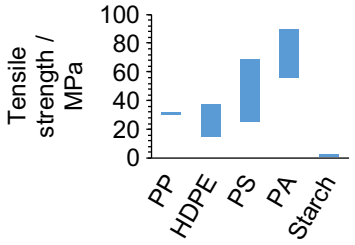

Figure 6 Approximate range of tensile strength comparison between starch films and some petrochemical polymers: Polypropylene (PP), high-density polyethylene (PE), polystyrene (PS) and polyamide (PA).[33, 49]

Another issue of starch-based films is the relatively low mechanical properties.[27] Compared to films of conventional polymers, starch films without other components show relatively low mechanical properties. For example, films of different types of starch generally showed maximum tensile strength around <1 MPa to a few MPa,[33] which is considerably lower than that of many petrochemical polymers (**Figure 6**).[49] While the water resistance and mechanical properties of starch films can be improved by blending with other polymers and nanoparticles,[27] the effect of such modifications is obviously largely affected by the material choice and the interaction between starch and other components.

GI.5. Strategies for improving water resistance starch-based blend films

To improve the low water resistance of starch-based blend films, various strategies have been previously developed, and popular strategies include hydrophobic modification of starch, doping with fillers and introducing crosslinks.

As mentioned above, one important cause for the low water resistance of starch-based films is the hydrophilicity of starch, due to the existence of large amount of hydrophilic hydroxyl groups on starch molecules. The introduction of hydrophobic groups, e.g. acetyl[50] and octenylsuccinate[51] groups, mainly through esterification on the hydroxyl group on starch,[52] can reduce the hydrophilicity of starch molecules; the number of hydroxy groups reduces in this process, which is also helpful for decreasing the hydrophilicity of starch.[53] However, water solubility can increase as the degree of substitution (D.S.) increases at low to intermediate D.S., as the increase in D.S. could hinder both inter- and intramolecular hydrogen bond formation (or, retrogradation).[54] To achieve water resistance by the introduction of hydrophobic groups, considerably high D.S. or sufficiently long alkyl chain is often required. However, the increase in D.S. and alkyl chain length can adversely impact the biodegradation of starch; it has

been reported that in activated sludge, both increase in D.S. and alkyl chain length significantly reduced the bioconversion potential of starch. As the microorganism density is much lower in seawater, it can be expected that the biodegradation of these starches would be even slower in seawater. The hydrophilicity of constitutional units, and the diffusion of water is also positively related to the degradation of polymers in aqueous environments,[15] which further affected the application prospect of hydrophobically-modified starch in developing marine ecosystem-friendly plastics.

As discussed above, the permanent loss of compact crystalline structure during gelatinization causes starch to lose its insolubility in water after film formation. Previously, starch-based blend film has been doped with a wide variety of nanofillers including natural nanofillers like cellulose nanocrystal[55] and cellulose nanofiber[56], inorganic nanoparticles like silica[57], calcium carbonate[58] and synthetic polymer nanoparticles like poly(methyl methacrylate-co-acrylamide)[59] nanospheres. These studies have seen improved water resistance indicated by decreased water uptake or water solubility, as the resulting films had more compact, high-density parts which could retard water penetration. Besides, mechanical strength can also be improved by the addition of fillers, which could simultaneously reinforce the matrix. However, the improvement on water resistance could be rather limited, as the hydrophilicity of starch between filler particles is not dramatically changed or only limitedly changed; as a result, starch between filler particles can still be solubilized by water. Additionally, as addition of fillers could cause the formation of more than one phases, doped film is more likely to exhibit inferior transparency.[60]

Introduction of intermolecular crosslinks connects polymer chains with chemical bonds, by which a stronger 3d molecular network is generated.[61] In particular, the introduction of crosslinks has been considered an effective means of improving the water resistance of polysaccharide-based materials:[61] By the introduction of crosslinks, the naturally occurring intermolecular interactions (e.g., hydrogen bonds) are strengthened, which contributes to improved water resistance. As discussed above, the intra- and intermolecular interactions are very important to the water resistance of starch, as they hold starch molecules together in water. Thus, it is likely that crosslinks could also improve the water resistance of starch. Indeed, previous research on introducing crosslinks of different chemical bonds to starch-based blend films have seen improvement of water resistance.[62–66] Besides, introduction of chemical crosslinks could likely yield films with better smoothness and transparency, as by nature it is not susceptible to the inhomogeneity caused by the introduction of fillers.

GI.6. Controllable dissolution/disintegration behavior for balancing ease of use and marine ecosystem protection

While starch-based blend films may have low water resistance, this susceptibility to water also rendered them low risk to marine ecosystem. After being discarded and entering the marine environment, starch-based blend films can quickly dissolve/disintegrate, which reduces the chance of being ingested

by or entangled with marine wildlife. However, improving the water resistance might offset this advantage, therefore there is a tradeoff between the rapid disintegration/dissolution and water resistance in daily usage.

In previous studies pertaining to improving the water resistance of starch films, the changes in material water resistance caused by these modifications usually do not change according to the environment that the material in question is in. However, rapid disintegration/dissolution and water resistance are usually not required simultaneously at the same stage of the material life cycle. Thus, the tradeoff between the rapid disintegration/dissolution after being discarded and leaked to the marine ecosystem and water resistance in daily usage might be overcome by different dissolution/disintegration behavior in aqueous environments under different stages of material lifecycle (**Figure 7**).

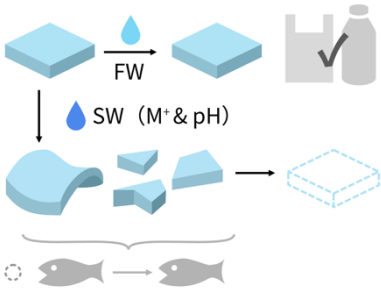

Figure 7 Schematic illustration of controlling disintegration behavior in aqueous environments for balancing ease of use and marine ecosystem protection.

Chemical properties of seawater differ from those of freshwater (e.g., rain or tap water) which plastic products typically encounter in everyday environments. In particular, seawater demonstrates a high ionic strength and slightly basic pH;[67] these different chemical properties can be used as chemical stimuli for cleaving certain types of chemical bonds. As discussed above, intermolecular crosslinks can greatly affect the stability of starch films. Therefore, starch-based films with different dissolution/disintegration behaviors in seawater and freshwater, can possibly be prepared by introducing chemical crosslinks with different susceptibilities to freshwater and seawater, as shown in **Figure 8**. In fresh water, the stability of the material is maintained by the crosslinks and remains stable. In seawater, the material is restored to its initial soluble state triggered by the cleavage of crosslinks; consequently, it rapidly dissolves or disintegrates without the assistance of seawater microorganisms. After the rapid disintegration and dissolution, the dissociated polymer chains can further undergo biodegradation when the biodegradation speed is no longer strongly related to the chance of ingestion and entanglement. By introducing microorganism-independent responsive disintegration/dissolution characteristics, the loss of shape and mechanical strength of the material in the seawater can be decoupled from biodegradation, which should shorten

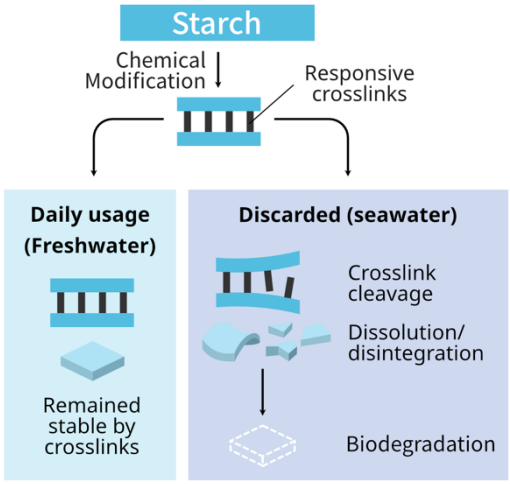

Figure 8 Schematic diagram of controlling disintegration behavior via formation and dissociation of intermolecular crosslinks.

the encounter window and reduce the ecological risk when the material is discarded and exposed to the marine environment.

The concept of controlling the mechanical properties of material in aqueous solution utilizing composition difference of the solution has previously been implemented on hydrogels in solutions which bear some similarities to seawater. For example, ionic bond-crosslinked alginate hydrogel microbeads were able to dissolve in phosphate solution due to the release of Ca^{2+} ions and the consequential dissociation of ionic crosslinks, and was used as vehicle a for the controlled release of drugs.[68] However, this concept has yet to be implemented on dry film materials without solvent, and seawater has not previously been used as a chemical signal or trigger. To prepare a starch film with seawater selective dissolution/disintegration property, crosslink bond candidates with proper selectivity to seawater have to be selected, and the material choice and crosslink introduction strategy would have to be designed from the ground up.

GI.7. In this work

In this thesis, intermolecular crosslinks including covalent and non-covalent crosslinks were utilized to improve the water resistance of starch-based blend films. To better reduce the risk of starch-based blend films on the marine ecosystem, starch films with controllable dissolution/disintegration behavior in freshwater and seawater were also developed by leveraging the stimuli-responsive properties of non-covalent bond crosslinks.

In the first chapter "Hemiacetal/acetal bond crosslinked starch/PVA blend film with improved water resistance", the effectiveness of intermolecular crosslinking on improving water resistance of

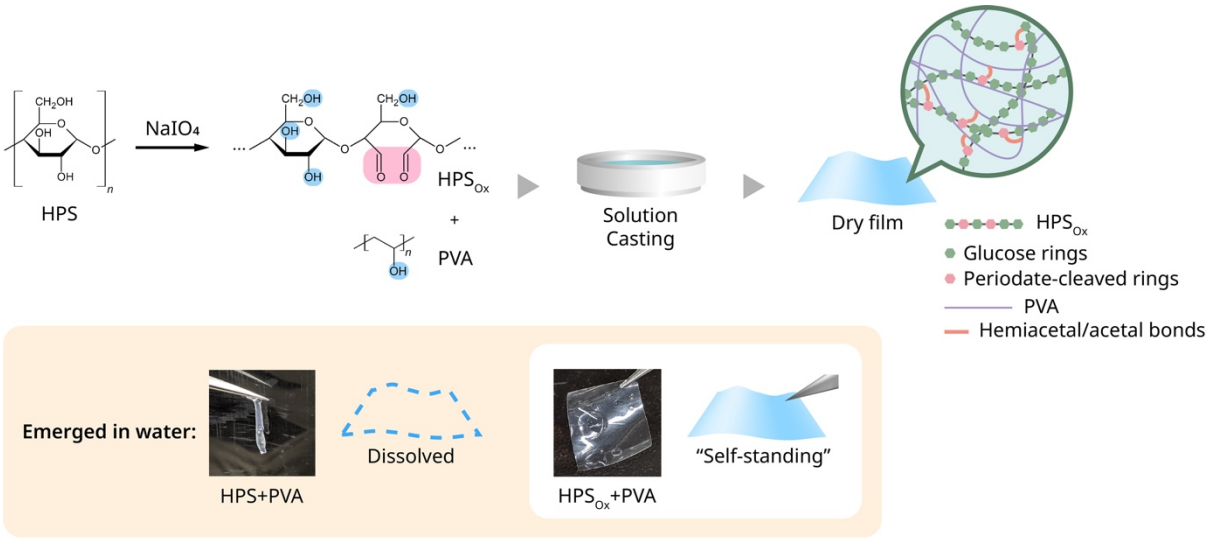

Figure 9 Schematic illustration of preparation process of HPS_{Ox}/PVA films, and the comparison of water stability of non-crosslinked HPS/PVA and hemiacetal/acetal bond crosslinked HPS_{Ox}/PVA films.

starch-based film was tested by the introducing a covalent crosslink, hemiacetal/acetal crosslink (**Figure 9**). Hydroxypropyl starch (HPS) was oxidized by periodate oxidation, and an oxidized HPS (HPS_{Ox})/PVA blend film, crosslinked by hemiacetal/acetal bond crosslinks using HPS_{Ox} as both structural material and crosslink agent. Compared to non-crosslinked HPS/PVA blend film prepared by simple blending, which dissolved immediately in water, the crosslinked film, HPS_{Ox}/PVA films showed drastically improved water resistance and mechanical strength due to the existence of crosslinks.

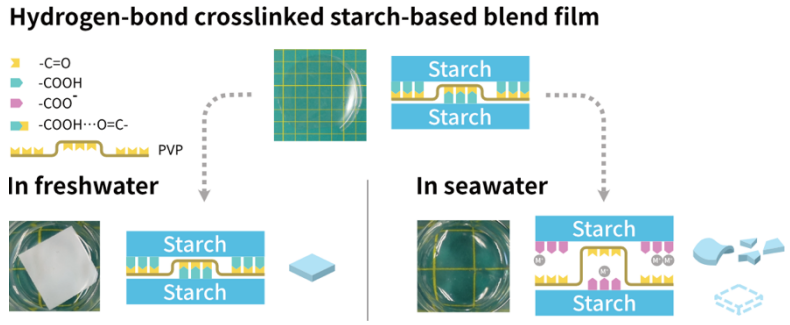

Figure 10 Schematic illustration of structure of TS-g-PAAc/PVP film, and its dissolution/disintegration in seawater and freshwater.

In the second chapter "A starch-based, crosslinked blend film with seawater-specific dissolution characteristics", the concept of controlling the dissolution/disintegration behavior of material in freshwater and seawater was being experimented with introducing a seawater-labile hydrogen bond crosslink to a starch-based blend film (**Figure 10**). A starch-based graft polymer, starch-g-poly(acrylic acid) (TS-g-PAAc) was first prepared by grafting polymerization, then a hydrogen bond-crosslinked TS-g-PAAc/PVP blend film was prepared by blending TS-g-PAAc with poly(vinyl pyrrolidone) (PVP)

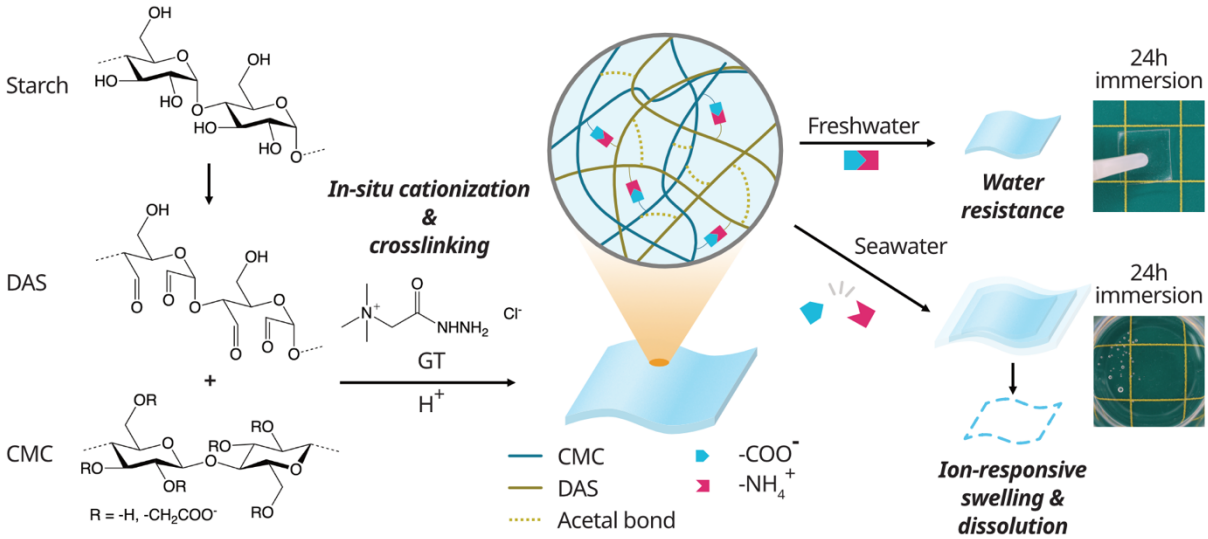

Figure 11 Schematic illustration of the preparation process of DAS/GT/CMC/GT film, and its ion-responsive dissolution/disintegration behavior.

and solution casting. After drying, the grafted starch was crosslinked with PVP by hydrogen bonds. While owing to the hydrogen bond-crosslinks, the film showed improved water resistance over unmodified starch films in DIW, in seawater the film was able to dissolve quickly as a result of disruption of the hydrogen bond crosslinks in the presence of weak acid anions.

In the third chapter "Dual-crosslinked starch/carboxymethyl cellulose blend film with ion-responsive dissolution properties", the concept of controlling the dissolution/disintegration behavior of material in freshwater and seawater was further extended by the developing alternative crosslinking mechanism which complements the seawater-responsive hydrogen bond crosslinks (**Figure 11**). A dialdehyde starch (DAS)/carboxymethyl cellulose (CMC) blend film is prepared via a modified solution casting process, during which DAS is gradually rendered cationic by a cationizing reagent, Girard's reagent T (GT) , and interacted with CMC to form ionic crosslinks. Meanwhile, the aldehyde groups on DAS also form acetal bonds with the -OH groups on both DAS and CMC, which further increases the wet strength. In solutions of low ionic strength encountered in daily life, such as freshwater, the film remains stable for both types of crosslinks. In high ionic strength solutions, such as seawater, the film swells rapidly and disintegrates owing to the cleavage of ionic crosslinks.

References

(1) Geyer, R.; Jambeck, J. R.; Law, K. L. Production, Use, and Fate of All Plastics Ever Made. *Sci. Adv.* **2017**, *3* (7), 25–29. https://doi.org/10.1126/sciadv.1700782.

(2) Jambeck, J. R.; Geyer, R.; Wilcox, C.; Siegler, T. R.; Perryman, M.; Andrady, A.; Narayan, R.; Law, K. L. Plastic Waste Inputs from Land into the Ocean. *Science* **2015**, *347* (6223), 768–771. https://doi.org/10.1126/science.1260352.

(3) Napper, I. E.; Thompson, R. C. Plastic Debris in the Marine Environment: History and Future Challenges. *Glob. Chall.* **2020**, *4* (6), 1900081. https://doi.org/10.1002/gch2.201900081.

(4) Law, K. L. Plastics in the Marine Environment. *Annu. Rev. Mar. Sci.* **2017**, *9* (1), 205–229. https://doi.org/10.1146/annurev-marine-010816-060409.

(5) Adyel, T. M. Accumulation of Plastic Waste during COVID-19. *Science* **2020**, *369* (6509), 1314–1315. https://doi.org/10.1126/science.abd9925.

(6) Vanapalli, K. R.; Sharma, H. B.; Ranjan, V. P.; Samal, B.; Bhattacharya, J.; Dubey, B. K.; Goel, S. Challenges and Strategies for Effective Plastic Waste Management during and Post COVID-19 Pandemic. *Sci. Total Environ.* **2021**, *750*, 141514. https://doi.org/10.1016/j.scitotenv.2020.141514.

(7) Horodytska, O.; Valdés, F. J.; Fullana, A. Plastic Flexible Films Waste Management – A State of Art Review. *Waste Manag.* **2018**, *77*, 413–425. https://doi.org/10.1016/j.wasman.2018.04.023.

(8) Lambert, S.; Wagner, M. Environmental Performance of Bio-Based and Biodegradable Plastics: The Road Ahead. *Chem. Soc. Rev.* **2017**, *46* (22), 6855–6871. https://doi.org/10.1039/C7CS00149E.

(9) Castro-Aguirre, E.; Iñiguez-Franco, F.; Samsudin, H.; Fang, X.; Auras, R. Poly(Lactic Acid)—Mass Production, Processing, Industrial Applications, and End of Life. *Adv. Drug Deliv. Rev.* **2016**, *107*, 333–366. https://doi.org/10.1016/j.addr.2016.03.010.
(10) Labet, M.; Thielemans, W. Synthesis of Polycaprolactone: A Review. *Chem. Soc. Rev.* **2009**, *38* (12), 3484. https://doi.org/10.1039/b820162p.
(11) Raza, Z. A.; Abid, S.; Banat, I. M. Polyhydroxyalkanoates: Characteristics, Production, Recent Developments and Applications. *Int. Biodeterior. Biodegrad.* **2018**, *126*, 45–56. https://doi.org/10.1016/j.ibiod.2017.10.001.
(12) Shen, M.; Song, B.; Zeng, G.; Zhang, Y.; Huang, W.; Wen, X.; Tang, W. Are Biodegradable Plastics a Promising Solution to Solve the Global Plastic Pollution? *Environ. Pollut.* **2020**, *263*, 114469. https://doi.org/10.1016/j.envpol.2020.114469.
(13) Moshood, T. D.; Nawanir, G.; Mahmud, F.; Mohamad, F.; Ahmad, M. H.; Abdul Ghani, A. Expanding Policy for Biodegradable Plastic Products and Market Dynamics of Bio-Based Plastics: Challenges and Opportunities. *Sustainability* **2021**, *13* (11), 6170. https://doi.org/10.3390/su13116170.
(14) Emadian, S. M.; Onay, T. T.; Demirel, B. Biodegradation of Bioplastics in Natural Environments. *Waste Manag.* **2017**, *59*, 526–536. https://doi.org/10.1016/j.wasman.2016.10.006.
(15) Bagheri, A. R.; Laforsch, C.; Greiner, A.; Agarwal, S. Fate of So-Called Biodegradable Polymers in Seawater and Freshwater. *Glob. Chall.* **2017**, *1* (4), 1700048. https://doi.org/10.1002/gch2.201700048.
(16) Dilkes-Hoffman, L. S.; Lant, P. A.; Laycock, B.; Pratt, S. The Rate of Biodegradation of PHA Bioplastics in the Marine Environment: A Meta-Study. *Mar. Pollut. Bull.* **2019**, *142*, 15–24. https://doi.org/10.1016/j.marpolbul.2019.03.020.
(17) Wang, G.-X.; Huang, D.; Ji, J.-H.; Völker, C.; Wurm, F. R. Seawater-Degradable Polymers—Fighting the Marine Plastic Pollution. *Adv. Sci.* **2021**, *8* (1), 2001121. https://doi.org/10.1002/advs.202001121.
(18) Balestri, E.; Menicagli, V.; Vallerini, F.; Lardicci, C. Biodegradable Plastic Bags on the Seafloor: A Future Threat for Seagrass Meadows? *Sci. Total Environ.* **2017**, *605–606*, 755–763. https://doi.org/10.1016/j.scitotenv.2017.06.249.
(19) Zuo, L.-Z.; Li, H.-X.; Lin, L.; Sun, Y.-X.; Diao, Z.-H.; Liu, S.; Zhang, Z.-Y.; Xu, X.-R. Sorption and Desorption of Phenanthrene on Biodegradable Poly(Butylene Adipate Co-Terephtalate) Microplastics. *Chemosphere* **2019**, *215*, 25–32. https://doi.org/10.1016/j.chemosphere.2018.09.173.
(20) Jiang, M.; Hu, L.; Lu, A.; Liang, G.; Lin, Z.; Zhang, T.; Xu, L.; Li, B.; Gong, W. Strong Sorption of Two Fungicides onto Biodegradable Microplastics with Emphasis on the Negligible Role of Environmental Factors. *Environ. Pollut.* **2020**, *267*, 115496. https://doi.org/10.1016/j.envpol.2020.115496.
(21) Weinstein, J. E.; Dekle, J. L.; Leads, R. R.; Hunter, R. A. Degradation of Bio-Based and

Biodegradable Plastics in a Salt Marsh Habitat: Another Potential Source of Microplastics in Coastal Waters. *Mar. Pollut. Bull.* **2020**, *160*, 111518. https://doi.org/10.1016/j.marpolbul.2020.111518.
(22) Green, D. S.; Boots, B.; Sigwart, J.; Jiang, S.; Rocha, C. Effects of Conventional and Biodegradable Microplastics on a Marine Ecosystem Engineer (Arenicola Marina) and Sediment Nutrient Cycling. *Environ. Pollut.* **2016**, *208*, 426–434. https://doi.org/10.1016/j.envpol.2015.10.010.
(23) Anderson, G.; Shenkar, N. Potential Effects of Biodegradable Single-Use Items in the Sea: Polylactic Acid (PLA) and Solitary Ascidians. *Environ. Pollut.* **2021**, *268*, 115364. https://doi.org/10.1016/j.envpol.2020.115364.
(24) Wang, C.; Yu, J.; Lu, Y.; Hua, D.; Wang, X.; Zou, X. Biodegradable Microplastics (BMPs): A New Cause for Concern? *Environ. Sci. Pollut. Res.* **2021**, *28* (47), 66511–66518. https://doi.org/10.1007/s11356-021-16435-4.
(25) Bertoft, E. Understanding Starch Structure: Recent Progress. *Agronomy* **2017**, *7* (3), 56. https://doi.org/10.3390/agronomy7030056.
(26) Robyt, J. F. Starch: Structure, Properties, Chemistry, and Enzymology.
(27) Do Val Siqueira, L.; Arias, C. I. L. F.; Maniglia, B. C.; Tadini, C. C. Starch-Based Biodegradable Plastics: Methods of Production, Challenges and Future Perspectives. *Curr. Opin. Food Sci.* **2021**, *38*, 122–130. https://doi.org/10.1016/j.cofs.2020.10.020.
(28) Vilpoux, O. F.; Santos Silveira Junior, J. F. Chapter 3 - Global Production and Use of Starch. In *Starchy Crops Morphology, Extraction, Properties and Applications*; Pascoli Cereda, M., François Vilpoux, O., Eds.; Academic Press, 2023; pp 43–66. https://doi.org/10.1016/B978-0-323-90058-4.00014-1.
(29) Maraveas, C. Environmental Sustainability of Greenhouse Covering Materials. *Sustainability* **2019**, *11* (21), 6129. https://doi.org/10.3390/su11216129.
(30) Bai, J.; Pei, H.; Zhou, X.; Xie, X. Reactive Compatibilization and Properties of Low-Cost and High-Performance PBAT/Thermoplastic Starch Blends. *Eur. Polym. J.* **2021**, *143*, 110198. https://doi.org/10.1016/j.eurpolymj.2020.110198.
(31) Cheng, T. H.; Ismail, N.; Kamaruding, N.; Saidin, J.; Danish-Daniel, M. Industrial Enzymes-Producing Marine Bacteria from Marine Resources. *Biotechnol. Rep.* **2020**, *27*, e00482. https://doi.org/10.1016/j.btre.2020.e00482.
(32) Soni, R.; Asoh, T.-A.; Hsu, Y.-I.; Uyama, H. Freshwater-Durable and Marine-Degradable Cellulose Nanofiber Reinforced Starch Film. *Cellulose* **2022**, *29* (3), 1667–1678. https://doi.org/10.1007/s10570-021-04410-8.
(33) Żołek-Tryznowska, Z.; Kałuża, A. The Influence of Starch Origin on the Properties of Starch Films: Packaging Performance. *Materials* **2021**, *14* (5), 1146. https://doi.org/10.3390/ma14051146.
(34) Mehyar, G. f.; Han, J. h. Physical and Mechanical Properties of High-Amylose Rice and Pea Starch Films as Affected by Relative Humidity and Plasticizer. *J. Food Sci.* **2004**, *69* (9), E449–E454. https://doi.org/10.1111/j.1365-2621.2004.tb09929.x.

(35) Lim, W. S.; Ock, S. Y.; Park, G. D.; Lee, I. W.; Lee, M. H.; Park, H. J. Heat-Sealing Property of Cassava Starch Film Plasticized with Glycerol and Sorbitol. *Food Packag. Shelf Life* **2020**, *26*, 100556. https://doi.org/10.1016/j.fpsl.2020.100556.
(36) Farahnaky, A.; Saberi, B.; Majzoobi, M. Effect of Glycerol on Physical and Mechanical Properties of Wheat Starch Edible Films. *J. Texture Stud.* **2013**, *44* (3), 176–186. https://doi.org/10.1111/jtxs.12007.
(37) Basiak, E.; Lenart, A.; Debeaufort, F. Effect of Starch Type on the Physico-Chemical Properties of Edible Films. *Int. J. Biol. Macromol.* **2017**, *98* (96), 348–356. https://doi.org/10.1016/j.ijbiomac.2017.01.122.
(38) Abral, H.; Soni Satria, R.; Mahardika, M.; Hafizulhaq, F.; Affi, J.; Asrofi, M.; Handayani, D.; Sapuan, S. M.; Stephane, I.; Sugiarti, E.; Muslimin, A. N. Comparative Study of the Physical and Tensile Properties of Jicama (Pachyrhizus Erosus) Starch Film Prepared Using Three Different Methods. *Starch/Staerke* **2019**, *71* (5–6), 1–9. https://doi.org/10.1002/star.201800224.
(39) Jumaidin, R.; Sapuan, S. M.; Jawaid, M.; Ishak, M. R.; Sahari, J. Characteristics of Thermoplastic Sugar Palm Starch/Agar Blend: Thermal, Tensile, and Physical Properties. *Int. J. Biol. Macromol.* **2016**, *89*, 575–581. https://doi.org/10.1016/j.ijbiomac.2016.05.028.
(40) Mathew, S.; Brahmakumar, M.; Abraham, T. E. Microstructural Imaging and Characterization of the Mechanical, Chemical, Thermal, and Swelling Properties of Starch–Chitosan Blend Films. *Biopolymers* **2006**, *82* (2), 176–187. https://doi.org/10.1002/bip.20480.
(41) Saberi, B.; Thakur, R.; Bhuyan, D. J.; Vuong, Q. V.; Chockchaisawasdee, S.; Golding, J. B.; Scarlett, C. J.; Stathopoulos, C. E. Development of Edible Blend Films with Good Mechanical and Barrier Properties from Pea Starch and Guar Gum. *Starch/Staerke* **2017**, *69* (1–2), 1–15. https://doi.org/10.1002/star.201600227.
(42) Raj, B.; Sankar, U. K.; Siddaramaiah. Low Density Polyethylene/Starch Blend Films for Food Packaging Applications. *Adv. Polym. Technol.* **2004**, *23* (1), 32–45. https://doi.org/10.1002/adv.10068.
(43) Godbole, S.; Gote, S.; Latkar, M.; Chakrabarti, T. Preparation and Characterization of Biodegradable Poly-3-Hydroxybutyrate-Starch Blend Films. *Bioresour. Technol.* **2003**, *86* (1), 33–37. https://doi.org/10.1016/S0960-8524(02)00110-4.
(44) Kim, S. R. B.; Choi, Y.-G.; Kim, J.-Y.; Lim, S.-T. Improvement of Water Solubility and Humidity Stability of Tapioca Starch Film by Incorporating Various Gums. *LWT - Food Sci. Technol.* **2015**, *64* (1), 475–482. https://doi.org/10.1016/j.lwt.2015.05.009.
(45) Chen, J.; Chen, F.; Meng, Y.; Wang, S.; Long, Z. Oxidized Microcrystalline Cellulose Improve Thermoplastic Starch-Based Composite Films: Thermal, Mechanical and Water-Solubility Properties. *Polymer* **2019**, *168*, 228–235. https://doi.org/10.1016/j.polymer.2019.02.026.
(46) Carvalho, A. J. F. Starch: Major Sources, Properties and Applications as Thermoplastic Materials. In *Monomers, Polymers and Composites from Renewable Resources*; Elsevier, 2008; pp

321–342. https://doi.org/10.1016/B978-0-08-045316-3.00015-6.
(47) Jiménez, A.; Fabra, M. J.; Talens, P.; Chiralt, A. Edible and Biodegradable Starch Films: A Review. *Food Bioprocess Technol.* **2012**, *5* (6), 2058–2076. https://doi.org/10.1007/s11947-012-0835-4.
(48) Yu, L.; Christie, G. Microstructure and Mechanical Properties of Orientated Thermoplastic Starches. *J. Mater. Sci.* **2005**, *40* (1), 111–116. https://doi.org/10.1007/s10853-005-5694-1.
(49) Sanivada, U. K.; Mármol, G.; Brito, F. P.; Fangueiro, R. PLA Composites Reinforced with Flax and Jute Fibers—A Review of Recent Trends, Processing Parameters and Mechanical Properties. *Polymers* **2020**, *12* (10), 2373. https://doi.org/10.3390/polym12102373.
(50) Bergel, B. F.; Dias Osorio, S.; da Luz, L. M.; Santana, R. M. C. Effects of Hydrophobized Starches on Thermoplastic Starch Foams Made from Potato Starch. *Carbohydr. Polym.* **2018**, *200*, 106–114. https://doi.org/10.1016/j.carbpol.2018.07.047.
(51) Li, J.; Ye, F.; Liu, J.; Zhao, G. Effects of Octenylsuccination on Physical, Mechanical and Moisture-Proof Properties of Stretchable Sweet Potato Starch Film. *Food Hydrocoll.* **2015**, *46*, 226–232. https://doi.org/10.1016/j.foodhyd.2014.12.017.
(52) Ruhul Amin, Md.; Anannya, F. R.; Mahmud, Md. A.; Raian, S. Esterification of Starch in Search of a Biodegradable Thermoplastic Material. *J. Polym. Res.* **2019**, *27* (1), 3. https://doi.org/10.1007/s10965-019-1983-2.
(53) Rivard, C.; Moens, L.; Roberts, K.; Brigham, J.; Kelley, S. Starch Esters as Biodegradable Plastics: Effects of Ester Group Chain Length and Degree of Substitution on Anaerobic Biodegradation. *Enzyme Microb. Technol.* **1995**, *17* (9), 848–852. https://doi.org/10.1016/0141-0229(94)00120-G.
(54) Colussi, R.; Pinto, V. Z.; El Halal, S. L. M.; Biduski, B.; Prietto, L.; Castilhos, D. D.; Zavareze, E. da R.; Dias, A. R. G. Acetylated Rice Starches Films with Different Levels of Amylose: Mechanical, Water Vapor Barrier, Thermal, and Biodegradability Properties. *Food Chem.* **2017**, *221*, 1614–1620. https://doi.org/10.1016/j.foodchem.2016.10.129.
(55) Noshirvani, N.; Hong, W.; Ghanbarzadeh, B.; Fasihi, H.; Montazami, R. Study of Cellulose Nanocrystal Doped Starch-Polyvinyl Alcohol Bionanocomposite Films. *Int. J. Biol. Macromol.* **2018**, *107*, 2065–2074. https://doi.org/10.1016/j.ijbiomac.2017.10.083.
(56) Frone, A. N.; Nicolae, C. A.; Gabor, R. A.; Panaitescu, D. M. Thermal Properties of Water-Resistant Starch - Polyvinyl Alcohol Films Modified with Cellulose Nanofibers. *Polym. Degrad. Stab.* **2015**, *121*, 385–397. https://doi.org/10.1016/j.polymdegradstab.2015.10.010.
(57) Ismail, H.; Zaaba, N. F. The Mechanical Properties, Water Resistance and Degradation Behaviour of Silica-Filled Sago Starch/PVA Plastic Films. *J. Elastomers Plast.* **2014**, *46* (1), 96–109. https://doi.org/10.1177/0095244312462163.
(58) Kisku, S. K.; Sarkar, N.; Dash, S.; Swain, S. K. Preparation of Starch/PVA/CaCO3 Nanobiocomposite Films: Study of Fire Retardant, Thermal Resistant, Gas Barrier and Biodegradable

Properties. *Polym. - Plast. Technol. Eng.* **2014**, *53* (16), 1664–1670. https://doi.org/10.1080/03602559.2014.919650.
(59) Yoon, S. D.; Park, M. H.; Byun, H. S. Mechanical and Water Barrier Properties of Starch/PVA Composite Films by Adding Nano-Sized Poly(Methyl Methacrylate-Co-Acrylamide) Particles. *Carbohydr. Polym.* **2012**, *87* (1), 676–686. https://doi.org/10.1016/j.carbpol.2011.08.046.
(60) Agarwal, S. Major Factors Affecting the Characteristics of Starch Based Biopolymer Films. *Eur. Polym. J.* **2021**, *160*, 110788. https://doi.org/10.1016/j.eurpolymj.2021.110788.
(61) Garavand, F.; Rouhi, M.; Razavi, S. H.; Cacciotti, I.; Mohammadi, R. Improving the Integrity of Natural Biopolymer Films Used in Food Packaging by Crosslinking Approach: A Review. *Int. J. Biol. Macromol.* **2017**, *104*, 687–707. https://doi.org/10.1016/j.ijbiomac.2017.06.093.
(62) Zhou, J.; Ma, Y.; Ren, L.; Tong, J.; Liu, Z.; Xie, L. Preparation and Characterization of Surface Crosslinked TPS/PVA Blend Films. *Carbohydr. Polym.* **2009**, *76* (4), 632–638. https://doi.org/10.1016/j.carbpol.2008.11.028.
(63) Nugroho, F. G.; Nizardo, N. M.; Saepudin, E. Synthesis of Citric Acid Crosslinked PVA/Tapioca Starch Bioplastic Reinforced with Grafted Cellulose; Depok, Indonesia, 2020; p 040040. https://doi.org/10.1063/5.0010357.
(64) Ramaraj, B. Crosslinked Poly(Vinyl Alcohol) and Starch Composite Films. II. Physicomechanical, Thermal Properties and Swelling Studies. *J. Appl. Polym. Sci.* **2007**, *103* (2), 909–916. https://doi.org/10.1002/app.25237.
(65) Priya, B.; Gupta, V. K.; Pathania, D.; Singha, A. S. Synthesis, Characterization and Antibacterial Activity of Biodegradable Starch/PVA Composite Films Reinforced with Cellulosic Fibre. *Carbohydr. Polym.* **2014**, *109*, 171–179. https://doi.org/10.1016/j.carbpol.2014.03.044.
(66) Chen, L.; Imam, S. H.; Gordon, S. H.; Greene, R. V. Starch-Polyvinyl Alcohol Crosslinked Film-Performance and Biodegradation. *J. Environ. Polym. Degrad.* **1997**, *5* (2), 111–117. https://doi.org/10.1007/BF02763594.
(67) Ishizu, M.; Miyazawa, Y.; Tsunoda, T.; Ono, T. Long-Term Trends in PH in Japanese Coastal Seawater. *Biogeosciences* **2019**, *16* (24), 4747–4763. https://doi.org/10.5194/bg-16-4747-2019.
(68) Voo, W.-P.; Ooi, C.-W.; Islam, A.; Tey, B.-T.; Chan, E.-S. Calcium Alginate Hydrogel Beads with High Stiffness and Extended Dissolution Behaviour. *Eur. Polym. J.* **2016**, *75*, 343–353. https://doi.org/10.1016/j.eurpolymj.2015.12.029.

Chapter 1. Hemiacetal/acetal bond crosslinked starch/PVA blend film with improved water resistance

1.1. Introduction

As described in general introduction, blending with other polymers has been established as an effective approach for improving the physical aspects of starch films. Among all polymers that can be blended with starch, poly(vinyl alcohol) (PVA), a water soluble polymer with a large amount of hydroxyl group whose structure is shown in **Figure 1-1**, has been considered to be a good candidate for blending with starch, due to its good mechanical strength and film-forming ability.[1] PVA can potentially be biodegraded by a broad panel of microorganisms, including bacteria[2–4] and fungi[5–7], which makes PVA more beneficial than other synthetic polymers. Additionally, the abundant -OH groups on PVA polymer chain open it for a large variety of chemical reactions.

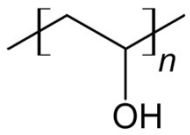

Figure 1-1 Molecular structure of PVA.

However, similar to other starch-based films, starch/PVA blend films are plagued by high humidity sensitivity[8,9] and disintegration in water[8], which greatly limited their practical usage. To improve the low water resistance of starch/PVA blends, doping with fillers and introducing crosslinks are two popular strategies. Doping starch/PVA blend film with hard particles or fillers generally yields films with improved water resistance,[10–14] as the doped films have more compact, high-density parts which could retard water penetration. However, as described before, the improvement is rather limited, and doped films are more likely to exhibit inferior smoothness and transparency as a result of introduction of multiple phases. Meanwhile, introducing crosslinks is an effective means of improving the water resistance of polysaccharide-based materials, and previous research on introducing crosslinks to starch/PVA films with different chemical bonds have seen improvement of water resistance.[8,15–18] Besides, introduction of chemical crosslinks could likely yield films with better smoothness and transparency, as by nature no secondary phases would be introduced to the film during this process. Nonetheless, there is still much room for improvement regarding the effects of crosslinks on water resistance. Even crosslinked starch/PVA films involved in aforementioned studies showed improved water resistance compared to non-crosslinked counterparts, nevertheless they still showed partial dissolution and relatively high swelling ratio in water.

Hemiacetal/acetal bond could be an ideal bond crosslink bond candidate for starch and PVA due to a number of reasons. Both starch and PVA contains a large amount of -OH groups, which can be used for the formation of hemiacetal/acetal bond crosslinks. The formation of hemiacetal/acetal bond also does not require harsh conditions. Additionally, with -OH groups being consumed during the crosslink introduction process, the hydrophilicity of the constituting polymers can also be decreased. However,

the introduction of hemiacetal/acetal crosslinks usually requires the use of small molecule aldehydes such as formaldehyde [19,20] and glutaraldehyde [21,22], which are known to be toxic and hazardous for the environment, making them potentially unsuitable for large-scale commercial production or biomedical-related applications. Additionally, due to the volatileness of these aldehyde reagents, aldehyde concentration is reduced in the drying process, and the evaporated crosslinking agent poses difficulty for operation and environmental risk.

The glycol cleavage of polysaccharides is an efficient, highly selective reaction that involves the cleavage between vicinal hydroxyl groups at the C-2 and C-3 positions of the anhydroglucose unit and the formation of two aldehyde groups in the presence of periodic acid or periodates, such as $NaIO_4$. It is a well-known method for the production of polysaccharide aldehyde derivatives,[23] and it has been widely accepted as compatible or nontoxic.[24–26] Besides, as the aldehyde groups introduced by oxidation is directly connected to the starch molecular chains, only one reaction is needed for the formation of each crosslinking, hence the reaction efficiency is also improved. In this section, aldehyde groups will be directly introduced to starch chains by $NaIO_4$ oxidation, and inter-/intra-species crosslinking occurs directly at the absence of external crosslinking agents.

This chapter focuses on improving the water resistance of starch/PVA blend film by introducing hemiacetal/acetal crosslinks using starch as both structural material and crosslinking agent (**Figure 1-2**). Oxidized hydroxypropyl starch (HPS_{Ox}) was prepared by iodate oxidation of hydroxypropyl starch (HPS), and then an HPS_{Ox}/PVA blend film was prepared by solution casting method. During the drying process, hemiacetal/acetal bonds formed between aldehyde groups on HPS_{Ox} and hydroxyl groups on both HPS_{Ox} and PVA under acidic conditions. The effects of the introduction of hemiacetal/acetal crosslinks were evaluated by observing swelling and dissolution/disintegration behavior in water and testing the mechanical properties of the films.

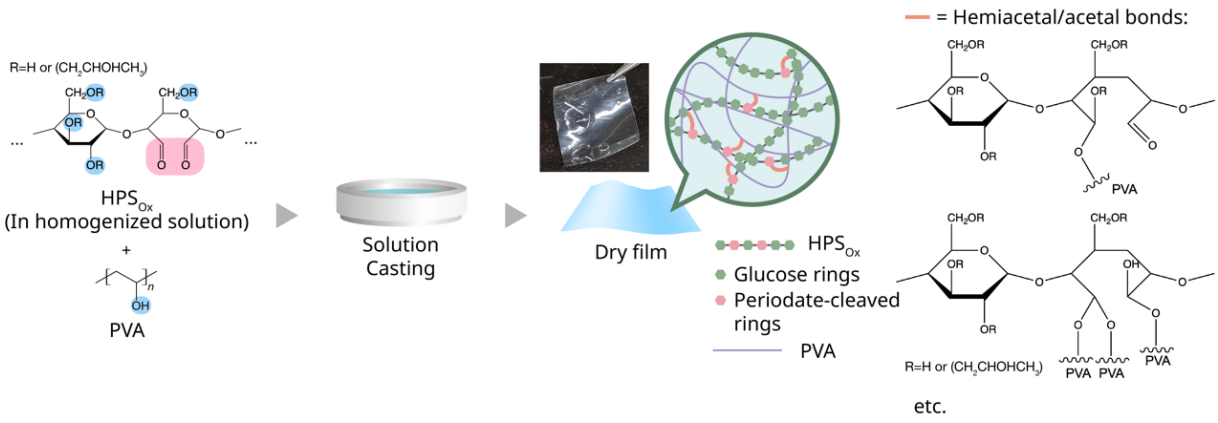

Figure 1-2 Schematic illustration of preparation process of crosslinked HPS_{Ox}/PVA film, and the proposed crosslinking mechanism.

1.2. Experimental

1.2.1. Materials

Hydroxypropyl tapioca starch (HPS) — molar substitution (MS): 0.1 — was provided by Nihon Shokuhin Kako Co., Ltd. (Japan). HPS was used as an alternative to unmodified counterparts that have a tendency to form aggregates during dialysis after oxidation. These aggregates might pose challenges in the following high-pressure homogenization. PVA (DP ≈ 2000, degree of hydrolysis ≈ 98.5%) was from Nacalai Tesque (Kyoto, Japan). Sodium periodate (JIS Special Grade), 25% glutaraldehyde solution (Wako First Grade), citric acid (Japanese food additive, ≧99.5%) and 1M hydrochloric acid were from Fujifilm Wako (Osaka, Japan). Glycerol (≧97.0%) was from Nacalai Tesque.

1.2.2. Preparation of oxidized hydroxypropyl starch (HPS_{Ox}) solution

An HPS paste (4 wt%) was prepared by mixing HPS and deionized water, followed by heating at 90°C in a water bath with stirring for approximately 30 min. A certain amount (0.05 g/ml starch paste) of sodium periodate was then added to the HPS paste and it was allowed to react for 1 h with stirring, away from light exposure. Oxidized HPS (HPS_{Ox}) paste was then transferred to dialysis tubing (Spectra/Por 6 standard regenerated cellulose dialysis tubing, prewetted, MwCO: 10 kD, Spectrum Chemical Mfg. Corp., USA) and dialyzed for three consecutive days. After the dialysis process, the volume of the HPS_{Ox} paste recovered from the dialysis process was adjusted to1.33 (in the case of preparing 3% wt solution) or 1.5 times (in the case of preparing 3% wt solution 2.67% wt solution) the volume before dialysis by diluting the paste with deionized water. It was then passed twice through a high-pressure homogenizer (Starburst Mini HJP-25001, Sugino Machine Ltd., Uozu, Toyama, Japan) at 200 MPa to obtain a homogeneous solution. To evaluate the extent of oxidation of HPS_{Ox}, homogenized HPS_{Ox} solution was titrated by simple iodometry using a slightly modified process of Hyon *et al*.[27] In brief, 5 ml of homogenized HPS_{Ox} solution was mixed with 10 ml 0.05 mol/L I2 solution and 10 ml 1 mol/L NaOH solution, then the mixture was allowed to react at room temperature for 15 min with stirring. Then, 7.5 ml of 6.25 v/v % H_2SO_4 was added to the mixture. Finally, the mixture is titrated with 0.1 mol/L $Na_2S_2O_3$ solution with diluted starch solution as indicator. The aldehyde concentration of HPS_{Ox} measured by this method was 3.57 mmol/g.

1.2.3. Preparation of sample films

PVA film. PVA aqueous solution was prepared by heating at 90°C in a water bath with stirring for approximately 30 min. Then, a certain amount of PVA solution was casted and dried overnight at 50°C in an oven.

HPS film. The HPS paste (3 wt%) was prepared by mixing HPS and deionized water, followed by heating at 90°C in a water bath with stirring for approximately 30 min. Glycerol of 25% HPS weight was added to the solution as a plasticizer to reduce the brittleness of the film. Then, a certain amount of

solution was casted and dried overnight at 50°C in an oven.

HPS/PVA blend film. HPS paste (4 wt%) was prepared by mixing HPS and deionized water, followed by heating at 90°C in a water bath with stirring for approximately 30 min. 2 wt% PVA solution was prepared by mixing PVA and deionized water, followed by heating at 90°C in a water bath with stirring for approximately 30 min. The HPS solution was then mixed with the PVA solution at a 1:1 volume ratio, yielding a mixed solution in which the concentrations of starch and PVA were 2% and 1%, respectively. Glycerol of 25% HPS weight was added to the solution as a plasticizer to reduce the brittleness of the film. Then, a certain amount of solution was casted and dried overnight at 50°C in an oven.

Glutaraldehyde crosslinked starch/PVA (HPS/PVA/GA) film. HPS paste (4 wt%) was prepared by mixing HPS and deionized water, followed by heating at 90°C in a water bath with stirring for approximately 30 min. The obtained HPS paste was then cooled to room temperature under ambient conditions. The cooled HPS paste was passed through a high-pressure homogenizer (Starburst Mini HJP-25001, Sugino Machine Ltd., Uozu, Toyama, Japan) at 100 MPa. A 2 wt% PVA solution was prepared by mixing PVA and deionized water, followed by heating at 90°C in a water bath with stirring for approximately 30 min. The obtained PVA solution was then cooled to room temperature under ambient conditions. The homogenized HPS solution was then mixed with PVA solution at a 1:1 volume ratio, yielding a mixed solution in which the concentrations for starch and PVA were 2% and 1%, respectively. A casting solution was obtained by adding a certain amount of glutaraldehyde solution (1% polymer weight of pure glutaraldehyde) and 1% v/v 1M HCl solution to the mixed solution. Finally, a certain amount of casting solution was casted and then dried overnight at 50°C in an oven.

Crosslinked oxidized hydroxypropyl starch/PVA (HPS$_{Ox}$/PVA) film. Homogenized HPS$_{Ox}$ paste (2.67% wt) was prepared as mentioned above, and PVA solution (4 wt%) was prepared and cooled to room temperature under ambient conditions. Homogenized HPS$_{Ox}$ solution was then mixed with PVA solution at a certain volume ratio. For casting solution of films with polymer weight ratio in dry film (HPS$_{Ox}$:PVA) = 1:1, 2:1 and 3:1, the mixing ratio was 3:1, 3:2 and 9:2, respectively. A casting solution was obtained by adding 1% v/v 1M HCl solution to the mixed solution. Finally, a certain amount of casting solution was casted and then dried overnight at 45°C in an oven.

1.2.4. Characterization

Short-term swelling profile. Sample films were cut into square pieces of approximately 1.5 × 1.5 cm. After the initial weight of the samples was measured, the sample pieces were immersed in deionized water at room temperature. At 10 and 30 min, the sample pieces were removed from the liquid environment, carefully wiped with Kimwipe™ wipes to remove any residual liquid on the surface, weighed, and then returned to the liquid. From 30 min on, the sample pieces were weighed every 30 min, until sample disintegration (during immersion or wiping) was observed or the immersion time had reached 2 h, depending on whichever comes first. At least three sample pieces were tested for each film

type. The swelling ratio (SR) at any given time t was defined as (wet weight at t − initial dry weight)/initial dry weight × 100%.

Water contact angle. The water contact angle (WCA) was measured with a DropMaster DM300 contact angle meter (Kyowa Interface Science Co., Ltd.) using the sessile drop method. A deionized water droplet (~1 μl) was applied to the sample surface with a manual precision syringe; then, the image of the water droplet was immediately captured by the charge-coupled-device camera of the system. The WCA was determined by the workstation connected to the system that corrected the baseline and fit the curve to a theoretical meridian curve. The contact angles of both sides of the droplet were measured and averaged.

Mechanical properties. The ultimate tensile strength (σ_{max}), Young's modulus (E), and elongation at maximum stress (%ε) of dry and wet HPS_{Ox}/PVA film was tested with a Shimadzu EZ Graph universal tester (Shimadzu Scientific Instruments, Columbia, Maryland, USA). A 100-N load cell and crosshead speed of 1 mm/min were used. The dry-film properties were measured immediately after drying had finished. For measurement of the wet HPS_{Ox}/PVA film properties, the samples were immersed in deionized water 1 h prior to testing and were carefully wiped with Kimwipe wipes to remove any residual liquid on the surface when loaded to the holder.

SEM imaging. SEM imaging of samples was performed on a Hitachi SU3500 scanning electron microscope (Hitachi High-Technologies Corp., Tokyo, Japan). Samples were sputtered with tin prior to imaging.

FT-IR analysis of HPS and HPS_{Ox}. Fourier-transform infrared (FT-IR) spectra of HPS and HPS_{Ox} were measured with a Nicolet iS5 FTIR spectrometer (Thermo Fisher Scientific, Waltham, Massachusetts, USA). HPS was tested as received. An HPS_{Ox} dry powder was obtained from freeze drying homogenized HPS_{Ox} solution.

Transmittance of HPS_{Ox}/PVA film. The transmittance of HPS_{Ox}/PVA film was measured over the whole visible spectrum with a Hitachi U-2810 UV-vis spectrophotometer. Samples were cut into sample strips of 5 mm, 20–30 μm thick, and then placed into a quartz cuvette with the sample perpendicular to the light path.

1.3. Results and discussion

1.3.1. Fabrication of glutaraldehyde crosslinked HPS/PVA blend film

First, crosslinked HPS/PVA films with glutaraldehyde as an external crosslinker was prepared, to assess the effects of acetal/hemiacetal crosslinking in HPS/PVA blend, and to verify that the reaction condition is proper for acetal/hemiacetal crosslinking. The effect of crosslinking was assessed by observation of water stability of the films. The water stability of HPS/PVA/GA film was assessed by immersing films in deionized water and measuring the swelling profile. Unlike HPS/PVA film prepared by simple blending of two polymers, which disintegrates and dissolves quickly upon contact with water,

HPS/PVA/GA film was able to maintain its shape without disintegration, as shown in **Figure 1-3**. Thus, it can be deduced that acetal/hemiacetal crosslinking has been generated during the drying process, and the given conditions is indeed effective for the formation of acetal/hemiacetal bonds. Though, HPS/PVA/GA film soon become very swollen upon contact with water, reaching ~160% SR when swelling equilibrium was reached (**Figure 1-3**). Additionally, Wet HPS/PVA/GA film generally have low wet strength, which is shown by the disintegration at minimal mechanical force, as well the fact that wet film does not have enough strength to support its own weight and drapes when removed from liquid environment, suggesting relatively low density of crosslinking in the films.

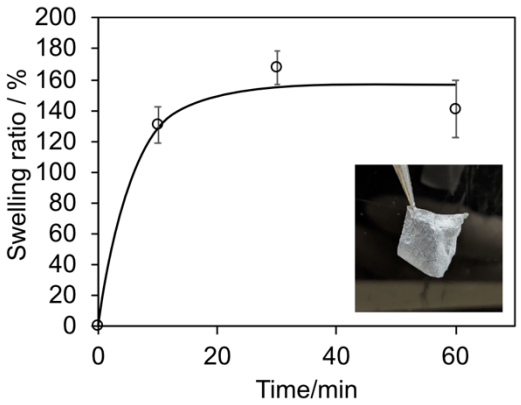

Figure 1-3 Swelling curve of HPS/PVA/GA film. Inset: mage of HPS/PVA/GA film after being immersed in water.

1.3.2. Preparation of uniform HPS_{Ox} solution

To fabricate uniform and transparent cast film, a uniform HPS_{Ox} solution is required. After HPS was oxidized by sodium periodate to synthesize HPS_{Ox}, loose aggregates were observed during purification by dialysis. This can be attributed to the partial crosslinking between HPS_{Ox} molecules, in which some aldehyde groups reacted with hydroxyl groups to form acetal/hemiacetal bonds, and/or a change in dispersibility in water were caused by functional group conversion. As these aggregates hinder uniform film production, after dialysis, aqueous counter collision (ACC) treatment was performed on the aggregated HPS_{Ox} paste to produce a uniform dispersion (**Figure 1-4 a).**)

The FT-IR spectrum of HPS_{Ox} was measured to determine the effect of the oxidation process (**Figure 1-4 b).**). Curves were normalized, with the highest peak at 1030 cm^{-1}, which is the C–O stretching peak within the glucose ring [28]. The peak at 1734 cm^{-1} is attributed to the characteristic absorption peak of carbonyl groups [29], which indicated the existence of free aldehyde groups in

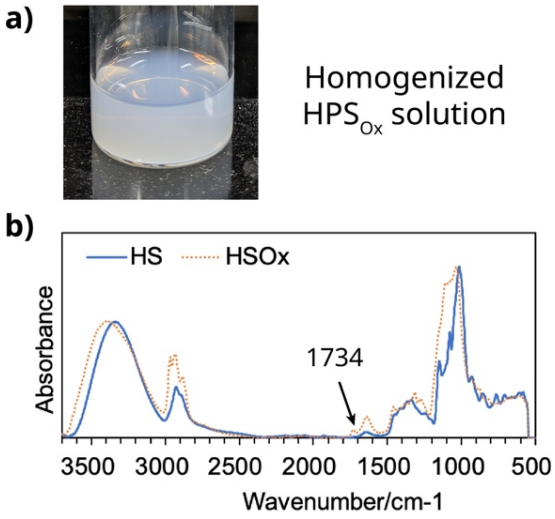

Figure 1-4 a). Homogenized HPS_{Ox} solution used for film casting; **b).** FT-IR spectra of HPS and HPS_{Ox}: the powder HPS_{Ox} sample was obtained from lyophilization of homogenized HPS_{Ox} solution.

$HPS_{Ox,}$ even after ACC treatment and the dialysis purification process. The peak around 1105 cm^{-1} can be attributed to C–O–C stretching of acetal linkage.[30] Although the underlying mechanism is yet to be fully understood, the increased peak intensity around 1105 cm^{-1} might imply that, in sole HPS_{Ox} prior to mixing and oven drying, there exists some degree of crosslinking, which might have developed during the dialysis process.

1.3.3. Appearance of HPS_{Ox}/PVA film

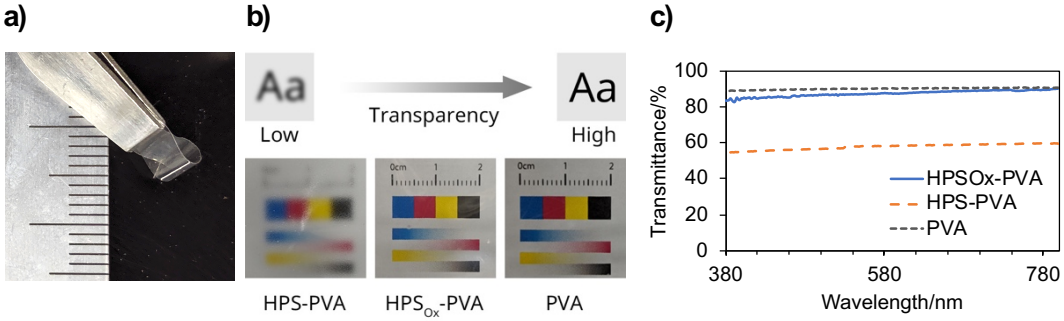

Figure 1-5 a). Flexed HPS_{Ox}/PVA film (HPS_{Ox}:PVA = 2:1) strip; **b).** HPS/PVA film (HPS:PVA = 2:1), HPS_{Ox}/PVA film (HPS_{Ox}:PVA = 2:1), and neat PVA film placed above printed background (samples were placed on a thin transparent glass sheet, and the glass sheet was elevated ~1 cm from the printed background); **c).** transmittance of HPS/PVA film (HPS:PVA = 2:1), HPS_{Ox}/PVA film (HPS_{Ox}:PVA = 2:1), and neat PVA film in visible range (380–800 nm).

Crosslinked HPS_{Ox}/PVA blend film (HPS_{Ox}:PVA = 2:1) was prepared by the process shown in **Figure 1-5**, utilizing the homogenized HPS_{Ox} solution prepared as previously mentioned. The appearance of the HPS_{Ox}/PVA film (HPS_{Ox}:PVA = 2:1) is shown in **Figure 1-5 a).** The HPS_{Ox}/PVA film was flexible and had a smooth, glossy surface (**Figure 1-5 a).**) The transparency of the HPS_{Ox}/PVA film is shown in **Figure 1-5 b).** Although printed text under the HPS/PVA film with the same HPS/PVA ratio can hardly be read because of its extremely rough surface, printed text and images under the HPS_{Ox}/PVA film can be read easily, indicating good transparency. The transmittance of HPS_{Ox}/PVA film in the visible range is shown in **Figure 1-5 c).** In the entire visible range, the HPS_{Ox}/PVA film has a high and consistent transmittance, varying between approximately 80% and 90%. Considering the smooth surface, the loss of light intensity during the transferring process is more likely to have resulted from scattering caused by material microstructure instead of scattering on a rough surface. The relatively high transmittance of HPS_{Ox}/PVA film, however, might be an indication of a homogeneous, relatively defect-free microscopic structure.

1.3.4. SEM analysis of HPS_{Ox}/PVA film

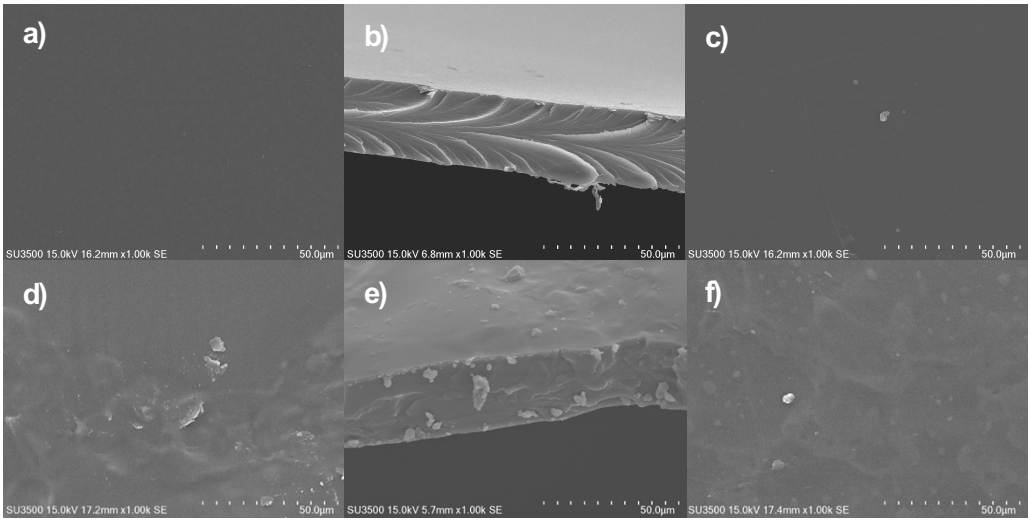

Figure 1-6 SEM images of **a).** top surface (blend–air surface), **b).** cross section, **c).** bottom surface (blend–substrate surface) of HPS_{Ox}/PVA film (HPS_{Ox}:PVA = 2:1); **d).** top surface, **e).** cross section, **f).**. bottom surface, of HPS/PVA film (HPS:PVA = 2:1), at 1000X magnification.

The SEM images of HPS/PVA and HPS_{Ox}/PVA film are shown in **Figure 1-6**. Compared with that of a simple-blend HPS/PVA film, the surface of the HPS_{Ox}/PVA film is much smoother, and this corresponds to the smooth, glossy surface observed in the optical images. No significant difference in surface smoothness was observed for top and bottom surfaces. This coincides with the conclusions drawn from the transmittance measurements, in which very few imperfections, such as cracks and aggregation, were observed in the cross section of HPS_{Ox}/PVA film, indicating a homogeneous, compact structure.

1.3.5. Water contact angle of HPS_{Ox}/PVA film

The WCA of HPS_{Ox}/PVA film was also tested (**Figure 1-7**). Interestingly, the WCA of HPS_{Ox}/PVA film was 72.2° ± 3.5°. Though the WCA of starch/PVA simple blend prepared in this study cannot be measured because it tends to swell and dissolve immediately upon contact with water, the WCA of HPS_{Ox}/PVA film is somewhat higher than the value reported in other research involving starch/PVA simple blends,[13,31,32] possibly indicating a slightly elevated surface hydrophobicity over simple blends of starch and PVA. No significant water uptake, film dissolution, and film deformation were

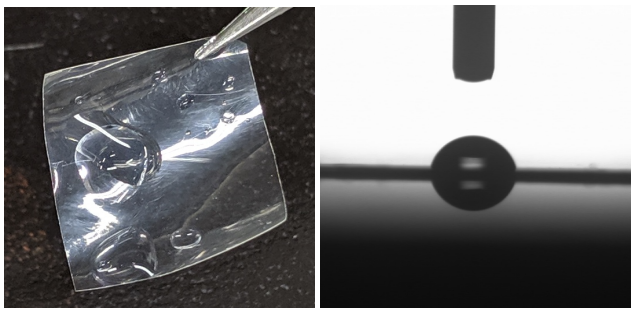

Figure 1-7 a). Image of water droplet left on immersed HPS_{Ox}/PVA film (HPS_{Ox}:PVA = 2:1) surface, when film was removed from water; **b).** mage of contact angle measurement of HPS_{Ox}/PVA film (HPS_{Ox}:PVA = 2:1).

observed during the testing process, implying improved water resistance.

A change in contact angle can be induced by the chemical properties of the constituent material and by the surface morphology. In some cases, starch/PVA blend film can have an abnormally high contact angle because of the high surface roughness.[32] However, considering the smooth surface morphology observed in the optical and SEM images, it seemed that the elevated contact angle values should not be attributed to higher surface roughness. Instead, the increased contact angle, or surface hydrophobicity was caused by the change in chemical properties—aldehyde groups introduced by periodate oxidation and hydrophobic ether bonds formed in the crosslinking process both have possibly decreased the hydrophilicity of the constituent material.

1.3.6. Water stability of HPS_{Ox}/PVA film

The water stability of the HPS_{Ox}/PVA film was investigated by immersing films in DIW. Glutaraldehyde crosslinked HPS/PVA blend film (HPS/PVA/GA) film was also prepared and used as a

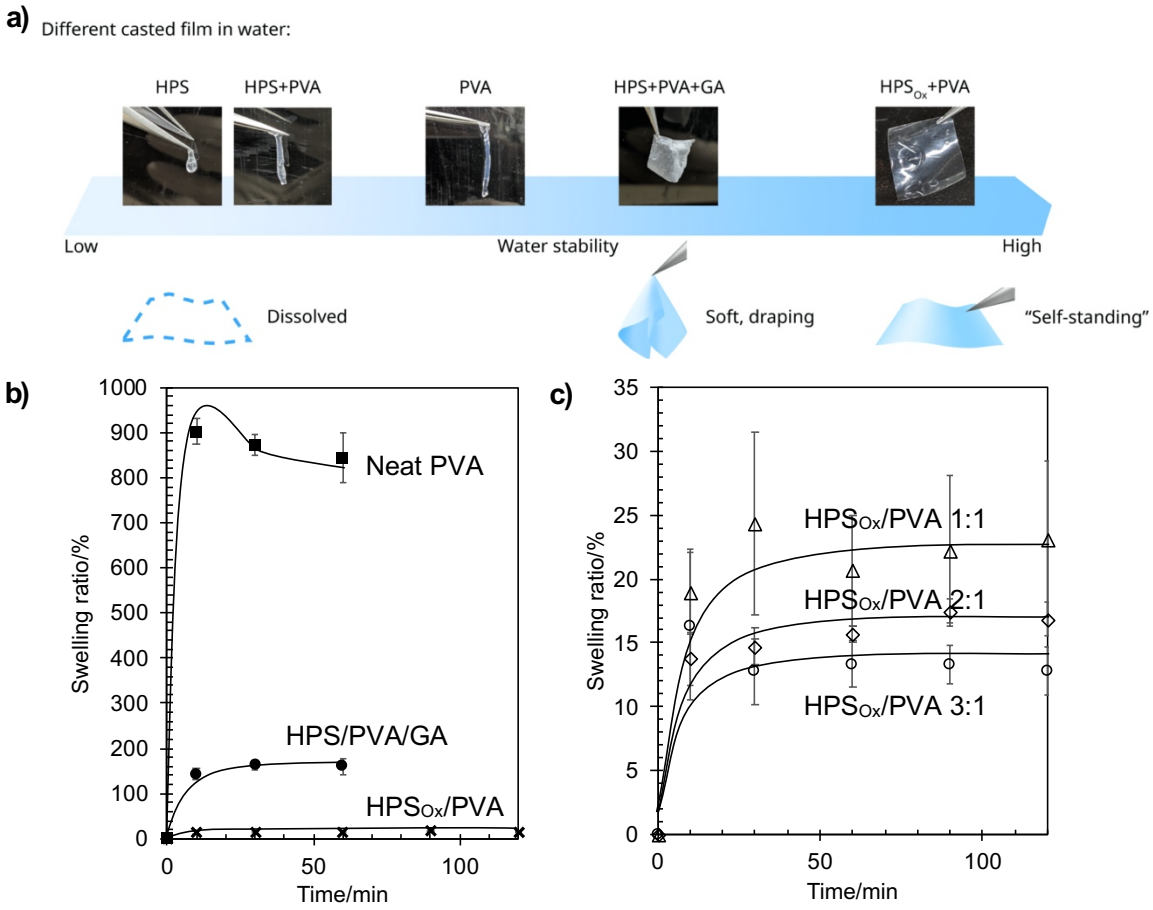

Figure 1-8 a). Images of films with different compositions after being immersed in water. **b).** swelling profile of neat PVA, HPS/PVA film crosslinked with glutaraldehyde (HPS/PVA/GA), and HPS_{Ox}/PVA film (HPS_{Ox}:PVA = 2:1), and **c).** swelling profile of HPS_{Ox}/PVA film with different HPS_{Ox}/PVA weight ratios: 1:1, 2:1, and 3:1.

benchmark for water resistance. While the HPS and HPS/PVA films immediately dissolved in water, HPS_{Ox}/PVA film maintained its shape as it did not disintegrate; HPS_{Ox}/PVA film even had sufficient strength to support its weight and remained "self-standing" (**Figure 1-8 a).**). Considering the free aldehyde groups in HPS_{Ox}, as demonstrated by the FTIR spectrum, this increased water resistance can be attributed to the acetal/hemiacetal crosslinking generated during the film-forming process. Thus, the HPS_{Ox}/PVA film had improved water stability. As shown in **Figure 1-8 b).**, the HPS_{Ox}/PVA film was also less swollen compared to the HPS/PVA/GA film when the swelling equilibrium was attained. This can be explained by the high crosslinking density consequent to the high aldehyde group concentration in HPS_{Ox}. In addition, the slightly elevated surface hydrophobicity might have also contributed to the observed higher water stability.

HPS_{Ox}/PVA films with different HPS_{Ox}/PVA weight ratios were also prepared, and their swelling behavior were compared to estimate how HPS_{Ox} affected the water uptake behavior of HPS_{Ox}/PVA films. The swelling curves of HPS_{Ox}/PVA films with different HPS_{Ox}/PVA weight ratios were shown in **Figure 1-8 c)**. As expected, the equilibrium swelling ratio decreased as the HPS_{Ox} proportion increased from 50% (HPS_{Ox}:PVA 1:1) to 67% (HPS_{Ox}:PVA 2:1), which is due to the increase in amount of aldehyde groups and consequently the crosslink density.

1.3.7. Mechanical performance of HPS_{Ox}/PVA film

The mechanical properties of both dry and wet HPS_{Ox}/PVA films were evaluated by tensile tests. The tensile parameters (Young's modulus (E), ultimate tensile strength (σ_{max}), elongation at maximum stress (%ε)) with different HPS_{Ox}:PVA weight ratios were shown in **Figure 1-9**. In the dry state, HPS_{Ox}/PVA films showed relatively high strength and stiffness, which was contributed by the introduction of crosslinks. After 1 h of immersion in DIW, the strength and stiffness decreased, and %ε increased, as expected. A possible explanation for why the HPS_{Ox}/PVA films became more ductile upon water uptake might be that water is an effective plasticizer for starch and PVA[33]. Nonetheless, a considerable part of strength and stiffness was retained, even after 1 h of immersion. This can be

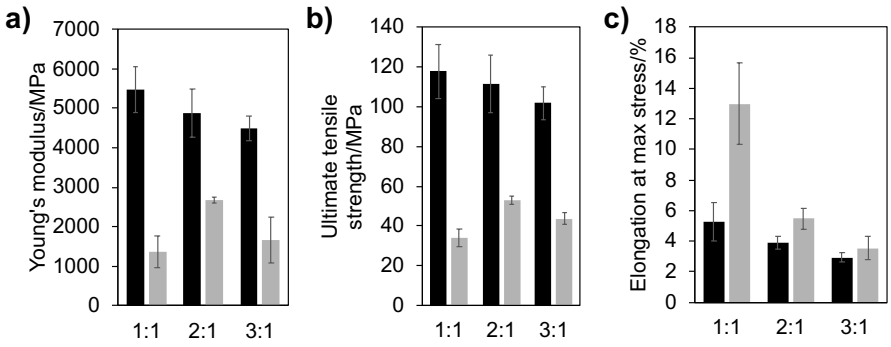

Figure 1-9 a). Young's modulus, **b).** ultimate tensile strength, **c).** elongation at maximum stress of HPS_{Ox}/PVA film with different HPS_{Ox}/PVA weight ratios (black bars: dry film; gray bars: wet film).

attributed to the low water uptake resulted from the high crosslink density and the compact structure formed during the crosslinking process. As the HPS_{Ox} proportion increased from 50% to 67%, both wet σ_{max} and E increased, in agreement with the swelling profile, which is attributed to the increased crosslink density. Unexpectedly, E, σ_{max}, %ε of the dry film decreased slightly as the HPS_{Ox} proportion increased from 50% to 75%. Given that 100% HPS_{Ox} can hardly be prepared and handled because of the significant shrinking in the drying/crosslinking process and the brittleness of the product, the slight decrease is possibly a consequence of early failure, as evident from decreasing %ε, caused by increased brittleness and increased defects derived from excessive shrinking in the crosslinking process. The slight decrease of wet film E and σ_{max} as the HPS_{Ox} proportion increased from 67% to 75% might also be attributed to the increased defects discussed above.

1.3.8. Influence of $NaIO_4$ dosage

HPS_{Ox} with different extent of oxidation was prepared by oxidation by different dosage of $NaIO_4$: 0.05 g/ml (1X), 0.025 g/ml (0.5X) and 0.0125 g/ml (0.25X), and influence of $NaIO_4$ dosage was analyzed by preparation of HPS_{Ox}/PVA films (W(HPS_{Ox}):W(PVA) in dry films: 2:1) with HPS_{Ox} oxidized by different dosage of $NaIO_4$.

As shown in **Figure 1-10**, the appearance of films with differently oxidized HPS_{Ox} varied vastly. While films with highest dosage, most oxidized HPS_{Ox} is smooth and transparent, films with less oxidized HPS_{Ox} has a rough surface and low transparency, and very rough, crater-like surface morphology can be seen in films with the least oxidized HPS_{Ox}. As the crater-like surface morphology can also be seen in (high pressure homogenized, non-oxidized HPS)/PVA films, it is highly possible that the increasing roughness is due to the increasing phase separation, which can be attributed to the decrease in crosslinking density consequential to the decrease in oxidation degree.

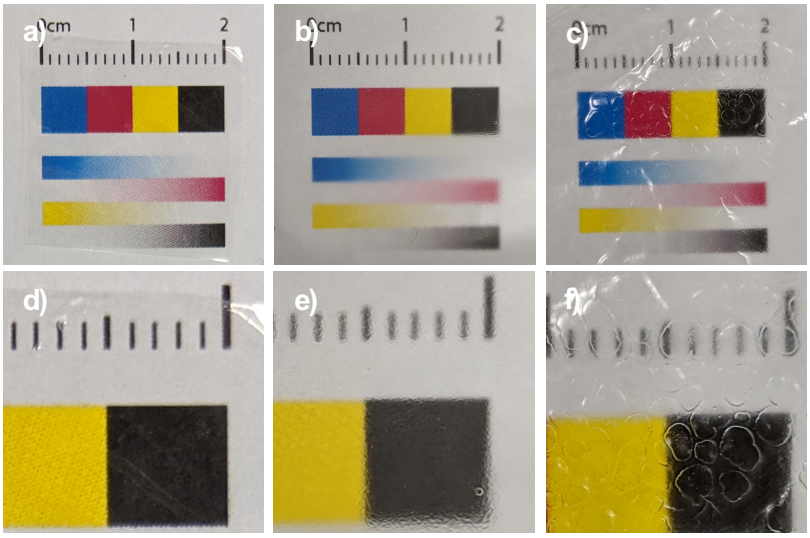

Figure 1-10 Image of dry HPS_{Ox}/PVA films (W(HPS_{Ox}):W(PVA) = 2:1 with HPS_{Ox} oxidized by different dosage of $NaIO_4$. **a).**, **d).** 1X; **b).**, **e).** 0.5X; **c).**, **f).** 0.25X

The water resistance of HPS_{Ox}/PVA films with differently oxidized HPS_{Ox} was also tested. Films with the least oxidized HPS_{Ox} swelled rapidly upon water immersion and became too weak for a complete swelling curve can be measured, reaching a swelling ratio of ~197% at 10 minutes of immersion. Though film with less oxidized HPS_{Ox} remained integrity, it became much more swollen than the counterpart with most oxidized HPS_{Ox} and was barely strong enough to maintain self-standing. Thus, the water resistance of HPS_{Ox}/PVA films is closely related to the extent of oxidation of HPS_{Ox}, which directly affects the aldehyde group concentration, and crosslinking density.

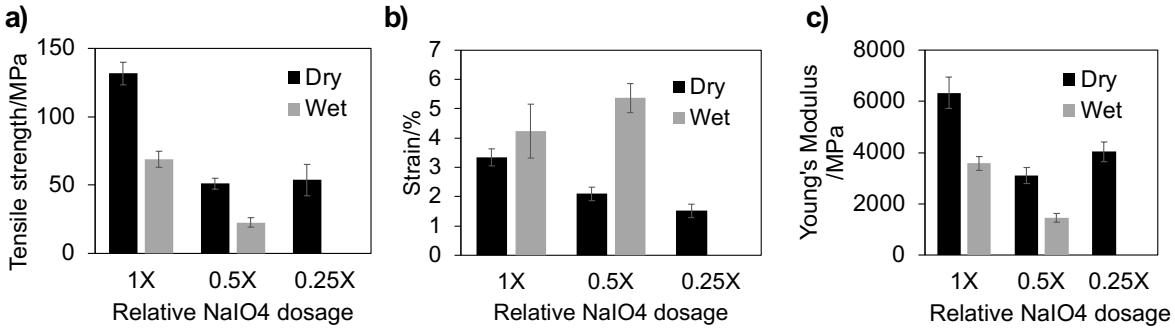

Figure 1-11 Mechanical properties of dry and wet HPS_{Ox}/PVA films with HPS_{Ox} oxidized by different dosage of $NaIO_4$. (black bars: dry film; gray bars: wet film).

The mechanical properties of HPS_{Ox}/PVA films with differently oxidized HPS_{Ox} were evaluated by tensile tests. The results are shown in **Figure 1-11**. Wet strength of HPS_{Ox}/PVA films with the least oxidized HPS_{Ox} was not tested, as its very low wet strength has presented great difficulty for tensile testing. In consistency with results of water resistance test, as the extent of oxidation decreases, both wet and dry strength and modulus of HPS_{Ox}/PVA films also decreases, which is due to the lowered crosslinking density.

In conclusion, physical properties including transparency, water resistance and mechanical properties of HPS_{Ox}/PVA films is greatly affected by the extent of oxidation of HPS_{Ox}, which affects the aldehyde concentration of HPS_{Ox} and the crosslinking density of the film. Also, to obtain transparent, water resistant film, a higher extent of oxidation of HPS_{Ox} is required, as the crosslinking density has to be higher than a certain threshold to eliminate any phase separation of two polymers.

1.4. Conclusions

Glutaraldehyde-crosslinked starch/PVA blend film with improved water resistance was successfully prepared under proper conditions, indicating that acetal/hemiacetal crosslinking is an effective strategy for improving the water resistance and strength of starch/PVA films. Based on this finding, a starch-derived polyaldehyde HPS_{Ox} was prepared, and a crosslinked, mainly starch film,

HPS_{Ox}/PVA film, was successfully prepared under the similar conditions. In the HPS_{Ox}/PVA film, HPS_{Ox} doubled as a building material and crosslinking agent, while PVA acted as a film-forming agent. HPS_{Ox}/PVA film showed improved water resistance and mechanical properties, indicating effective acetal/hemiacetal crosslinking. In addition, the HPS_{Ox}/PVA film had a relatively high surface smoothness and transparency, which resulted from the homogenous, compact structure of the film. Further inspection revealed that the improvement in the strength of the wet film was chiefly due to the addition of HPS_{Ox} and the consequential crosslinking reaction. Sufficient extent of oxidation degree and crosslinking density is essential for the formation of homogenous, strong film, while the crosslinking reaction was not highly sensitive to acid catalyst type if proper pH was reached. Thus, acetal/hemiacetal crosslinking of the starch/PVA films with oxidized starch as a crosslinker was demonstrated to be a simple-to-operate, yet effective strategy for improving the performance of starch/PVA films in packaging applications.

References

(1) Akhavan, A.; Khoylou, F.; Ataeivarjovi, E. Preparation and Characterization of Gamma Irradiated Starch/PVA/ZnO Nanocomposite Films. *Radiat. Phys. Chem.* **2017**, *138* (February), 49–53. https://doi.org/10.1016/j.radphyschem.2017.02.057.

(2) Kim, B. C.; Sohn, C. K.; Lim, S. K.; Lee, J. W.; Park, W. Degradation of Polyvinyl Alcohol by Sphingomonas Sp. SA3 and Its Symbiote. *J. Ind. Microbiol. Biotechnol.* **2003**, *30* (1), 70–74. https://doi.org/10.1007/s10295-002-0010-4.

(3) Yamatsu, A.; Matsumi, R.; Atomi, H.; Imanaka, T. Isolation and Characterization of a Novel Poly(Vinyl Alcohol)-Degrading Bacterium, Sphingopyxis Sp. PVA3. *Appl. Microbiol. Biotechnol.* **2006**, *72* (4), 804–811. https://doi.org/10.1007/s00253-006-0351-4.

(4) Mori, T.; Sakimoto, M.; Kagi, T.; Sakai, T. Isolation and Characterization of a Strain of Bacillus Megaterium That Degrades Poly(Vinyl Alcohol). *Biosci. Biotechnol. Biochem.* **1996**, *60* (2), 330–332. https://doi.org/10.1271/bbb.60.330.

(5) Jecu, L.; Gheorghe, A.; Rosu, A.; Raut, I.; Grosu, E.; Ghiurea, M. Ability of Fungal Strains to Degrade PVA Based Materials. *J. Polym. Environ.* **2010**, *18* (3), 284–290. https://doi.org/10.1007/s10924-010-0173-4.

(6) Tsujiyama, S. ichi; Nitta, T.; Maoka, T. Biodegradation of Polyvinyl Alcohol by Flammulina Velutipes in an Unsubmerged Culture. *J. Biosci. Bioeng.* **2011**, *112* (1), 58–62. https://doi.org/10.1016/j.jbiosc.2011.03.004.

(7) Qian, D.; Du, G.; Chen, J. Isolation and Culture Characterization of a New Polyvinyl Alcohol-Degrading Strain: Penicillium Sp. WSH02-21. *World J. Microbiol. Biotechnol.* **2004**, *20* (6), 587–591. https://doi.org/10.1023/B:WIBI.0000043172.83610.08.

(8) Chen, L.; Imam, S. H.; Gordon, S. H.; Greene, R. V. Starch-Polyvinyl Alcohol Crosslinked Film-Performance and Biodegradation. *J. Environ. Polym. Degrad.* **1997**, *5* (2), 111–117. https://doi.org/10.1007/BF02763594.
(9) Tian, H.; Yan, J.; Rajulu, A. V.; Xiang, A.; Luo, X. Fabrication and Properties of Polyvinyl Alcohol/Starch Blend Films: Effect of Composition and Humidity. *Int. J. Biol. Macromol.* **2017**, *96*, 518–523. https://doi.org/10.1016/j.ijbiomac.2016.12.067.
(10) Ismail, H.; Zaaba, N. F. The Mechanical Properties, Water Resistance and Degradation Behaviour of Silica-Filled Sago Starch/PVA Plastic Films. *J. Elastomers Plast.* **2014**, *46* (1), 96–109. https://doi.org/10.1177/0095244312462163.
(11) Yoon, S. D.; Park, M. H.; Byun, H. S. Mechanical and Water Barrier Properties of Starch/PVA Composite Films by Adding Nano-Sized Poly(Methyl Methacrylate-Co-Acrylamide) Particles. *Carbohydr. Polym.* **2012**, *87* (1), 676–686. https://doi.org/10.1016/j.carbpol.2011.08.046.
(12) Kisku, S. K.; Sarkar, N.; Dash, S.; Swain, S. K. Preparation of Starch/PVA/CaCO3 Nanobiocomposite Films: Study of Fire Retardant, Thermal Resistant, Gas Barrier and Biodegradable Properties. *Polym. - Plast. Technol. Eng.* **2014**, *53* (16), 1664–1670. https://doi.org/10.1080/03602559.2014.919650.
(13) Noshirvani, N.; Hong, W.; Ghanbarzadeh, B.; Fasihi, H.; Montazami, R. Study of Cellulose Nanocrystal Doped Starch-Polyvinyl Alcohol Bionanocomposite Films. *Int. J. Biol. Macromol.* **2018**, *107*, 2065–2074. https://doi.org/10.1016/j.ijbiomac.2017.10.083.
(14) Frone, A. N.; Nicolae, C. A.; Gabor, R. A.; Panaitescu, D. M. Thermal Properties of Water-Resistant Starch - Polyvinyl Alcohol Films Modified with Cellulose Nanofibers. *Polym. Degrad. Stab.* **2015**, *121*, 385–397. https://doi.org/10.1016/j.polymdegradstab.2015.10.010.
(15) Zhou, J.; Ma, Y.; Ren, L.; Tong, J.; Liu, Z.; Xie, L. Preparation and Characterization of Surface Crosslinked TPS/PVA Blend Films. *Carbohydr. Polym.* **2009**, *76* (4), 632–638. https://doi.org/10.1016/j.carbpol.2008.11.028.
(16) Nugroho, F. G.; Nizardo, N. M.; Saepudin, E. Synthesis of Citric Acid Crosslinked PVA/Tapioca Starch Bioplastic Reinforced with Grafted Cellulose; Depok, Indonesia, 2020; p 040040. https://doi.org/10.1063/5.0010357.
(17) Ramaraj, B. Crosslinked Poly(Vinyl Alcohol) and Starch Composite Films. II. Physicomechanical, Thermal Properties and Swelling Studies. *J. Appl. Polym. Sci.* **2007**, *103* (2), 909–916. https://doi.org/10.1002/app.25237.
(18) Priya, B.; Gupta, V. K.; Pathania, D.; Singha, A. S. Synthesis, Characterization and Antibacterial Activity of Biodegradable Starch/PVA Composite Films Reinforced with Cellulosic Fibre. *Carbohydr. Polym.* **2014**, *109*, 171–179. https://doi.org/10.1016/j.carbpol.2014.03.044.
(19) Duong, A.; Steinmaus, C.; McHale, C. M.; Vaughan, C. P.; Zhang, L. Reproductive and Developmental Toxicity of Formaldehyde: A Systematic Review. *Mutat. Res. - Rev. Mutat. Res.* **2011**, *728* (3), 118–138. https://doi.org/10.1016/j.mrrev.2011.07.003.

(20) Kim, K. H.; Jahan, S. A.; Lee, J. T. Exposure to Formaldehyde and Its Potential Human Health Hazards. *J. Environ. Sci. Health - Part C Environ. Carcinog. Ecotoxicol. Rev.* **2011**, *29* (4), 277–299. https://doi.org/10.1080/10590501.2011.629972.
(21) Zeiger, E.; Gollapudi, B.; Spencer, P. Genetic Toxicity and Carcinogenicity Studies of Glutaraldehyde - A Review. *Mutat. Res. - Rev. Mutat. Res.* **2005**, *589* (2), 136–151. https://doi.org/10.1016/j.mrrev.2005.01.001.
(22) Leung, H. W. Ecotoxicology of Glutaraldehyde: Review of Environmental Fate and Effects Studies. *Ecotoxicol. Environ. Saf.* **2001**, *49* (1), 26–39. https://doi.org/10.1006/eesa.2000.2031.
(23) Tomasik, P. Chemical Modifications of Polysaccharides. *Chem. Funct. Prop. Food Sacch.* **2003**, *2013*, 123–130.
(24) Šedová, P.; Buffa, R.; Kettou, S.; Huerta-Angeles, G.; Hermannová, M.; Leierová, V.; Šmejkalová, D.; Moravcová, M.; Velebný, V. Preparation of Hyaluronan Polyaldehyde - A Precursor of Biopolymer Conjugates. *Carbohydr. Res.* **2013**, *371*, 8–15. https://doi.org/10.1016/j.carres.2013.01.025.
(25) Zhang, X.; Yang, Y.; Yao, J.; Shao, Z.; Chen, X. Strong Collagen Hydrogels by Oxidized Dextran Modification. *ACS Sustain. Chem. Eng.* **2014**, *2* (5), 1318–1324. https://doi.org/10.1021/sc500154t.
(26) Kamoun, E. A. N-Succinyl Chitosan-Dialdehyde Starch Hybrid Hydrogels for Biomedical Applications. *J. Adv. Res.* **2016**, *7* (1), 69–77. https://doi.org/10.1016/j.jare.2015.02.002.
(27) Hyon, S. H.; Nakajima, N.; Sugai, H.; Matsumura, K. Low Cytotoxic Tissue Adhesive Based on Oxidized Dextran and Epsilon-Poly- l -Lysine. *J. Biomed. Mater. Res. - Part A* **2014**, *102* (8), 2511–2520. https://doi.org/10.1002/jbm.a.34923.
(28) Willfahrt, A.; Steiner, E.; Hötzel, J.; Crispin, X. Printable Acid-Modified Corn Starch as Non-Toxic, Disposable Hydrogel-Polymer Electrolyte in Supercapacitors. *Appl. Phys. Mater. Sci. Process.* **2019**, *125* (7), 1–10. https://doi.org/10.1007/s00339-019-2767-6.
(29) Sun, B.; Hou, Q.; Liu, Z.; Ni, Y. Sodium Periodate Oxidation of Cellulose Nanocrystal and Its Application as a Paper Wet Strength Additive. *Cellulose* **2015**, *22* (2), 1135–1146. https://doi.org/10.1007/s10570-015-0575-5.
(30) Figueiredo, K. C. S.; Alves, T. L. M.; Borges, C. P. Poly(Vinyl Alcohol) Films Crosslinked by Glutaraldehyde under Mild Conditions. *J. Appl. Polym. Sci.* **2009**, *111* (6), 3074–3080. https://doi.org/10.1002/app.29263.
(31) Shi, R.; Zhu, A.; Chen, D.; Jiang, X.; Xu, X.; Zhang, L.; Tian, W. In Vitro Degradation of Starch/PVA Films and Biocompatibility Evaluation. *J. Appl. Polym. Sci.* **2009**, *115* (1), 346–357. https://doi.org/10.1002/app.31136.
(32) Jayasekara, R.; Harding, I.; Bowater, I.; Christie, G. B. Y.; Lonergan, G. T. Preparation, Surface Modification and Characterisation of Solution Cast Starch PVA Blended Films. *Polym. Test.* **2004**, *23* (1), 17–27. https://doi.org/10.1016/S0142-9418(03)00049-7.

(33) Zhang, X.; Jiang, X.; Jiang, T.; Gan, L.; Zhang, X.; Dai, H. The Plasticizing Mechanism and Effect of Calcium Chloride on Starch/Poly(Vinyl Alcohol) Films. *Carbohydr. Polym.* **2012**, *90* (4), 1677–1684. https://doi.org/10.1016/j.carbpol.2012.07.050.

Chapter 2. A Starch-Based, Crosslinked Blend Film with Seawater-Specific Dissolution Characteristics

2.1. Introduction

As previously mentioned, while starch-based blend films have low water resistance, this susceptibility to water also allows them to quickly dissolve/disintegrate after being leaked to the marine environment. In previous studies pertaining to improving the water resistance of starch films, the changes in material water resistance caused by these modifications usually do not change according to the environment that the material in question is in, therefore there is a tradeoff between the rapid dissolution/disintegration and water resistance in daily usage. This tradeoff might be overcome by different dissolution/disintegration behavior under different environments, as rapid dissolution/disintegration and water resistance are usually not required simultaneously at the same stage of the material life cycle.

As seen in the last chapter, the dissolution/disintegration behavior of starch-based material can be greatly affected by introduction of crosslinks, thus it may also be controlled by formation and disruption of crosslinks. Compared to freshwater, which is more typically encountered in daily life, seawater demonstrates high ionic strength and slightly basic pH.[1] The chemical characteristics of seawater can be used as chemical signals for triggering the disruption of chemically responsive crosslinks, such as ionic crosslinks and hydrogen bond crosslinks. Previously, the concept of mechanical property control via ion/pH-responsive crosslinks under similar conditions have already implemented on hydrogels; for example, it has been reported that the mechanical properties of an alginate/PSS hydrogel can be manipulated via the formation and removal of ionic bond crosslinks.[2] Thus, it might be possible to achieve seawater-specific dissolution/disintegration behavior of starch-based film via the introduction of responsive crosslinks. However, this concept has not yet been implemented on films, and few or no research involved using seawater as a trigger.

This chapter focuses on introducing microorganism-independent seawater-responsive dissolution/disintegration characteristics to starch films by introducing seawater-responsive crosslinks, as a demonstration of the concept of balancing the tradeoff between eco-safety and ease of use with different dissolution/disintegration behavior under different environments. Previously it has been reported that strong, water-stable hydrogen bonds can form between the carboxylic acid groups of poly(acrylic acid) (PAAc) and carbonyl groups of poly(vinyl pyrrolidone) (PVP), two non-toxic, biodegradable[3,4] water soluble polymers. Also, it is possible that this type of hydrogen bond can be disrupted in seawater, as it can be cleaved under conditions similar to that of seawater. It has been reported that a PAAc/PVP layer-by-layer film can dissolve in NaCl solution, due to the pKa decrease

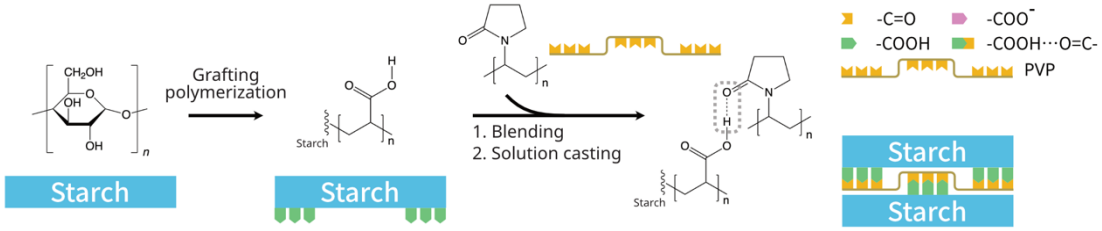

Figure 2-1 Schematic illustration of preparation process of TS-g-PAAc/PVP blend film.

of PAAc and consequential deprotonation of -COOH at high ionic strengh.[5] Also, this type of hydrogen bond can also be disrupted at elevated pH, due to the deprotonation of the -COOH groups on PAAc.[6] Additionally, PAAc chain segments can be introduced to starch with multiple methods,[7–9] thus this type of hydrogen bond can possibly be introduced to starch films. In this chapter, a starch-based blend film, TS-g-PAAc/PVP film, with different dissolution/disintegration behavior in freshwater and seawater was prepared by introducing aforementioned type of hydrogen bonds as seawater-responsive crosslinks (**Figure 2-1**). Its seawater-responsive dissolution/disintegration behavior was observed, and the seawater-responding mechanism was also elucidated.

2.2. Experimental

2.2.1. Materials

Unmodified tapioca starch (TS) was obtained from Nihon Shokuhin Kako Co., Ltd. (Japan). Ammonium persulfate (APS; ACS reagent grade, ≥98.0%) and polyvinylpyrrolidone (PVP) K30 (Mw ~40 kDa) were purchased from Sigma-Aldrich (USA). Acetone (≥99.8%), acrylic acid monomer (≥ 98.5%), 0.1 mol/L acetate buffer solution (pH 5.0), and 0.1 mol/L phosphate buffer solution (pH 6, 7, and 7.6) were obtained from Nacalai Tesque (Kyoto, Japan). Dimethyl sulfoxide (DMSO) was purchased from Fujifilm Wako (Osaka, Japan). Artificial seawater (SW) was obtained as a mixed salt from Fujifilm Wako (Japan), and an artificial seawater solution was prepared by dissolving the salt in a prescribed volume of deionized water (DIW). The detailed composition of the mixed salt is listed in **Table 2-1**. All materials were used as received.

2.2.2. Preparation of starch-g-polyacrylic acid copolymer (TS-g-PAAc)

Tapioca starch-g-poly(acrylic acid) (TS-g-PAAc) was prepared via free-radical polymerization. Starch (5 g) was dispersed in 90 mL of water and the mixture was purged with N_2 for 15 min to avoid air being trapped in gelatinized solution, followed by heating to 80 ℃ for approximately 30 min. After the mixture had properly gelatinized, it was cooled to 55 ℃. Subsequently, a predetermined amount of APS was dissolved in 5 mL of water and added to the mixture. After the APS solution was mixed

Table 2-1 Components of artificial seawater.

Components	mg/L	Components	mg/L
$MgCl_2 \cdot 6H_2O$	9474	LiCl	1
$CaCl_2 \cdot 2H_2O$	1326	KI	0.07
Na_2SO_4	3505	$CoCl_2 \cdot 6H_2O$	0.0002
KCl	597	$AlCl_3 \cdot 6H_2O$	0.008
$NaHCO_3$	171	$FeCl_3 \cdot 6H_2O$	0.005
KBr	85	$Na_2WO_4 \cdot 2H_2O$	0.0002
$Na_2B_4O_7 \cdot 2H_2O$	34	$(NH_4)_6Mo_7O_{24} \cdot 4H_2O$	0.02
$SrCl_2$	12	$MnCl_2$	0.0008
NaF	3	NaCl	20747

thoroughly with the starch paste, a predetermined amount of acrylic acid monomer was slowly added to the mixture. The mixture was then allowed to react for 3 h with the reaction vessel sealed. The product was precipitated in 1 L of acetone and collected by centrifugation. The collected precipitate was then washed 5 times with acetone by centrifugation. Finally, the washed precipitate was dried in an oven at 50 ℃.

2.2.3. Determination of grafting ratio (GR%) of TS-g-PAAc

The GR% of TS-g-PAAc was determined by conductometric titration with a conductometer (LAQUA F-74, Horiba, Japan). TS-g-PAAc (0.2 g) was added to 250 mL of DIW. Subsequently, the mixture was stirred at 50 ℃ until the solid was completely dissolved. To restore all the –COOH groups to the protonated state, 200 μL of 1 M HCl was added to the solution. The solution was then titrated against 0.05 mol/L NaOH solution (Fujifilm Wako, Japan).

The GR% of starch is defined as:

$$GR = \frac{(\text{Weight of PAAc in TS} - \text{g} - \text{PAAc})}{(\text{Weight of TS in TS} - \text{g} - \text{PAAc})} \times 100\%$$

$$= \frac{V_{NaOH} \times c_{NaOH} \times M_{AAc}}{m_{TS-g-PAAc} - V_{NaOH} \times c_{NaOH} \times M_{AAc}}$$

where V_{NaOH}: Volume of NaOH solution consumed during the titration; c_{NaOH}: concentration of NaOH used in the titration; M_{AAc}: molar mass of the AAc monomer; $m_{TS\text{-}g\text{-}PAAc}$: weight of TS-g-PAAc used in the titration.

2.2.4. Film preparation

TS-g-PAAc/PVP blend film. A 3% w/v DMSO solution of TS-g-PAAc (synthesized with 0.5 g of APS and 10 mL of AAc) and PVP was prepared by dissolving TS-g-PAAc or PVP directly in DMSO. The PVP and the TS-g-PAAc solutions were then mixed at volume ratios of 2:1, 4:1, or 4:1. Finally, 15 mL of the mixed solution was cast in a Petri dish and dried in a well-ventilated drying oven at 45 ℃ for 2 d.

Starch film. Tapioca starch (0.6 g) was dissolved in 20 mL of DIW; the slurry was then incubated at 90 ℃. After the mixture was properly gelatinized, glycerol equivalent to 10% of the weight of starch was added to the solution. The solution was then allowed to cool to room temperature and was cast in a fluoropolymer Petri dish. Finally, the film was dried in a well-ventilated drying oven at 50 ℃ for 1 d.

Humidity conditioning of films. After drying, the water content of the film was adjusted using humidity conditioning. The films were placed in a desiccator with a bottle of saturated K_2CO_3 solution, which would maintain the humidity in the desiccator at a relative humidity (RH) of approximately 43% at room temperature. [10] The films were retained in the desiccator for at least 1 d and stored thereafter. Samples that were subjected to Fourier transform infrared (FTIR) tests were not humidity-conditioned and were stored in a desiccator at ~30% RH.

2.2.5. Characterization

A Nicolet iS5 FTIR spectrometer with an attenuated total reflectance attachment (Thermo Fisher Scientific, Waltham, MA, USA) was used to measure the FTIR spectra of the TS-g-PAAc and TS-g-PAAc/PVP films. A Hitachi SU3500 scanning electron microscope (SEM; Hitachi High-Technologies Corp., Tokyo, Japan) was used to study the morphologies of the samples. The ultimate tensile strength (σ_{max}), Young's modulus (E), and elongation at maximum stress (%ε) of the dry TS-g-PAAc/PVP films were measured using a Shimadzu EZ Graph universal tester (Shimadzu Scientific Instruments, Columbia, MD, USA) with a 100 N load cell and a crosshead speed of 10 mm/min. The humidity-conditioned samples were subsequently tested at approximately 45% RH. The dissolution behavior of the TS-g-PAAc film was studied by immersing pieces of the samples in different solutions. The samples were cut into square pieces of 1 cm × 1 cm and placed into the wells of 12-well plates, each containing 3 mL of a given solution. The change in the sample pieces over time was captured with a digital camera at predetermined time points after the sample came into contact with the solution.

2.3. Results and discussion

2.3.1. Influence of reaction parameters on TS-g-PAAc synthesis

TS-g-PAAc was synthesized by free-radical polymerization with different amounts of APS initiator and AAc monomer to understand the effect of these parameters on the GR% and to determine

the optimal conditions for the TS-g-PAAc synthesis. Different APS dosages (0.1, 0.5, and 0.9 g) were combined with AAc dosages of 5 and 10 mL each, yielding six combinations in total. The FTIR spectra of all six combinations were compared with those of the unmodified starch. As shown in **Figure 2-2**, in the spectra of TS-g-PAAc synthesized with all six APS/AAc combinations, a stretching peak of –C=O is observed at 1708 cm^{-1}, which indicates that the PAAc chain segments are successfully grafted to the starch. The carboxylate content of TS-g-PAAc was measured by conductometric titration, and the GR% was calculated accordingly. The GR of TS-g-PAAc synthesized with different amounts of APS/AAc combination monomer is shown in **Figure 2-3**. The GR% increases with the increase in the APS and AAc dosages. The GR% only slightly increases at higher initiator dosages; however, it significantly increases with the increase in the monomer dosage. Thus, the contribution of the monomer dosage to the GR% is more significant than that of the initiator dosage, which agrees with some previously reported observations. [7,8]

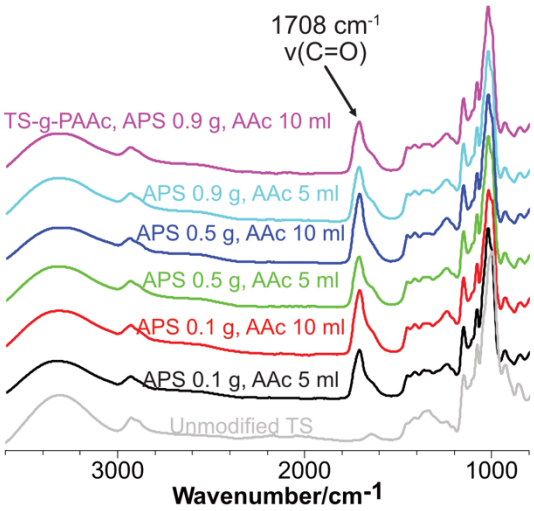

Figure 2-2 FTIR spectra of unmodified TS and TS-g-PAAc prepared with different initiator and monomer dosage.

When 0.9 g of APS was used for the synthesis of TS-g-PAAc, the reaction mixture after free-radical polymerization was visually less viscous than its counterparts with lower APS dosages. As APS evidently destroys other polysaccharides with D-anhydroglucose units,[11–13] the additional APS possibly results in excess oxidation and partial degradation of the starch chains. Thus, TS-g-PAAc samples synthesized with 0.5 g of APS and 10 mL of AAc were used for preparing TS-g-PAAc/PVP films, which have the highest GR% second only to TS-g-PAAc synthesized with 0.9 g of APS and 10 mL of AAc. A high GR could be helpful for achieving a higher density of hydrogen bond crosslinks or crosslink density, and consequently, a high film strength.

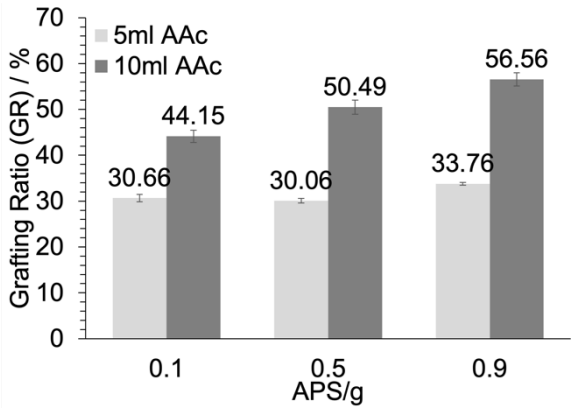

Figure 2-3 Grafting ratio (GR%) of TS-g-PAAc synthesized with different APS and AAc monomer dosage.

2.3.2. Observation of the film forming process

Both TS-g-PAAc and PVP are hydrophilic and individually soluble in water. However, a homogenous casting solution is not obtained using

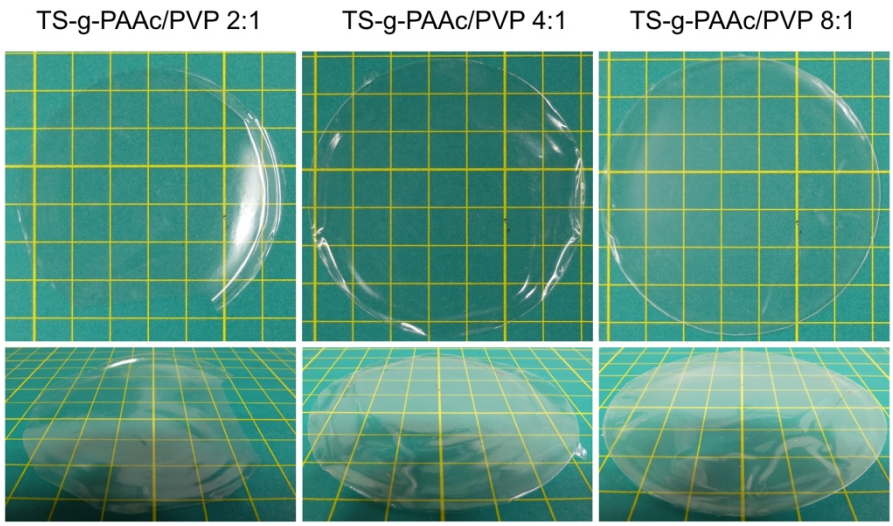

Figure 2-4 Image of dry TS-g-PAAc/PVP films with different TS-g-PAAc:PVP ratios.

water as a solvent because strong hydrogen bonds are formed between the two polymers, and precipitation is observed consequently. As a polar solvent, DMSO exhibits good solubility in starch, poly(acrylic acid) (PAAc), and PVP, and can effectively dissolve TS-g-PAAc. In addition, DMSO is a strong acceptor of hydrogen bonds; this prevents hydrogen bonds from forming between TS-g-PAAc

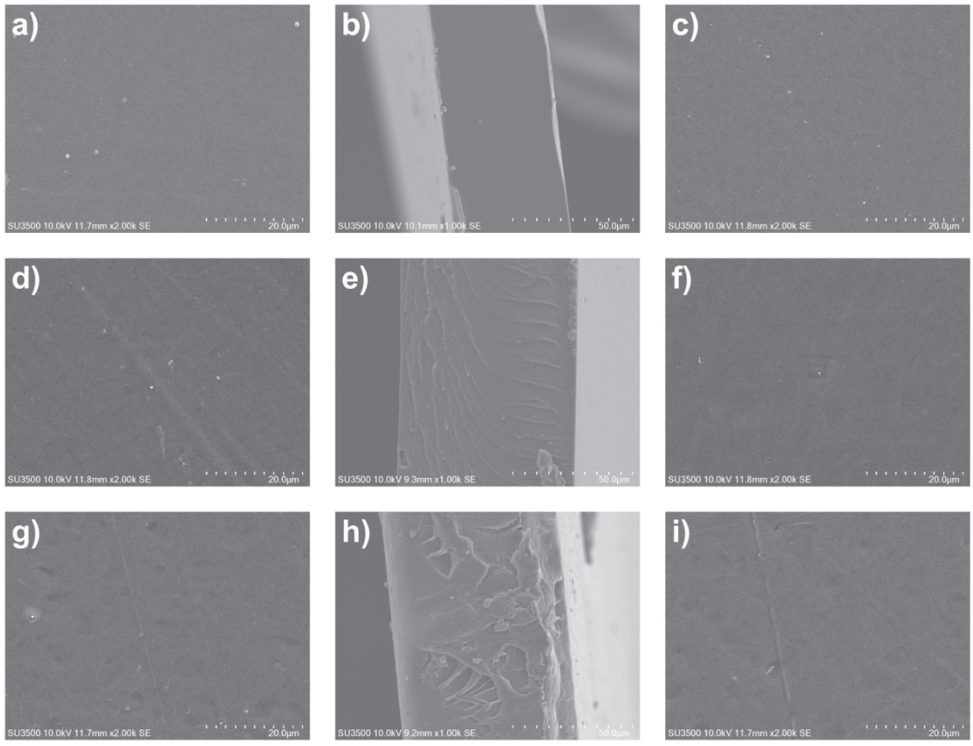

Figure 2-5 Scanning electron microscopy (SEM) images of the TS-g-PAAc/PVP blend film. **a).**, **d).**, **g).**: Top surfaces of TS-g-PAAc/PVP (2:1, 4:1, and 8:1) films; **b).**, **e).**, **f).**: Cross sections of TS-g-PAAc/PVP (2:1, 4:1, and 8:1) films; **g).**, **h).**, **i)**.: Bottom surfaces of TS-g-PAAc/PVP (2:1, 4:1, and 8:1) films.

and PVP and allows a homogenous casting solution to be prepared. Therefore, the TS-g-PAAc/PVP blend film was prepared by solution casting using DMSO as the solvent. Films with three different TS-g-PAAc:PVP weight ratios (2:1, 4:1, and 8:1) were prepared and examined.

In preliminary tests, PAAc/PVP blend film was not obtained from the solution casting method using DMSO as the solvent because of the low film-forming ability of PAAc and PVP. The film-forming ability of PAAc was significantly improved when it was grafted onto starch, and the TS-g-PAAc/PVP blend film was obtained using the same method. The TS-g-PAAc dissolved well in DMSO, and after it was mixed with the PVP DMSO solution, the homogeneous state of the solution remained unchanged. A clear, homogenous film with a smooth, glossy surface was prepared from the homogenous casting solution (**Figure 2-4**). The homogeneity of the films was further confirmed by the SEM images of the films (**Figure 2-5**). The surface of the film is microscopically smooth, and no interface is observed on the surface or cross section. The TS-g-PAAc film was slightly brittle when freshly taken out of the drying oven; however, aft er humidity conditioning, the film eventually became flexible. This change in flexibility can be explained by the fact that water is a good plasticizer for films.

2.3.3. Hydrogen bond formation between TS-g-PAAc and PVP

Hydrogen bond formation between TS-g-PAAc and PVP was observed by analyzing the shift of the –C=O stretching peak in the FTIR spectra of the two polymers. In **Figure 2-6**, for TS-g-PAAc, the typical –C=O stretching peak of carboxylic acid is identified at 1708 cm^{-1}, whereas the –C=O stretching peak of the amide group is identified at 1651 cm^{-1} in the spectrum of PVP. After mixing and drying, a shift is observed in the peak position of the –C=O peak of both polymers. The –C=O stretching peak of TS-g-PAAc shifts to 1718 cm^{-1} and that of PVP shifts to 1632 cm^{-1}. The distance and direction shifting of the C=O stretching peaks of the TS-g-PAAc carboxylic acid groups and PVP amide groups correspond with those of a previously reported PAAc/PVP blend.[14] The blue shift of -C=O stretching peak of PAAc is the result of disruption of intramolecular hydrogen bonding in PAAc.[15] Thus, it can be deduced that hydrogen bonds are formed between the COOH group of TS-g-PAAc and the –C=O group of PVP during the d rying process.

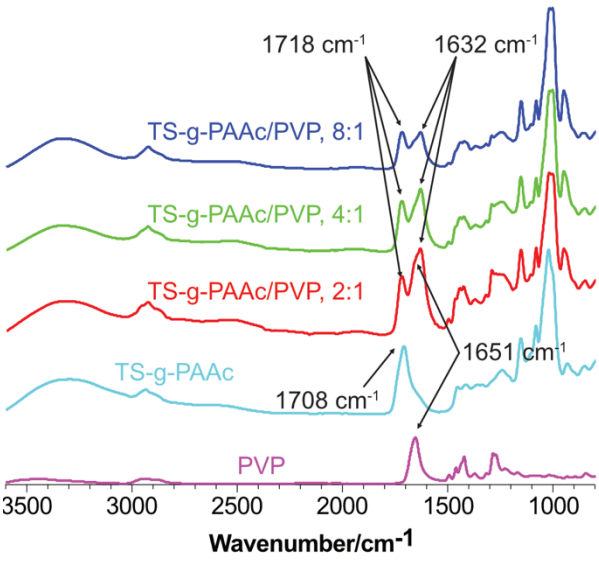

Figure 2-6 FTIR spectra of TS-g-PAAc, PVP, and TS-g-PAAc/PVP blend film for different TS-g-PAAc:PVP weight ratios.

The component of the non-shifted PVP–C=O peak is not visible in the spectra of the blend films with lower PVP contents,

whereas it is visible in the spectrum of the TS-g-PAAc:PVP 2:1 films. Therefore, the excess PVP or PVP chain segments are not involved in hydrogen bonding in TS-g-PAAc:PVP 2:1 films. The "optimized" TS-g-PAAc:PVP for maximum density of hydrogen bond crosslinks should be achieved in the range of TS-g-PAAc:PVP = 2:1 to 4:1; the density of hydrogen bond crosslinks should first increase for these ratios, then decrease as PVP contents decrease.

2.3.4. Mechanical properties of TS-g-PAAc/PVP blend film

The mechanical properties of the neat TS-g-PAAc and TS-g-PAAc/PVP blend films were determined using tensile tests. The tensile curves of the films are shown in **Figure 2-7** and the corresponding parameters are listed in **Table 2-2**. All blend films exhibit a higher ultimate tensile strength than that of the neat TS-g-PAAc film, which is attributed to the formation of a hydrogen bond crosslinking network. As the PVP fraction in the blend film decreases, the nature of the blend film shifts from strong and stiff to ductile and stretchable. This can be explained by the change in density of hydrogen bond crosslinks and the resultant crosslinking network structure; the density of hydrogen bond crosslinks is high at high PVP fractions, and thus limiting the movement of chain segments. As

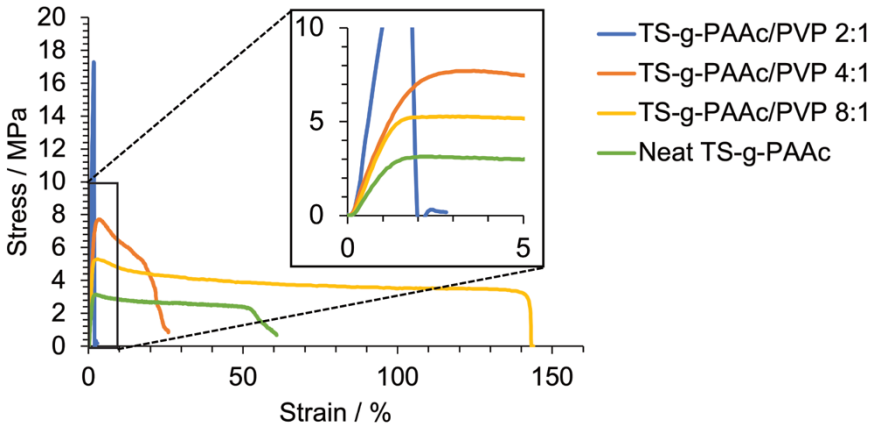

Figure 2-7 Mechanical properties of the TS-g-PAAc/PVP blend film with different TS-g-PAAc:PVP blending ratios. Crosshead speed used in tensile test: 10mm/min.

Table 2-2 Tensile parameters of the TS-g-PAAc/PVP blend film with different TS-g-PAAc:PVP blending ratios. σ_{max}: ultimate tensile strength. E: tensile modulus. ε: strain at break

Film type	**σ_{max}/MPa**	**E/MPa**	**ε**
Neat TS-g-PAAc	2.9±0.1	330±27	0.194±0.025
TS-g-PAAc:PVP (2:1)	18.5±1.8	1344±132	0.016±0.001
TS-g-PAAc:PVP (4:1)	7.5±0.3	466±21	0.211±0.036
TS-g-PAAc:PVP (8:1)	5.8±0.3	484±27	1.425±0.163

the PVP fraction decreases, the density of hydrogen bond crosslinks simultaneously decreases. Consequently, the chain segment mobility is improved in films with a relatively low PVP fraction, resulting in a low ultimate tensile strength. Nevertheless, owing to the existence of PAAc/PVP hydrogen bonds, the resistance of the chain segment movement in the blend film is larger than that of the neat TS-g-PVP film, and the elongation at break is higher than that for the neat TS-g-PVP film at low PVP fractions.

2.3.5. Dissolution/disintegration behavior of TS-g-PAAc/PVP in different solutions

Prior to the dissolution/disintegration test, the swelling behavior of the TS-g-PAAc film in DIW was tested by immersing TS-g-PAAc in DIW. The films were cut into square pieces of 1 cm × 1 cm and placed in Petri dishes containing a sufficient volume of DIW. The swelling process was monitored by a camera. The images at 0 min and 24 h of immersion are shown in **Figure 2-8.** As the PVP fraction decreases, the swelling of the TS-g-PAAc/PVP blend film increases, which indicates that the TS-g-PAAc/PVP 2:1 blend film demonstrates the highest crosslinking density, whereas that of the TS-g-PAAc/PVP 8:1 blend film is the lowest. This result concurs with the interpretation of the mechanical properties of the films; the hydrogen bond and crosslinking densities simultaneously decrease with decreasing PVP content. As the TS-g-PAAc/PVP 2:1 film has the highest density of hydrogen bond crosslinks, its dissolution/disintegration behavior is the easiest to observe and is considered for all dissolution/disintegration tests.

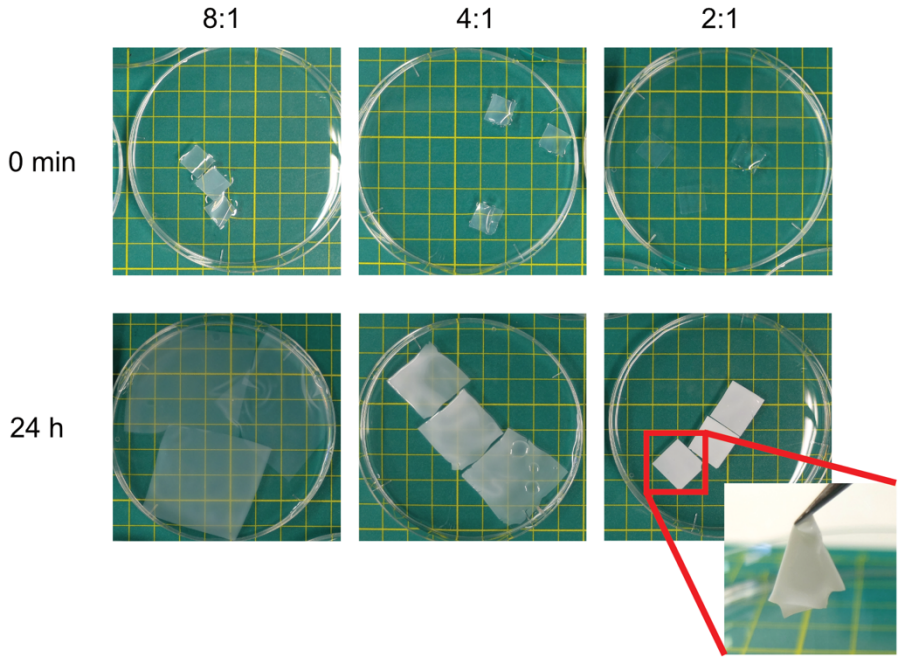

Figure 2-8 Immersion test of TS-g-PAAc/PVP films with different TS-g-PAAc:PVP ratio in deionized water.

The dissolution/disintegration behavior of the TS-g-PAAc/PVP (weight ratio 2:1) blend film sample pieces was being observed in DIW, 3.5% NaCl water solution, and artificial seawater (SW) (**Figure 2-9**). Unmodified starch film dissolved quickly in DIW. In contrast, the TS-g-PAAc/PVP film initially swelled when immersed in DIW; however, no dissolution was observed thereafter. As PAAc and PVP are also known to be readily soluble in water, this difference in solubility indicated that water-stable hydrogen bonds were generated between the TS-g-PAAc and PVP, possibly owing to the formation of ladder-like structures and hydrophobic effects.[16] When immersed in SW, the initial behavior of the film was similar to that in freshwater; however, as the immersion time increases, the film was gradually eroded from the edge and finally dissolved. This dissolution behavior can be ascribed to deprotonation; when immersed in seawater, the protonated carboxy groups gradually deprotonated to a degree wherein the ladder structure was no longer stable and cleaved, thereby returning the TS-g-PAAc to a non-crosslinked state. The film gradually dissolved as the poly mer chains are washed away.

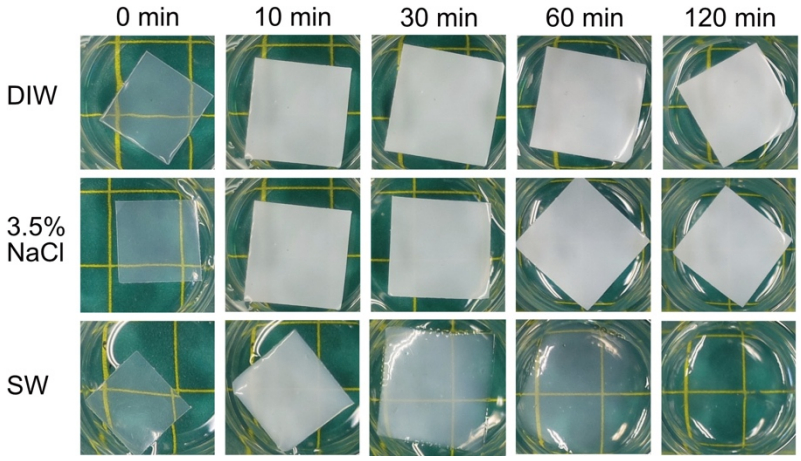

Figure 2-9 Dissolution behavior of the TS-g-PAAc/PVP (2:1) blend film in DIW, 3.5% w/v NaCl solution, and SW.

While the TS-g-PAAc/PVP film dissolved in SW, no dissolution was observed when the film was immersed in 3.5% w/v NaCl solution, which has approximately the same salinity as that of seawater. As both 3.5% w/v NaCl solution and SW have relatively high ionic strength, it is unlikely that the deprotonation of TS-g-PAAc and subsequent dissolution are driven solely by the presence of ions. SW is similar to 3.5% w/v NaCl solution in many ways, the higher pH of SW is a major differentiator of the two solutions. Considering deprotonation can be also triggered by high pH, it is possible that this higher pH is the major cause of the dissolution.

2.3.6. Dissolution mechanism of TS-g-PAAc/PVP in SW

TS-g-PAAc can be deprotonated by either or both of the following factors: the shift of pKa of PAAc chain blocks on TS-g-PAAc towards a low value at high salt concentration,[5,17] or the high pH of seawater.[1] To understand the dissolution mechanism of the TS-g-PAAc/PVP blend film in seawater, the

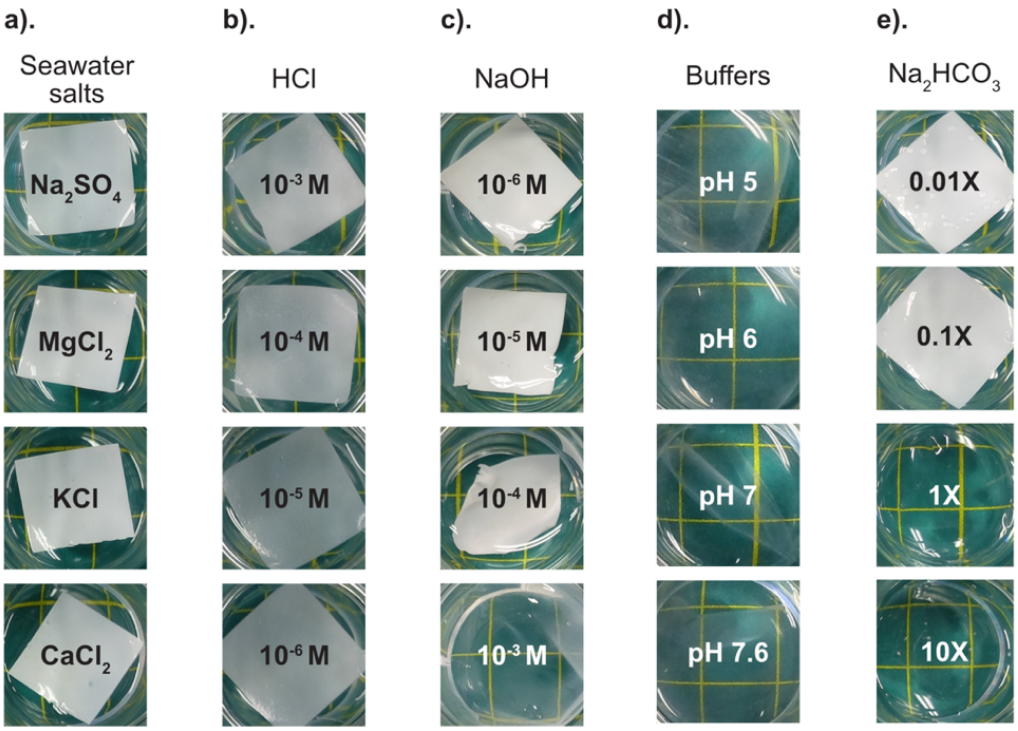

Figure 2-10 TS-g-PAAc/PVP 2:1 film after 24h immersion in different water solution. **a).** In solution of major salts species in SW, of their respective concentrations in SW. **b).** HCl solution. **c).** NaOH solution. **d).** In pH 5 acetate buffer, pH 6, 7 and 7.6 phosphate buffer. **e).** In Na_2CO_3 solution with concentration that is 0.01, 0.1, 1 and 10 times (X) of its concentration in SW.

film was tested in different solutions (salt species with a high concentration in artificial seawater, strong acid and base, and buffer). TS-g-PAAc/PVP 2:1 film samples after 24h immersion were shown in **Figure 2-10**. Initially, the TS-g-PAAc/PVP film samples were immersed in solutions of different salts with their respective concentrations in artificial seawater. The five selected salt species exhibit the highest content in artificial seawater, other than NaCl ($MgCl_2$, $CaCl_2$, Na_2SO_4, KCl, and $NaHCO_3$). As shown in **Figure 2-10 a).** and **e).**, samples in most salt solutions demonstrated no dissolution, regardless of the valency of metal ions, whereas the sample in $NaHCO_3$ solution dissolved. As $NaHCO_3$ renders seawater pH basic, the deprotonation and the resultant dissolution were initially assumed to be pH-responsive rather than cation-responsive.

To determine the switching pH of the film, its dissolution behavior under different pH conditions was investigated. The film was first immersed in a solution of a strong base (NaOH) and a strong acid (HCl) of different concentrations to eliminate the influence of ions and ionic strength. In particular, no dissolution was observed until the NaOH concentration was increased to 10^{-3} M, with a pH considerably higher than that of seawater and the deprotonation pH of PAAc predicted by the pKa of PAAc (**Figure 2-10 b).** and **c)**). To further investigate the dissolution mechanism of the TS-g-PAAc/PVP film, the film was immersed in commercial buffer solutions with a pH in the range of 5-7.6 and an ionic strength of

0.1 mol/L. In contrast to the dissolution behavior in the strong acid and base solution series, samples dissolved in all buffers that were tested, irrespective of the pH and type of buffer (**Figure 2-10 d).**).

Considering the dissolution behavior of the TS-g-PAAc/PVP film in four solution series, the dissolution mechanism can be deduced as follows: As all solutions in which the film dissolved contain a large amount of weak acid and its salts or NaOH, the dissolution behavior of the film may not solely be controlled by the pH. In water and low-concentration strong base solutions, the only H^+-accepting species in the solution is OH^-, whose concentration is insufficient. Consequently, the deprotonation of the PAAc segments is considerably slow even at a relatively high pH, and no dissolution is observed until $[OH^-]$ is increased to a sufficient level by NaOH. In solutions with weak acid anions (buffer, artificial seawater, and $NaHCO_3$ solution), the concentration of weak acid anions $[A^-]$ is higher than that of $[OH^-]$ in strong base solutions with a similar pH; thus, the protons on the PAAc segments are rapidly transferred to A^-. In conclusion, instead of the protonation/deprotonation equilibrium shift of the PAAc chain segments at higher ionic strengths, the dissolution behavior of the TS-g-PAAc/PVP film is more probably caused by the change in the deprotonation kinetics of PAAc chain segments induced by weak acid anions, which greatly increases the deprotonation speed and shortens the dissolution time.

Additionally, the dissolution response for different $NaHCO_3$ concentrations of the film was tested by immersing the film in solutions with $NaHCO_3$ concentrations that were 0.01, 0.1, 1, and 10 times the Na_2CO_3 concentration in seawater (**Figure 2-10 e).**). Within the observation period of 24 h, the film immersed in the 0.01 times and 0.1 times solutions did not dissolve, whereas the film immersed in the other two solutions dissolved. As the concentration is increased from 1 time to 10 times, the dissolution rate of the film also increased. Therefore, the dissolution of the film occurs at a threshold concentration of $NaHCO_3$; the dissolution speed of the film increases when the $NaHCO_3$ concentration is increased beyond this threshold.

2.4. Conclusions

Acrylic acid-modified starch (TS-g-PAAc) was prepared as a non-covalently crosslinked blend film by free-radical grafting polymerization. Subsequently, a TS-g-PAAc/PVP blend film was prepared using PVP, a strong acceptor for hydrogen bonding, as a polymeric crosslinker. Strong water-stable hydrogen bonds that are generated between the PVP and the grafted PAAc chain segments of TS-g-PAAc prevent the film from dissolving in DIW. In artificial seawater, the carboxy groups on TS-g-PAAc rapidly deprotonate, thereby destroying the hydrogen bond network structure and enabling TS-g-PAAc to be freely dissolved. The blend film quickly dissolves when immersed in seawater. The deprotonation of TS-g-PAAc is attributed to the reaction between TS-g-PAAc and bicarbonate groups in artificial seawater. This technique provides a potential recourse for the ocean plastic problem. Furthermore, it may be suitable for single-use applications in fields such as packaging, healthcare, and agriculture.

References

(1) Ishizu, M.; Miyazawa, Y.; Tsunoda, T.; Ono, T. Long-Term Trends in PH in Japanese Coastal Seawater. *Biogeosciences* **2019**, *16* (24), 4747–4763. https://doi.org/10.5194/bg-16-4747-2019.

(2) Qian, C.; Asoh, T.-A.; Uyama, H. Dimensionally Stable and Mechanically Adaptive Polyelectrolyte Hydrogel. *Macromol. Rapid Commun.* **2020**, *41* (22), 2000406. https://doi.org/10.1002/marc.202000406.

(3) Kurakula, M.; Rao, G. S. N. K. Pharmaceutical Assessment of Polyvinylpyrrolidone (PVP): As Excipient from Conventional to Controlled Delivery Systems with a Spotlight on COVID-19 Inhibition. *J. Drug Deliv. Sci. Technol.* **2020**, *60*, 102046. https://doi.org/10.1016/j.jddst.2020.102046.

(4) Arkaban, H.; Barani, M.; Akbarizadeh, M. R.; Pal Singh Chauhan, N.; Jadoun, S.; Dehghani Soltani, M.; Zarrintaj, P. Polyacrylic Acid Nanoplatforms: Antimicrobial, Tissue Engineering, and Cancer Theranostic Applications. *Polymers* **2022**, *14* (6), 1259. https://doi.org/10.3390/polym14061259.

(5) Lin, W.; Guan, Y.; Zhang, Y.; Xu, J.; Zhu, X. X. Salt-Induced Erosion of Hydrogen-Bonded Layer-by-Layer Assembled Films. *Soft Matter* **2009**, *5* (4), 860–867. https://doi.org/10.1039/B813614A.

(6) Jin, S.; Liu, M.; Zhang, F.; Chen, S.; Niu, A. Synthesis and Characterization of PH-Sensitivity Semi-IPN Hydrogel Based on Hydrogen Bond between Poly(N-Vinylpyrrolidone) and Poly(Acrylic Acid). *Polymer* **2006**, *47* (5), 1526–1532. https://doi.org/10.1016/j.polymer.2006.01.009.

(7) Yu, W.; Wang, Y.; Li, A.; Yang, H. Evaluation of the Structural Morphology of Starch-Graft-Poly(Acrylic Acid) on Its Scale-Inhibition Efficiency. *Water Res.* **2018**, *141*, 86–95. https://doi.org/10.1016/j.watres.2018.04.021.

(8) Witono, J. R.; Noordergraaf, I. W.; Heeres, H. J.; Janssen, L. P. B. M. Graft Copolymerization of Acrylic Acid to Cassava Starch—Evaluation of the Influences of Process Parameters by an Experimental Design Method. *Carbohydr. Polym.* **2012**, *90* (4), 1522–1529. https://doi.org/10.1016/j.carbpol.2012.07.024.

(9) Gök, M. K.; Özgümüş, S.; Demir, K.; Cirit, Ü.; Pabuccuoğlu, S.; Cevher, E.; Özsoy, Y.; Bacınoğlu, S. Development of Starch Based Mucoadhesive Vaginal Drug Delivery Systems for Application in Veterinary Medicine. *Carbohydr. Polym.* **2016**, *136*, 63–70. https://doi.org/10.1016/j.carbpol.2015.08.079.

(10) Greenspan, L. Humidity Fixed Points of Binary Saturated Aqueous Solutions. *J. Res. Natl. Bur. Stand. Sect. Phys. Chem.* **1977**, *81A* (1), 89. https://doi.org/10.6028/jres.081A.011.

(11) Cheng, M.; Qin, Z.; Liu, Y.; Qin, Y.; Li, T.; Chen, L.; Zhu, M. Efficient Extraction of Carboxylated Spherical Cellulose Nanocrystals with Narrow Distribution through Hydrolysis of Lyocell Fibers by Using Ammonium Persulfate as an Oxidant. *J. Mater. Chem. A* **2014**, *2* (1), 251–258. https://doi.org/10.1039/C3TA13653A.

(12) Leung, A. C. W.; Hrapovic, S.; Lam, E.; Liu, Y.; Male, K. B.; Mahmoud, K. A.; Luong, J. H. T. Characteristics and Properties of Carboxylated Cellulose Nanocrystals Prepared from a Novel One-Step Procedure. *Small* **2011**, *7* (3), 302–305. https://doi.org/10.1002/smll.201001715.
(13) Mascheroni, E.; Rampazzo, R.; Ortenzi, M. A.; Piva, G.; Bonetti, S.; Piergiovanni, L. Comparison of Cellulose Nanocrystals Obtained by Sulfuric Acid Hydrolysis and Ammonium Persulfate, to Be Used as Coating on Flexible Food-Packaging Materials. *Cellulose* **2016**, *23* (1), 779–793. https://doi.org/10.1007/s10570-015-0853-2.
(14) Guan, Y.; Yang, S.; Zhang, Y.; Xu, J.; Han, C. C.; Kotov, N. A. Fabry−Perot Fringes and Their Application To Study the Film Growth, Chain Rearrangement, and Erosion of Hydrogen-Bonded PVPON/PAA Films. *J. Phys. Chem. B* **2006**, *110* (27), 13484–13490. https://doi.org/10.1021/jp061548g.
(15) Biswas, A.; Willet, J. L.; Gordon, S. H.; Finkenstadt, V. L.; Cheng, H. N. Complexation and Blending of Starch, Poly(Acrylic Acid), and Poly(N-Vinyl Pyrrolidone). *Carbohydr. Polym.* **2006**, *65* (4), 397–403. https://doi.org/10.1016/j.carbpol.2006.01.035.
(16) Tsuchida, E.; Osada, Y.; Ohno, H. Formation of Interpolymer Complexes. *J. Macromol. Sci. Part B* **1980**, *17* (4), 683–714. https://doi.org/10.1080/00222348008212832.
(17) Dickhaus, B. N.; Priefer, R. Determination of Polyelectrolyte PKa Values Using Surface-to-Air Tension Measurements. *Colloids Surf. Physicochem. Eng. Asp.* **2016**, *488*, 15–19. https://doi.org/10.1016/j.colsurfa.2015.10.015.

Chapter 3. Dual-crosslinked Starch/Carboxymethyl Cellulose Blend Film with Ion-responsive Dissolution Properties

3.1. Introduction

Polyion complexes (PICs) is a class of polymeric materials consisting of two oppositely charged polyelectrolytes crosslinked by ionic bonds. Due to the ionic bond crosslinks, PICs are able to remain stable in low ionic strength solutions, e.g., freshwater; meanwhile in solution of high ionic strength, e.g. salt solutions, the ionic bonds dissociates due to the ionic shielding effect, causing the material to dissolve.[1] As seawater has significantly higher ionic strength compared to freshwater and many common solutions in daily life, it is likely a starch-based film with both water resistance in daily scenarios and rapid disintegration/weakening after being discarded and leaked to the sea can be realized via the development of a starch-based PIC film.

Previously, various types of PICs including hydrogels and micelles have been prepared.[2–6] Nevertheless, the preparation of starch-based PIC films can be challenging for several reasons. Natural-based polymers with ionizable amine groups, such as chitosan, have been the most used natural-based options of polycation for preparing various PICs.[7] However, these amine-rich polymers exhibit cationic properties only at low pH values, rendering them unsuitable for the preparation of dry films without a solvent. Moreover, realizing complexation via the direct mixing of charged starch with polymeric counterions is difficult to achieve. Owing to the rapid formation of ionic crosslinks, the newly formed PIC might precipitate from the solution, which not only might prevent further complexation, but also render the film-forming step challenging, if not impossible.

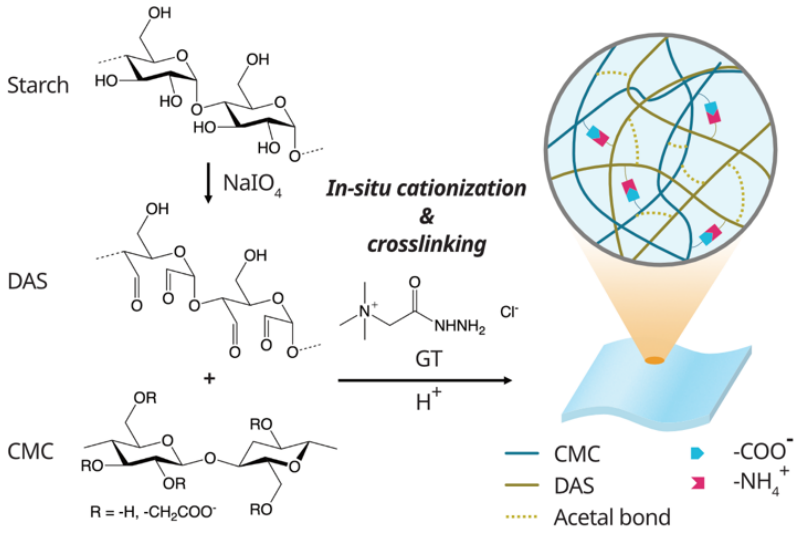

Figure 3-1 Schematic illustration of preparation process of DAS/CMC/GT/HCl blend film.

In this chapter, an ionic bond-crosslinked starch-based dry PIC film with seawater-selective or ion-responsive dissolution ability was prepared via a new solution-casting approach that does not rely on pH-dependent ionization and avoids the direct mixing of polycations and polyanions. (**Figure 3-1**) Starch was first converted to dialdehyde starch to increase its reactivity. Then, a biodegradable[8], natural-based polyanion with excellent water solubility and film forming characterisitics[9], i.e., CMC, is mixed with dialdehyde starch (DAS), which does not contain charged groups, and a composite film is prepared via solution casting. During the drying process, DAS is gradually converted into a cationic polymer using Girard's reagent T (GT), which reacts with -CHO groups and has previously been used to introduce quaternary ammonium groups into dialdehyde cellulose under mild conditions via imine bond formation.[10,11] Owing to the newly introduced cationic groups, DAS forms ionic crosslinks with CMC. In the meanwhile, acetal bond crosslinks are introduced by the reaction between the aldehyde groups on DAS and -OH groups on both DAS and CMC. The selective dissolution/disintegration behavior of the films is observed by immersing them in modeled freshwater and seawater environments.

3.2. Experimental

3.2.1. Materials

Unmodified tapioca starch (TS) was provided by Matsutani Chemical Industry Co., Ltd. (Japan) and used as is. CMC (Mw ~250 KDa, degree of substitution (D.S.: 0.7) and GT (for HPLC derivatization, 99.0%–101.0%) were obtained from Sigma–Aldrich (USA). Sodium periodate, sodium chloride, sodium sulfate, magnesium chloride, 1M hydrochloric acid (volumetric analysis grade), and glycerol were obtained from Fujifilm Wako (Osaka, Japan), and all were of JIS Special Grade unless specified otherwise. Calcium chloride (JIS special grade) was obtained from Kanto Chemical (Tokyo, Japan). Dialysis tube (Spectra/Por® 6 standard regenerated cellulose dialysis tubing, pre-wetted, MwCo: 10 kDa) was obtained from Spectrum Chemical Mfg. Corp. (USA). Artificial seawater (SW) was obtained as a mixed salt from Fujifilm Wako, and an SW solution was prepared by dissolving the salt in deionized water (DIW) in an amount specified in the manufacturer's instructions. The composition of the mixture is listed in **Table 2-1**.

3.2.2. Preparation of DAS suspension

A DAS suspension was prepared using a previously reported periodate oxidation method.[12] TS was mixed with DIW to obtain a 4% w/v suspension. Subsequently, the suspension was heated in a 90 °C water bath for approximately 30 min to gelatinize the TS. After gelatinization, the solution was cooled to room temperature (RT) under ambient conditions. Next, 0.05 g/mL of $NaIO_4$ was added to the cooled starch solution, and the solution was allowed to react for 1 h at RT with stirring, during which the starch was oxidized to DAS. After the reaction, the DAS solution was transferred to a dialysis tube (MwCo 10 KDa) and dialyzed against DIW for three days. Finally, the volume of the contents in the dialysis

tube was adjusted to 1.5 times the initial volume, and the mixture was processed via high-pressure homogenization using a high-pressure homogenizer (Starburst Mini HJP-25001, Sugino Machine Ltd., Uozu, Toyama, Japan) at 200 MPa for two passes. The degree of DAS oxidation was determined via iodometric titration, using a previously reported method.[12]

3.2.3. Preparation of blend films

A 3% CMC solution was prepared by directly dissolving CMC in DIW. CMC solution was added to the DAS suspension at a -CHO/-COO^- molar ratio of 1:0.75, 1:0.5 and 1:0.25, and the mixture was stirred and heated at 45 °C for 30 min. Subsequently, the mixture was cooled to RT under ambient cooling and further cooled in an ice/water bath. Next, pH of the solution was adjusted to 3.8 with 1M HCl. Subsequently, GT was added to casting solutions at a molar ratio of -COO^-: GT = 1:1. After the GT was completely dissolved, 15 mL of the mix solution was transferred promptly to a fluoropolymer Petri dish and then dried overnight at 45 °C. The final product is referred to as DAS/CMC*a*/GT/HCl, where *a* signifies the -CHO/-COO^- molar ratio; for example, the -CHO/-COO^- molar ratio is 1:0.5 when *a* is 0.5. Films prepared without HCl and GT, either or both, were also prepared and referred to by names that indicate their respective compositions; for example, films prepared without HCl and GT were referred to as DAS/CMC, and films prepared without HCl were referred to as DAS/CMC/GT.

3.2.4. Post-processing of DAS/CMC/GT/HCl blend film

First, the DAS/CMC/GT/HCl blend film was washed by immersing the film in 250 mL of DIW for approximately 2.5 h, and this step was repeated after the first washing was completed. After being washed using DIW twice, samples for all tests other than those for scanning electron microscopy (SEM) observation and swelling behavior comparison among DAS/CMC, DAS/CMC/GT, DAS/CMC/HCl and DAS/CMC/GT/HCl films were transferred to 50 mL of 15, 20 and 25% v/v glycerol water solution and stored in the solution for another 2.5 h. Samples for SEM observation and swelling behavior comparison among DAS/CMC, DAS/CMC/GT, DAS/CMC/HCl and DAS/CMC/GT/HCl films were immersed in 50 mL of DIW for another 2.5 h. Finally, film samples were removed from the glycerol solution or DIW, wiped to remove residual liquid on the surface, and dried overnight at 45 °C.

3.2.5. Characterization

FTIR analysis. The periodate oxidation of TS and the reaction between DAS and GT were analyzed using FTIR. The FTIR spectra of TS, DAS, and DAS/CMC film and DAS/CMC/GT/HCl film samples were measured using a Nicolet iS5 FTIR spectrometer with an attenuated total reflectance attachment (Thermo Fisher Scientific, Waltham, MA, USA), and the spectra were compared.

Microscopic morphology observation of DAS/CMC/GT/HCl blend film. The microscopic morphologies of both the surfaces and the cross-section (generated by stretching the film in an ambient

environment) of the DAS/CMC/GT/HCl film samples were observed via SEM (Hitachi SU3500 scanning electron microscope, Hitachi High-Technologies Corp., Tokyo, Japan).

Mechanical properties of DAS/CMC/GT/HCl blend film. To test the mechanical properties of dry DAS/CMC/GT/HCl films, DAS/CMC/GT/HCl films processed using glycerol solution of different concentrations and with different DAS/CMC ratios (processed by 20% glycerol solution) were cut into sample strips measuring 5 mm wide, and the ultimate tensile strength (σ_{max}), Young's modulus (E), and strain at break (ε_{break}) of the dry samples were measured using a Shimadzu EZ Graph universal tester (Shimadzu Corporation, Kyoto, Japan) with a 100 N load cell at a crosshead speed of 1 mm/min. To test the mechanical properties of wet DAS/CMC/GT/HCl films, with different DAS/CMC ratios (processed by 20% glycerol solution) were cut into sample strips measuring 5 mm wide and then immersed in DIW for 30 min. Subsequently, the σ_{max}, E, and ε_{break} of the wet samples were measured using a Shimadzu Autograph AGS-X universal tester (Shimadzu Corporation, Kyoto, Japan) with a 50 N load cell at crosshead speed of 5 mm/min.

Swelling/disintegration test of DAS/CMC/GT/HCl blend film. The DAS/CMC0.5/GT/HCl blend films were cut into pieces measuring approximately 1 cm × 1 cm. Subsequently, the samples were weighed using an analytical balance and placed into the wells of well plates; next, 3 mL of the solution was added to each well. To test the seawater-responsive and ion-responsive swelling behaviors, the solutions used were DIW, NaCl solutions of different concentrations (0.2%, 1%, 3.5%, and 5% w/v), SW, and different salt solutions with ionic strengths equivalent to that of the 3.5% NaCl solution (4.5% w/v KCl solution, 2.8% w/v Na_2SO_4 solution, 1.9% w/v $MgCl_2$ solution, and 2.2% w/v $CaCl_2$ solution). These salt species were selected because of their high concentrations in SW.

The weights of the samples were measured before and after 10, 30, 60, and 120 min of immersion, and the swelling ratio (SR) of the films was calculated as follows:

$$SR(\%) = \frac{W_t - W_0}{W_0} \times 100\%$$

where W_0 is the weight of the sample before immersion, and W_t is the weight of the sample at time *t*. After the sample established contact with the solution, images of the samples were captured at 10, 30, 60 and 120 min and 24 h using a digital camera.

3.3. Results and Discussion

3.3.1. Preparation of DAS

To enable starch to form imines with GT, aldehyde groups were introduced into starch via periodate oxidation. The oxidation of TS was monitored via FTIR and iodometric titration. As shown in **Figure 3-2**, a new peak at approximately 1732 cm^{-1}, which was attributed to the -C=O peak of the aldehyde groups,[13] appeared in the FTIR spectrum of DAS. Thus, TS was successfully oxidized to DAS. The degree of DAS oxidation was determined via iodometric titration. The oxidation degree of DAS

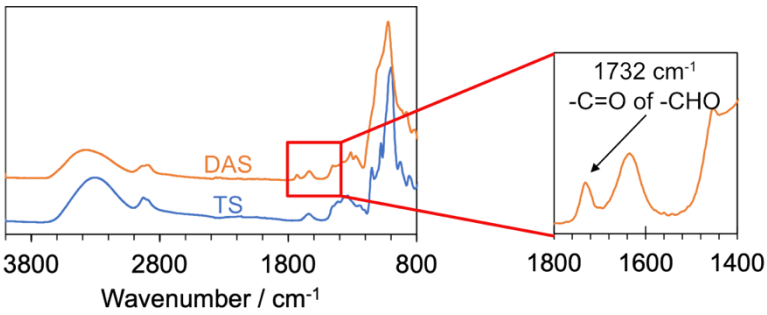

Figure 3-2 FTIR spectra of unmodified tapioca starch and DAS.

determined via this method was 51.7 ± 0.5%.

3.3.2. Appearance and microscopic morphology of DAS/CMC/GT/HCl film

The visual appearance of the DAS/CMC/GT/HCl film is shown in **Figure 3-3 a). and b)**. The DAS/CMC/GT/HCl film is transparent and has a smooth, glossy surface. This smooth transparency and surface morphology may indicate the high homogeneity of the structure. After the film was prepared via solution casting, it was washed with water to remove excess reagents, and all samples other than those used for SEM observation and swelling behavior comparison among DAS/CMC, DAS/CMC/GT, DAS/CMC/HCl and DAS/CMC/GT/HCl films were washed with a glycerol solution to introduce glycerol as a plasticizer. Whereas the film was slightly brittle immediately after drying, the flexibility of the film improved after it was washed and processed using a glycerol solution. However, regardless of the solution used in the final washing step (water or glycerol), no noticeable changes in the visual

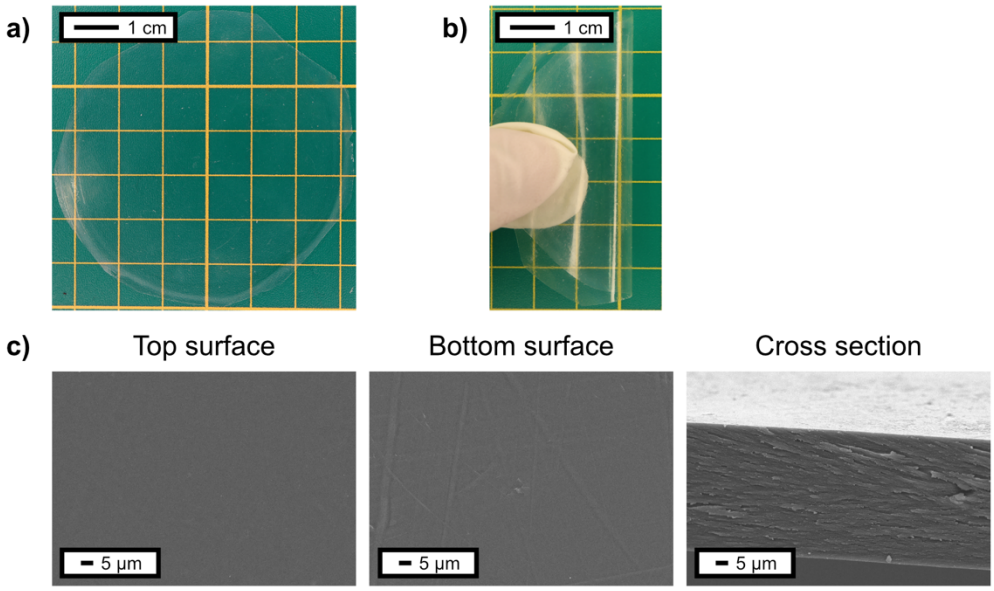

Figure 3-3 Macroscopic and microscopic appearance of DAS/CMC/GT/HCl film. **a).** Optical image of DAS/CMC/GT/HCl film. **b).** Image of DAS/CMC/GT/HCl film being bent. **c).** SEM imaged of top surface, bottom surface and cross-section of DAS/CMC/GT/HCl film.

appearance of the film were observed after washing and drying.

The microscopic morphologies of the DAS/CMC/GT/HCl films were observed via SEM; both the top and bottom surfaces and cross-sections of the film were observed via SEM. As shown in **Figure 3-3 c).**, the DAS/CMC/GT/HCl film was microscopically smooth on both surfaces, and no inhomogeneity was observed at the cross-section of the film, which is consistent with speculations based on visual observation. Thus, the smooth surface morphology and highly transparent appearance of the DAS/CMC/GT/HCl film is attributable to its high microscopic homogeneity.

3.3.3. Reaction between DAS and GT

The reaction between the DAS/CMC films was analyzed by comparing the FTIR spectra of the DAS/CMC and DAS/CMC/GT/HCl films. As shown in **Figure 3-4**, peaks originating from the GT structure is presented clearly in the spectrum of the DAS/CMC/GT/HCl film, including a sharp peak at 1691 cm^{-1}, which is due to the carbonyl group in GT,[10] and a peak at 923 cm^{-1}, which is due to the nitrogen–nitrogen bond in GT.[14] Considering the high water solubility of GT and the fact that the films were washed thoroughly after preparation, the GT-related peaks in the DAS/CMC/GT/HCl spectrum were attributed to GT bound to the polymer chain via imine bond formation.[10,11] Therefore, GT is likely to have reacted with DAS during drying.

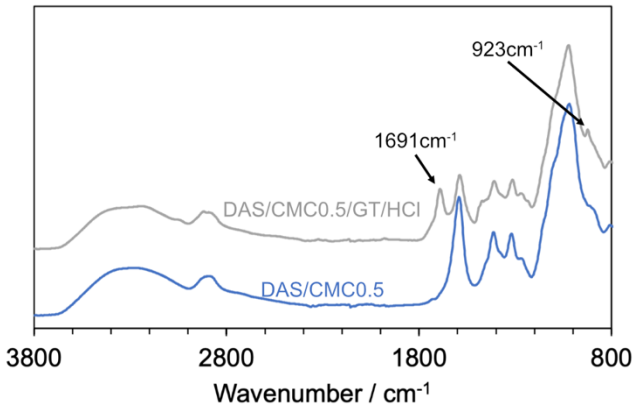

Figure 3-4 FTIR spectra of DAS/CMC0.5 and DAS/CMC0.5/GT/HCl films

3.3.4. Ionic-responsive swelling behavior of DAS/CMC/GT/HCl film

The ionic swelling-responsive behavior of the DAS/CMC/GT/HCl film was first tested by immersing the film samples in freshwat er and seawater. Two solutions, i.e., 3.5% NaCl and SW, were selected as models for seawater, and DIW was used as the model for freshwater. The extent of swelling over time was measured by the weight change, as shown in **Figure 3-5 a)**, and the swelling/dissolution processes of the DAS/CMC/GT/HCl film in DIW, 3.5% NaCl, and SW were observed, as shown in **Figure 3-5 b)**. Whereas pure TS film dissolved rapidly in DIW,[15] DAS/CMC/GT/HCl film reached swelling equilibrium in 30–60 min and remained stable even after 1 day of immersion. By contrast, the film exhibited significantly different swelling and disintegration behaviors in the 3.5% NaCl solution. The film remained swollen without reaching equilibrium and eventually became extremely swollen, weak after one day of immersion, and almost non-removable from the solution. This rapid swelling and

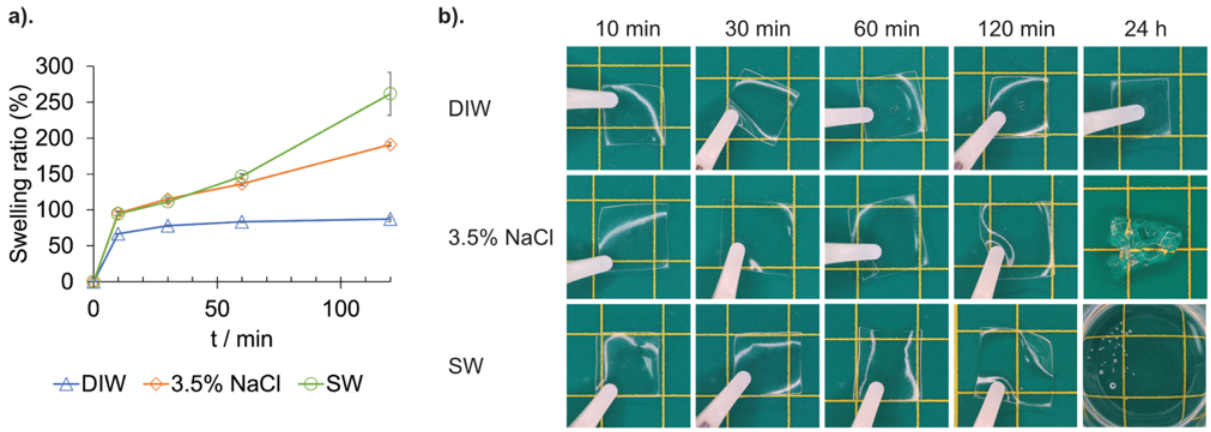

Figure 3-5 a). Swelling curve of DAS/CMC0.5/GT/HCl films in DIW, 3.5% NaCl, and SW. **b).** Swelling and disintegration behavior of DAS/CMC0.5/GT/HCl films in DIW, 3.5% NaCl, and SW.

disintegration can be explained by the rapid cleavage of ionic bonds triggered by ion exchange, which caused the polymer chains to be bounded only by acetal crosslinks. Acetal crosslinking alone might be insufficient to counteract the swelling force resulted from the osmotic pressure difference between the inside and outside of the film; consequently, the film swelled and disintegrated rapidly. Interestingly, regardless of the existence of divalent cations such as Ca^{2+} and Mg^{2+} in SW, which might crosslink CMC and decrease/prevent the swelling of the film, the film continued to swell and eventually completely disintegrated in SW.

To better understand the ion-responsive swelling/disintegration process, the effect of the ionic strength on the swelling/dissolution behavior of the film was investigated by observing the swelling and dissolution/disintegration behaviors in NaCl solutions of different concentrations. As shown in **Figure 3-6 a)**, as the concentration of NaCl increased, swelling occurred faster in the samples,

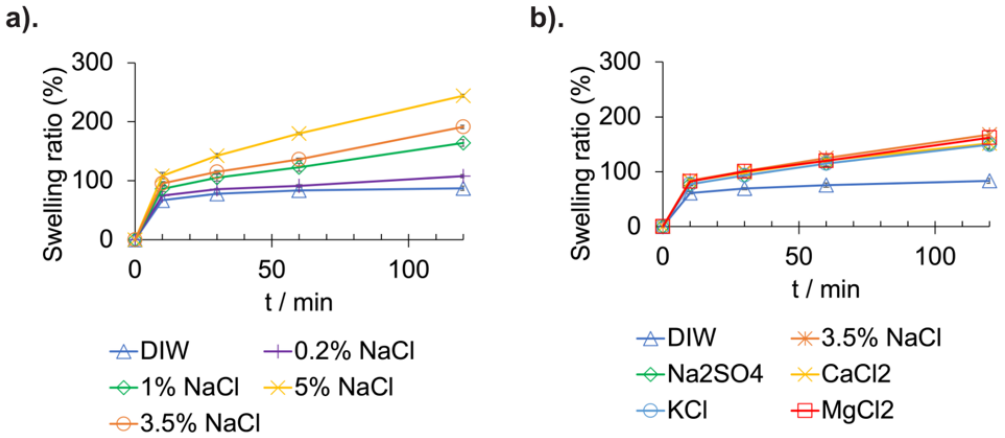

Figure 3-6 a). Swelling curve of DAS/CMC0.5/GT/HCl films in NaCl solution of different concentrations. **b).** Swelling curve of DAS/CMC0.5/GT/HCl films in different salt solutions with ionic strength equivalent to that of 3.5% NaCl solution.

indicating that the swelling behavior of the film is associated significantly with the ionic strength of the solution. A higher ionic strength may have caused more ionic bonds to cleave, which impaired the strength of the network and allowed the film to swell more. In addition to the swelling process, the final state in the solution was determined by the ionic strength. As shown in **Figure 3-7**, in low ionic strength solutions such as DIW and 0.2% NaCl, the film remained stable after 24 h of immersion. Meanwhile, in high ionic strength solutions such as 3.5% and 5% NaCl solutions, the film swelled rapidly and became extremely swollen, weak, or disintegrated/dissolved. In the medium NaCl solution, the state of the film after 24 h of immersion was between that of the film immersed in high- and low-concentration NaCl solutions. Similarly, this might be due to the increased ionic crosslink cleavage at higher ionic concentrations; when sufficient ionic crosslinks were cleaved, the expansion force caused by the osmotic pressure difference successfully overcame the binding force provided by the crosslinks and disrupted the crosslinked network.

In addition, the effect of ion type on the swelling/dissolution proper ties of the film was investigated by observing the swelling and dissolution/disintegration behavior in different salt solutions with ionic strengths similar to that of the 3.5% NaCl solution. The salt species used in this study were selected mainly because of their abundance in seawater. As shown in **Figure 3-6 b).**, the swelling ratios of the film samples immersed in all salt solutions were almost identical to that of the film samples immersed in the 3.5% NaCl solution. No significant difference was observed between the swelling processes of the samples immersed in different solutions, as shown in **Figure 3-8**. Thus, the swelling/disintegration behavior was mainly determined by the ionic strength, and the ion types and valency of the seawater ions did not significantly affect the swelling of

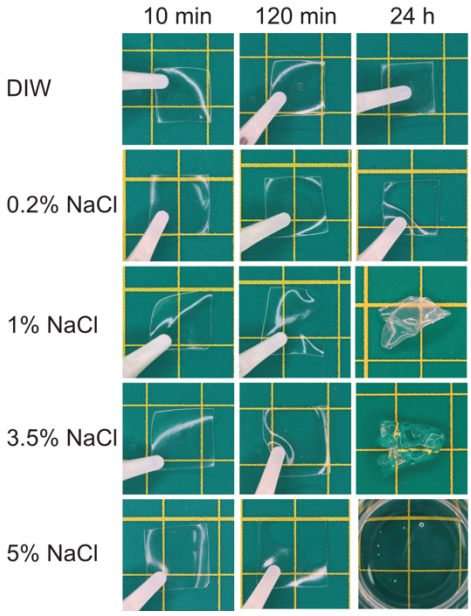

Figure 3-7 Swelling/dissolution process of DAS/CMC/GT/HCl films in NaCl solution of different concentration.

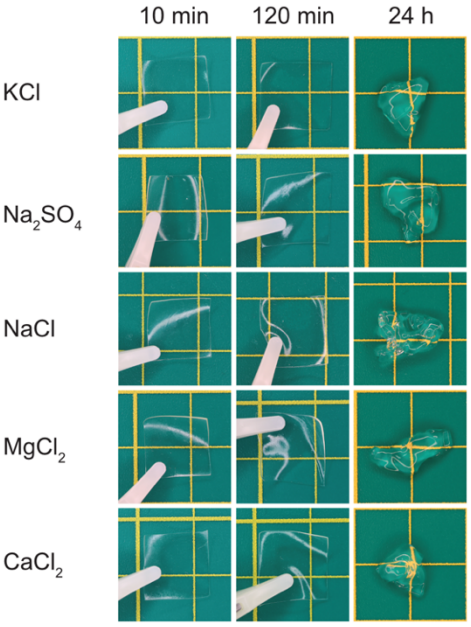

Figure 3-8 Swelling/dissolution process of DAS/CMC/GT/HCl films in salt solutions with the same ionic strength as 3.5% NaCl solution.

the DAS/CMC/GT/HCl film. Some anionic polysaccharides have been reported to form tight chelation structures around Ca^{2+} and Mg^{2+} and exhibit a strong tendency for gelation in the presence of these ions, e.g., alginic acid. However, in the case of CMC, neither was reported, which might explain the extremely similar swelling behavior of DAS/CMC/GT/HCl films in all tested solutions. The faster swelling and complete disintegration of the DAS/CMC/GT/HCl films in SW compared with that in 3.5% NaCl might be solely due to the difference in the ionic strength. Whereas the weight concentrations of SW and 3.5% NaCl were similar, the ionic strength of SW was much higher because of the significant number of divalent cations.

3.3.5. Contribution of ionic and acetal crosslinks

DAS/CMC blended films without either or both types of crosslinks were prepared by preparing DAS/CMC/GT/HCl films without GT and/or HCl. An acidic environment is essential for acetal bond formation. The swelling/disintegration behavior of the films by immersing the film in DIW and 3.5% NaCl solution was compared to understand the contribution of two types of crosslinks to water

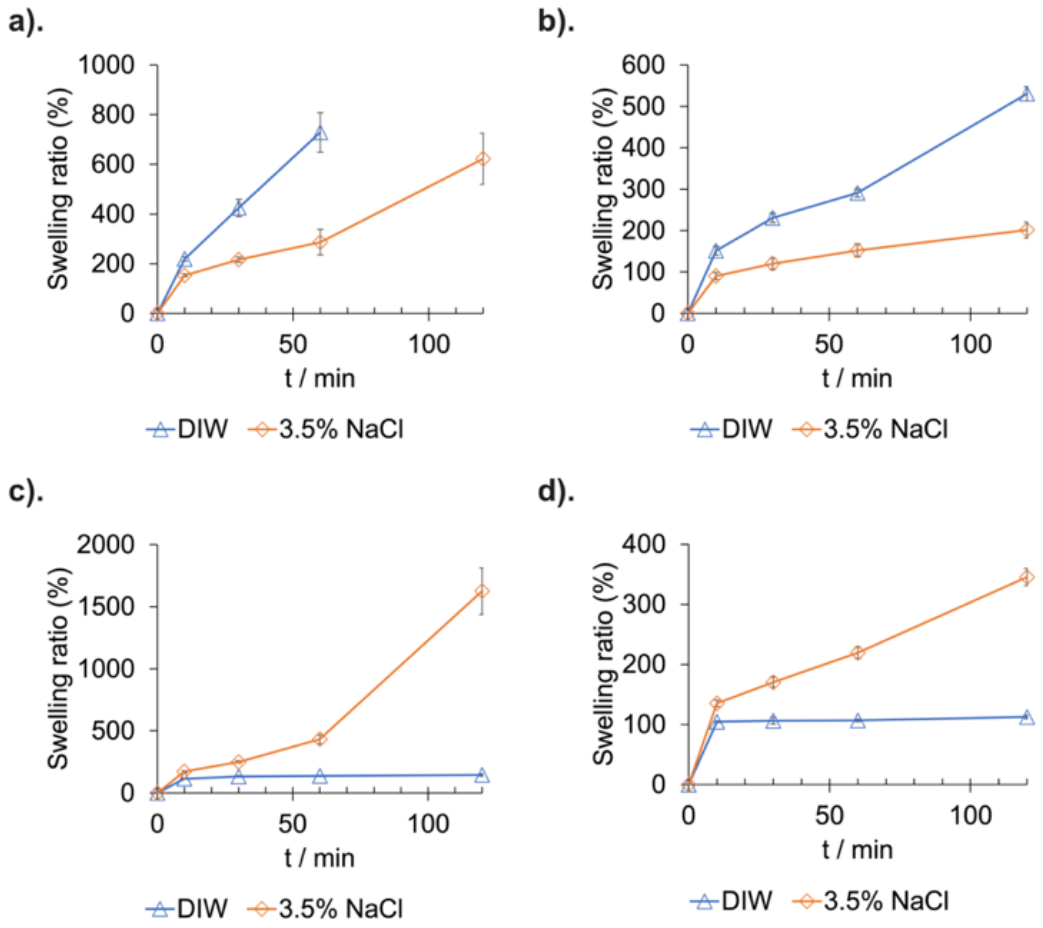

Figure 3-9 Swelling curves of **a).** DAS/CMC0.5, **b).** DAS/CMC0.5/HCl, **c).** DAS/CMC0.5/GT and **d).** DAS/CMC0.5/GT/HCl films in DIW and 3.5% NaCl solution.

resistance and the ion-responsive swelling/dissolution process of the DAS/CMC/GT/HCl film, and the swelling curves of 4 types of films are shown in **Figure 3-9**.

The DAS/CMC film, which contained neither type of crosslink, continued to swell in both the NaCl solution and DIW, and eventually disintegrated. Owing to the numerous carboxylate groups, the molecular structure of the DAS/CMC film resembled that of typical super absorbent polymers (SAPs). The DAS/CMC film swelled more significantly in DIW to the extent that it became excessively swollen and weak to be weighted 2 h after immersion. Meanwhile, DAS/CMC swelled less in the NaCl solution, which is characteristic of SAPs owing to the reduced osmotic pressure difference and the counterion shielding effect.[16] The molecular structure of the DAS/CMC/HCl film is similar to that of DAS/CMC, with the only difference that the DAS/CMC/HCl film is crosslinked via acetal bonds. Even when acetal crosslinks were introduced, the DAS/CMC/HCl film could not reach swelling equilibrium in DIW, suggesting that the binding force provided by the acetal bonds alone was insufficient to counteract the expansion force owing to the osmotic pressure difference. By contrast, both types of films with ionic bonds, i.e., DAS/CMC/GT and DAS/GT/CMC/HCl, reached swelling equilibrium in DIW, swelled continuously, disintegrated in the NaCl solution, and swelled more in the NaCl solution. Thus, ionic bonds are essential for maintaining the water resistance of films in low ionic strength solutions. The formation of ionic bonds not only provided additional bonding force to the network, which counteracted the expansion force, but also shielded the charge on the carboxylate groups, thus reducing the expansion force.

Compared with their respective counterparts without acetal bonds, films with acetal bonds swelled noticeably less in both the DIW and NaCl solutions. Thus, acetal bonds, in addition to ionic bonds, provide additional binding forces. Because acetal bonds are not susceptible to high ionic strengths, their contribution to the binding force should be equal for all solution types.

3.3.6. Mechanical properties of DAS/CMC/GT/HCl film

The mechanical properties of the dry DAS/CMC/GT/HCl film were evaluated via tensile tests, and the effect of glycerol concentration and DAS/CMC ratio on mechanical properties of dry films were tested. The stress-strain curve of DAS/CMC0.5/GT/HCl films processed with 15, 20 and 25% of glycerol solution were shown in **Figure 3-10 a)**, and the mechanical properties were summarized in **Figure 3-10 c)**, **d)**, and **e)**. During the glycerol processing step, films were allowed to reach swelling equilibrium in glycerol solution; thus, the amount of glycerol introduced to the film depends solely on the concentration of glycerol solution used for the processing. As the glycerol concentration during glycerol processing increased, the strain at the breakage of the film increased significantly, indicating that glycerol is an effective plasticizer for the DAS/CMC/GT/HCl film. However, the strength of the film decreased as the glycerol concentration increased, which might have been caused by excessive reduction of hydrogen bond formation due to an increase in the glycerol content. At lower glycerol concentrations (15% and 20%), the DAS/CMC/GT/HCl films exhibited good balance between ε_{break} and

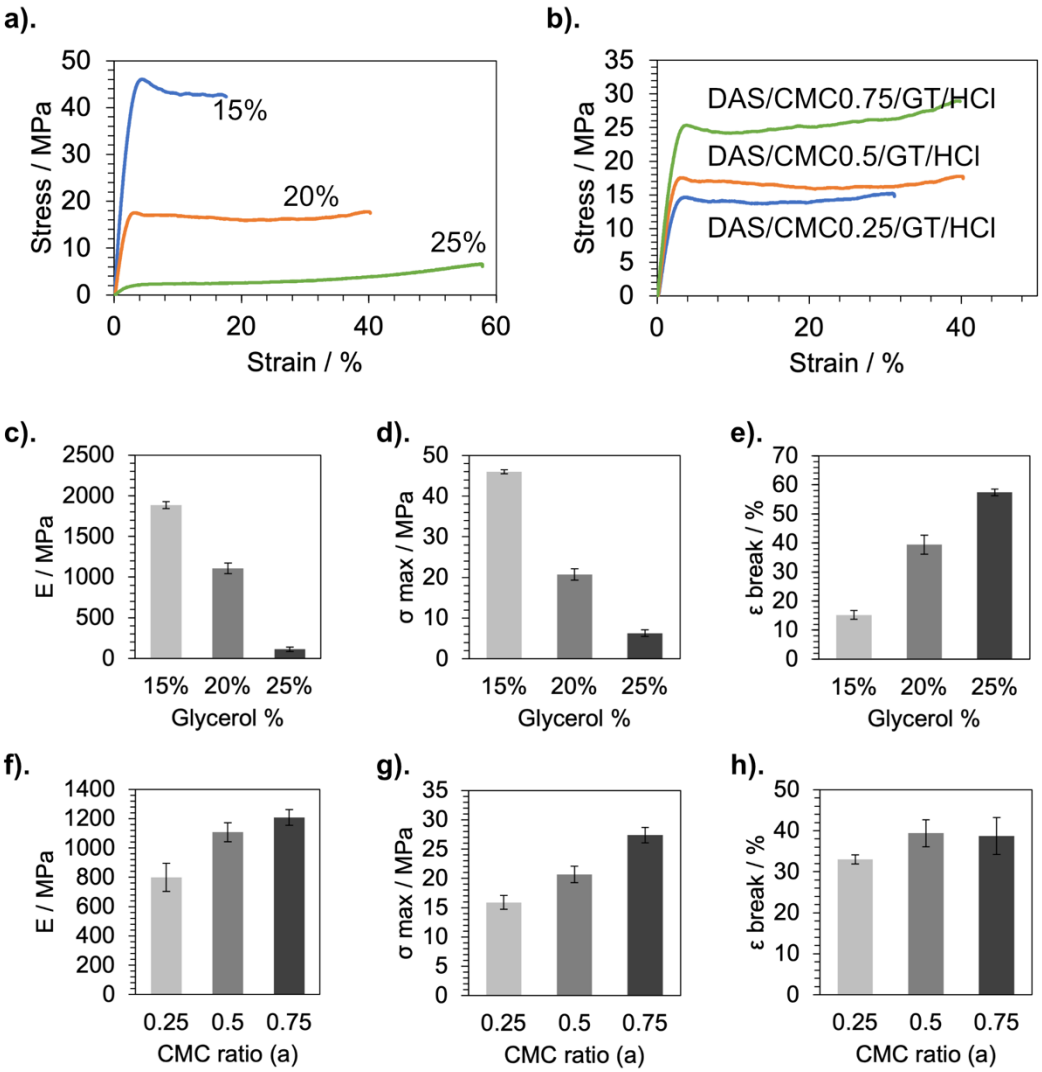

Figure 3-10 Mechanical properties of wet DAS/CMC/GT/HCl films. **a).** Stress–strain curve of DAS/CMC/GT/HCl films with different CMC ratios (processed by 20% glycerol solution), immersed in DIW for 30 min: DAS/CMC0.25/GT/HCl, DAS/CMC0.5/GT/HCl, DAS/CMC0.75/GT/HCl films. **b).** E, **c).** σ_{max} and **d).** ε_{break} of DAS/CMC0.25/GT/HCl, DAS/CMC0.5/GT/HCl, DAS/CMC0.75/GT/HCl films. **f).** E, **g).** σ_{max} and **h).** ε_{break} of DAS/CMC0.25/GT/HCl, DAS/CMC0.5/GT/HCl, DAS/CMC0.75/GT/HCl films (processed by 20% glycerol solution). CMC ratio (a) refers to the number after CMC in DAS/CMCa/GT/HCl sample name, which indicated the -CHO/-COO^- molar ratio; for example, the -CHO/-COO^- molar ratio is 1:0.5 when a is 0.5.

σ_{max}. The stress-strain curve of DAS/CMC/GT/HCl films with different DAS/CMC ratios were shown in **Figure 3-10 b)**, and the mechanical properties were summarized in **Figure 3-10 f)**, **g)**, and **h)**. As CMC proportion increased, ε_{break} and σ_{max} also increased. Compared to DAS, CMC has better film-forming ability and strength; while a film can be prepared with solely CMC, the same cannot be realized with solely DAS. Thus, the increase in CMC proportion increased the strength and ductility of the film.

The mechanical properties of the wet DAS/CMC/GT/HCl films were also tested, and the effect of

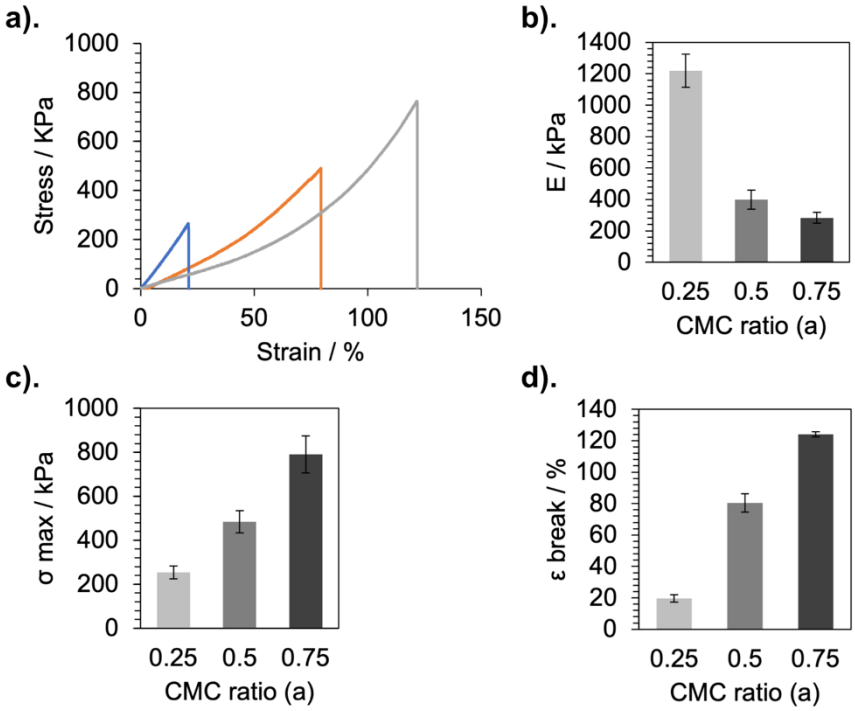

Figure 3-11 Mechanical properties of wet DAS/CMC/GT/HCl films. **a).** Stress–strain curve of DAS/CMC/GT/HCl films with different CMC ratios (processed by 20% glycerol solution), immersed in DIW for 30 min: DAS/CMC0.25/GT/HCl, DAS/CMC0.5/GT/HCl, DAS/CMC0.75/GT/HCl films. **b).** E, **c).** σ_{max} and **d).** ε_{break} of DAS/CMC0.25/GT/HCl, DAS/CMC0.5/GT/HCl, DAS/CMC0.75/GT/HCl films.

and DAS/CMC ratio on the mechanical properties of wet films were tested. The immersion time of 30 minutes was chosen to ensure the film samples reached swelling equilibrium. The stress–strain curve of the wet DAS/CMC/GT/HCl film is shown in **Figure 3-11 a)**, and the mechanical properties were summarized in **Figure 3-11 b)**, **c)**, and **d)**. Although the strength of the film decreased owing to water uptake after immersion, the films retained some strength, and the wet strength of the film (especially, film with DAS/CMC ratio of 1:0.5 and 1:0.75) were even comparable to that of some cellulose nanofiber-based blend films.[17] As DAS and CMC are both individually soluble in water, and DAS/CMC film without both type of crosslinks could not maintain stable in water, the binding force provided by crosslinks must be the major source of stability and mechanical strength of wet DAS/CMC/GT/HCl film. As mentioned before, GT was added to casting solutions at a constant molar ratio of $-COO^-$: GT = 1:1 across films with different DAS/CMC ratio, which was to minimize the amount uncoupled charged groups in the film. As a result, when CMC ratio increase, the GT dosage would also increase, leaving less -CHO available for the formation of acetal bond crosslinks. Thus, the change in mechanical properties reflects the different contribution of two types of crosslinks to the water resistance of the film. When CMC proportion is low, more -CHO bonds are available for the formation of acetal bond crosslinks; as a result, DAS/CMC0.25/GT/HCl film showed the highest *E* among the films tested. However, unlike ionic bonds, acetal bonds are not dynamic; combined with the fact that CMC has

higher strength compared to DAS, DAS/CMC0.25/GT/HCl film showed the lowest ε_{break} and σ_{max}. As CMC proportion increases, strength of the film indicated by σ_{max} also increased as expected. The ductility of the film indicated by σ_{max} also increased noticeably as CMC proportion increases. Due to its dynamic nature, the ionic crosslinks could dynamically cleave and reform during the elongation process, thus the films with higher CMC proportion and ionic bond crosslink proportion showed higher σ_{max}.

3.4. Conclusions

In this study, a starch-based blend film, DAS/CMC/GT/HCl, crosslinked by ionic and acetal crosslinks was prepared via solution casting, and its ion-responsive disintegration/dissolution behavior and mechanical properties were investigated. A chemically reactive starch derivative, DAS, was prepared via the dialdehyde oxidation of TS and then blended with CMC. The nonionic property of DAS allowed homogenous mixing with CMC, which contributed to the homogenous structure of the film. GT was added to the mixture to introduce positively charged quaternary ammonium groups into DAS, which bounded to DAS via imine bond formation during the film formation via solution casting. When cationic groups were introduced into DAS via GT, the DAS became cationic gradually, interacted with CMC, and formed ionic crosslinks. The formation of ionic crosslinks was confirmed by the improved stability of DAS/CMC/GT/HCl compared with the stability of films without ionic crosslinks in DIW. Owing to the ionic crosslinks, the DAS/CMC/GT/HCl film showed ion-responsive swelling behavior and finally disintegrated in high ionic strength solutions, including SW. The ion-responsive disintegration of DAS/CMC/GT/HCl was affected only by the ionic strength of the solution and not by the ion type, which might be explained by the weaker interaction between CMC and divalent cations in seawater. Acetal crosslinks introduced to the DAS/CMC/GT/HCl film during the preparation process further improved the water stability of the DAS/CMC/GT/HCl film but did not prevent the film from disintegrating in high ionic strength solutions. This study demonstrated that ionic crosslink could be a potential solution for overcoming the tradeoff between water resistance and rapid disintegration in marine ecosystems in polymer, which is essential to the development of future marine ecosystem-friendly single-use plastics.

References

(1) Luo, F.; Sun, T. L.; Nakajima, T.; Kurokawa, T.; Ihsan, A. B.; Li, X.; Guo, H.; Gong, J. P. Free Reprocessability of Tough and Self-Healing Hydrogels Based on Polyion Complex. *ACS Macro Lett.* **2015**, No. 4, 961–964. https://doi.org/10.1021/acsmacrolett.5b00501.

(2) He, M.; Shi, L.; Wang, G.; Cheng, Z.; Han, L.; Zhang, X.; Wang, C.; Wang, J.; Zhou, P.; Wang, G. Biocompatible and Biodegradable Chitosan/Sodium Polyacrylate Polyelectrolyte Complex

Hydrogels with Smart Responsiveness. *Int. J. Biol. Macromol.* **2020**, *155*, 1245–1251. https://doi.org/10.1016/j.ijbiomac.2019.11.092.
(3) Li, G.; Zhang, G.; Sun, R.; Wong, C.-P. Dually PH-Responsive Polyelectrolyte Complex Hydrogel Composed of Polyacrylic Acid and Poly (2-(Dimthylamino) Ethyl Methacrylate). *Polymer* **2016**, *107*, 332–340. https://doi.org/10.1016/j.polymer.2016.11.037.
(4) Insua, I.; Liamas, E.; Zhang, Z.; A. Peacock, A. F.; Marie Krachler, A.; Fernandez-Trillo, F. Enzyme-Responsive Polyion Complex (PIC) Nanoparticles for the Targeted Delivery of Antimicrobial Polymers. *Polym. Chem.* **2016**, *7* (15), 2684–2690. https://doi.org/10.1039/C6PY00146G.
(5) Hu, Q.; Zhang, Y.; Wang, T.; Sun, W.; Tong, Z. PH Responsive Strong Polyion Complex Shape Memory Hydrogel with Spontaneous Shape Changing and Information Encryption. *Macromol. Rapid Commun.* **2021**, *42* (9), 2000747. https://doi.org/10.1002/marc.202000747.
(6) Ishii, S.; Kaneko, J.; Nagasaki, Y. Dual Stimuli-Responsive Redox-Active Injectable Gel by Polyion Complex Based Flower Micelles for Biomedical Applications. *Macromolecules* **2015**, *48* (9), 3088–3094. https://doi.org/10.1021/acs.macromol.5b00305.
(7) Emmanuel, B. D.; Abu-Thabit, N. Y.; Ngwuluka, N. C. Responsive Polyelectrolyte Complexes Based on Natural Polysaccharides for Drug Delivery Applications. In *Stimuli Responsive Polymeric Nanocarriers for Drug Delivery Applications, Volume 1*; Elsevier, 2018; pp 267–287. https://doi.org/10.1016/B978-0-08-101997-9.00014-X.
(8) VanGinkel, C. G.; Gayton, S. The Biodegradability and Nontoxicity of Carboxymethyl Cellulose (DS 0.7) and Intermediates. *Environ. Toxicol. Chem.* **1996**, *15* (3), 270–274. https://doi.org/10.1002/etc.5620150307.
(9) Feddersen, R. L.; Thorp, S. N. SODIUM CARBOXYMETHYLCELLULOSE. In *Industrial Gums*; Elsevier, 1993; pp 537–578. https://doi.org/10.1016/B978-0-08-092654-4.50024-3.
(10) Sirviö, J.; Honka, A.; Liimatainen, H.; Niinimäki, J.; Hormi, O. Synthesis of Highly Cationic Water-Soluble Cellulose Derivative and Its Potential as Novel Biopolymeric Flocculation Agent. *Carbohydr. Polym.* **2011**, *86* (1), 266–270. https://doi.org/10.1016/j.carbpol.2011.04.046.
(11) Hujaya, S. D. Polyion Complex Hydrogels from Chemically Modified Cellulose Nanofibrils: Structure-Function Relationship and Potential for Controlled and PH-Responsive Release of Doxorubicin. *Acta Biomater.* **2018**, 12.
(12) Jia, Y.; Asoh, T.-A.; Hsu, Y.-I.; Uyama, H. Wet Strength Improvement of Starch-Based Blend Films by Formation of Acetal/Hemiacetal Bonding. *Polym. Degrad. Stab.* **2020**, *177*, 109197. https://doi.org/10.1016/j.polymdegradstab.2020.109197.
(13) Yu, J.; Chang, P. R.; Ma, X. The Preparation and Properties of Dialdehyde Starch and Thermoplastic Dialdehyde Starch. *Carbohydr. Polym.* **2010**, *79* (2), 296–300. https://doi.org/10.1016/j.carbpol.2009.08.005.
(14) El-Ayaan, U.; Kenawy, I. M.; Abu El-Reash, Y. G. Synthesis, Thermal and Spectral Studies of

First-Row Transition Metal Complexes with Girard-T Reagent-Based Ligand. *J. Mol. Struct.* **2007**, *871* (1–3), 14–23. https://doi.org/10.1016/j.molstruc.2007.01.054.
(15) Jia, Y.; Hsu, Y.-I.; Uyama, H. A Starch-Based, Crosslinked Blend Film with Seawater-Specific Dissolution Characteristics. *Carbohydr. Polym.* **2023**, *299*, 120181. https://doi.org/10.1016/j.carbpol.2022.120181.
(16) Zhang, W.; Wang, P.; Liu, S.; Chen, J.; Chen, R.; He, X.; Ma, G.; Lei, Z. Factors Affecting the Properties of Superabsorbent Polymer Hydrogels and Methods to Improve Their Performance: A Review. *J. Mater. Sci.* **2021**, *56* (29), 16223–16242. https://doi.org/10.1007/s10853-021-06306-1.
(17) Soni, R.; Asoh, T.-A.; Uyama, H. Cellulose Nanofiber Reinforced Starch Membrane with High Mechanical Strength and Durability in Water. *Carbohydr. Polym.* **2020**, *238*, 116203. https://doi.org/10.1016/j.carbpol.2020.116203.

Conclusions

In this study, control of the dissolution/disintegration behavior of starch-based blend film was attempted by the introduction of three different types of intermolecular crosslinks including covalent and non-covalent, responsive crosslinks, and the dissolution/disintegration behavior of crosslinked blend film in different solution environments was characterized. This research showed that the dissolution/disintegration behavior of starch-based blend film can be effectively controlled via the introduction and the disruption of intermolecular crosslinks, and dissolution/disintegration behavior control of starch-based blend film in different aqueous environments, namely seawater and freshwater, can be realized with crosslink bond types that respond to the chemical characteristics of seawater and proper selection of modification method.

In Chapter 1, HPS was oxidized by periodate oxidation. The oxidized product, HPS_{Ox}, was blended with PVA; hemiacetal/acetal bond crosslinked starch/PVA blend film, HPS_{Ox}/PVA film, was prepared by solution casting. With the presence of acid, -CHO on HPS_{Ox} reacted with -OH groups on both HPS_{Ox} and PVA, forming hemiacetal/acetal bond crosslinks. The hemiacetal/acetal bond crosslinked HPS_{Ox}/PVA film showed drastically improved water resistance, which is due to the high crosslinking density consequent to the high aldehyde group concentration in HPS_{Ox}. Thus, using periodate-oxidized starch as both constitutional material and crosslinking agent is a simple-to-operate, yet effective strategy for improving the water resistance of starch-based blend films. Chapter 1 confirmed that intermolecular crosslinks have a great influence on the dissolution/disintegration behavior of starch-based blend films in aqueous environment.

In Chapter 2, utilizing the findings from Chapter 1, the dissolution/disintegration behavior of a starch-based blend film in freshwater and seawater was controlled by the introduction of a seawater-responsive hydrogen bond crosslink. PAAc chain segments were grafted to TS by grafting polymerization, and the grafted starch, TS-g-PAAc was blended with PVP to form a hydrogen-bond crosslinked film, TS-g-PAAc/PVP film by solution casting. With the grafted PAAc chain segments, the grafted starch, TS-g-PAAc was able to form strong, water stable hydrogen bond crosslinks with PVP during the drying process, which contributed to the improved water resistance of the film over unmodified starch film. Whereas the pure starch film dissolved rapidly in DIW, TS-g-PAAc film was able to remain stable due to the crosslinks. In seawater, TS-g-PAAc film was also able to rapidly disintegrate and dissolve in SW due to the deprotonation of -COOH groups on PAAc chain segments, which may greatly reduce the risk of the film to marine wildlife after being leaked to the marine ecosystem. Chapter 2 demonstrated that the dissolution/disintegration behavior of a starch-based blend film in freshwater and seawater can be controlled by the formation and disruption of intermolecular crosslinks.

In Chapter 3, the concept of dissolution/disintegration behavior of starch-based blend films was

further extended by the development of alternative responsive mechanism to the hydrogen bond crosslink featured in Chapter 2. A starch-based blend DAS was prepared from TS by periodate oxidation, and a DAS/CMC blend film crosslinked by both ionic and acetal crosslinks, DAS/CMC/GT/HCl film, was prepared by a modified solution casting process, during which DAS in DAS/CMC mixture is gradually rendered cationic by a GT, and interacted with CMC to form ionic crosslinks. While introducing ionic bond crosslinks via direct blending of polycation and polyanion can lead to aggregation which renders film formation difficult if not impossible, this issue was addressed by the modified solution casting process. During the drying process, acetal bonds also formed between -CHO on DAS and -OH on both CMC and DAS. DAS/CMC/GT/HCl film was stable in DIW and reached swelling equilibrium, which is due to both type of crosslinks. By contrast, the film continued to swell and finally disintegrated in high ionic strength solutions like 3.5% NaCl solution and SW due to the cleavage of ionic crosslinks. While the ionic responsive dissolution/disintegration properties of the film were contributed by ionic crosslinks, both types of crosslinks contributed to the water resistance in low ionic strength solutions like DIW. Chapter 3 again exemplified that the dissolution/disintegration behavior in freshwater and seawater can be controlled by the formation and disruption of intermolecular crosslinks, and implied the versatility of crosslink-based dissolution/disintegration behavior control.

From the results of this study, it can be concluded that the dissolution/disintegration behavior control of starch-based films in freshwater and seawater can be a potential strategy for balancing the ecological risk of starch-based films to the marine ecosystem and the ease of use in daily life. Findings in this study are expected to contribute to the development of future starch-based single-use materials which pose lower risk to the marine ecosystem.

List of publications

1. Wet Strength Improvement of Starch-based Blend Films by Formation of Acetal/hemiacetal Bonding

Yuxiang JIA, Taka-Aki Asoh*, Yu-I Hsu, Hiroshi Uyama*

Polymer Degradation and Stability **2020**, *177*, 109197.

10.1016/j.polymdegradstab.2020.109197.

2. A Starch-based, Crosslinked Blend film with Seawater-specific Dissolution Characteristics

Yuxiang JIA, Yu-I Hsu*, Hiroshi Uyama*

Carbohydrate Polymers **2023**, *299*, 120181.

10.1016/j.carbpol.2022.120181.

3. Dual-Crosslinked Starch/Carboxymethyl Cellulose Blend Film with Ion-responsive Dissolution Properties

Yuxiang JIA, Yu-I Hsu*, Hiroshi Uyama*

Polymer Degradation and Stability

Accepted

Acknowledgements

This work was conducted in Uyama Lab., Department of Applied Chemistry, Graduate School of Engineering, Osaka University, from 2018 to 2023, and I am sincerely grateful for the immeasurable support I have received from many during this period.

I would like to express my deepest gratitude to Prof. Hiroshi Uyama, my research supervisor, without whose expertise, constructive critics and advice, this research work would not be possible. My gratitude extends to the rest of the thesis committee, Prof. Takeshi Hayashi and Prof. Satoshi Minakata, for their advice during the preparation of this thesis.

I would like to express my sincere appreciation to Assoc. Prof Yu-I Hsu, for her continued guidance and support on my research work and publication writing. My gratitude would also extend to Dr. Takaaki Asoh (Tokyo University of Science), for his kind advice on my research work and research funding acquisition, during his incumbency as Assoc. Prof. in Uyama Lab.

Special thanks to Assist. Prof. Akihide Sugawara and Dr. Yasushi Takeuchi, for their insightful advice.

I would also like to extend my thanks to the rest of members of Uyama Lab., for their help in research and daily life. You always lend a helping hand when I was confronted with big and small barriers.

Finally, I would like to thank my parents deeply for their companionship and encouragement.

2023.06

Yuxiang JIA